NIRS

HIMAC

NIRS-M-99
HIMAC-006

Proceedings of the Third Workshop on Physical and Biological Research with Heavy Ions

Edited by
Koichi Ando
Tatsuaki Kanai

September 2 - 3, 1993

National Institute of Radiological Sciences
9-1, Anagawa 4-chome, Inage-ku, Chiba-shi 263 JAPAN

Editor's note

The clinical trial of the heavy-ion radiation therapy at NIRS will start in 1994. In the clinical trial, it is very important to discuss what particle is best for the radiotherapy. The physicist and biologist took part in the decision of the particle to be used for the first radiotherapy through the biophysical experiments at RIKEN Ring Cyclotron. We would like to express sincere gratitude to the Insti. Phys. Chem. Res., who provided us an opportunity to do heavy ion experiments using the RRC. It becomes more important of the cooperation between physicist, biologist and medical doctors in searching the best method of the heavy-ion radiotherapy. Significance of this biophysical research meeting will be more and more important from now on.

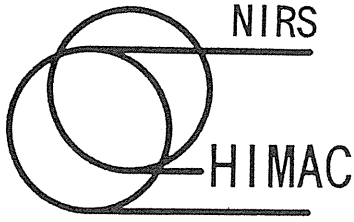

NIRS-M-99
HIMAC-006

Proceedings of the Third Workshop on Physical and Biological Research with Heavy Ions

Edited by
Koichi Ando
Tatsuaki Kanai

September 2 - 3, 1993

National Institute of Radiological Sciences

9-1, Anagawa 4-chome, Inage-ku, Chiba-shi 263 JAPAN

Foreword

In the National Institute of Radiological Sciences (NIRS), construction of a heavy ion medical accelerator (HIMAC) facility is just before its completion. As the preparatory studies to start the clinical trial of cancer treatment in near future, various kinds of physical and biological researches have been performed by using mainly heavy ion beams provided by RIKEN Ring-Cyclotron facility.

Most of these studies are not only the works preparatory to the clinical trial but also milestones of the important researches in the field of radiation biology itself, and therefore should be continued in the HIMAC facility.

I believe that this workshop which is quite informative and fruitful will stimulate further collaboration works among related researchers in the whole world.

Yasuo Hirao, Ph.D.

Director-General,
NIRS

Proceedings of the Third Workshop on Physical and Biological Reseach with Heavy Ions

I. PROPOSALS FOR A CLINICAL TRIAL

1. Biological and physical proposals for a heavy-ion clinical trial.
   T.Kanai, and Bio-Phys. Group of RIKEN Ring Cyclotron Users.

II. PHYSICS

2. Effects of object size on a function to convert X-ray CT numbers into the water equivalent path length of charged particle beam.
   S.Minohara, T.Kanai, M.Endo, and K.Kawachi.
3. Secondary-electron emission monitor.
   M.Sudou and T.Kanai.
4. Silicon diodes as detectors in relative dosimetry of heavy ions.
   A.Fukumura, K.Hoshino, M.Takeshita, T.Kanai, S.Minohara, and M.Sudou.
5. Beam end point measurement with positron emitting secondary beams.
   T.Tomitani, M.Kanazawa, M.Sudou, F.Soga, T.Kanai, Y.Sato, M.Inabe, A.Yoshida, and Y.Watanabe.
6. Tracking and LET measurements of cosmic ray nuclei for space radiobiological studies.
   K. Ogura, T.Hayashi, T.Kojima, M.Matsushima, S.Nagaoka, K.Nakano, T. Takahashi, H.Yamada, and F.Yatagai.
7. Track structure of heavy ions and inactivation model for microorganisms.
   T.Takahashi, F.Yatagai, and M.Suzuki.
8. Microscopical investigation of cellular effects of 135 MeV/amu carbon along the path of the beam.
   M. Furuse, F.Soga, and S.Matsumoto.

III. CELL LETHALITY

9. Difference in the LET-RBE and - OER response to heavy-ions revealed by accelerated ions and cell strains.
   Y.Furusawa, K.Fukutsu, H.Itsukaichi, K.Eguchi-Kasai, H.Ohara, F.Yatagai, and T.Kanai.
10. Response of plateau-phase cultures and multicellular spheroids of human osteosarcoma cells to carbon beam irradiation.
    N.Kubota, M.Kakehi, S.Matsubara, F.Yatagai, T.Kanai, and T.Inada.

11. RBEs of various human monolayer cells irradiated with carbon beams.
H. Ito, S.Yamashita, I. Nishiguchi, N.Shigematsu, Wei-jei Ka, A.Kubo, F.Yatagai, and T.Kanai.

IV. GENETIC DAMAGE

12. Chromosome aberrations induced by 135 MeV/u of carbon and neon beams by RRC.
H. Ohara, M.Minamihisamatu, T.Kanai, K.Eguchi-Kasai, H.Itsukaichi, K.Fukutsu, F.Yatagai, and K.Sato.

13. Sensitivity of ts85 mutant strain from mouse FM3A cells to heavy ions.
F. Yatagai, K.Nakano, T.Kanai, K.Saito, and F.Hanaoka.
14. Enhancement of cell killing by split exposure of high LET heavy ion beams.
K.Eguchi-Kasai, H.Itsukaichi, M.Murakami, K.Fukutsu, Y.Furusawa, T.Kanai, K.Shimizu, and K.Sato.
15. LET dependency of mutation induction at the HGPRT locus and molecular characterization of mutations in human cells irradiated with accelerated heavy ions.
M.Watanabe, M.Suzuki, Y.Kase, F.Yatagai, T.Kanai, and T.Kato.
16. The effects of cell death and mutation induction irradiated with accelerated carbon ion beams with spread out Bragg peak.
M.Suzuki, M.Watanabe, Y.Kase, T.Kanai, F.Yatagai, T.Karto, and S.Matsubara.

V. TISSUE LEVEL

17. Effects of high LET radiation on murine skin and tumors.
K.Ando, S.Koike, M.Iizuka, T.Aruga, N.Hori, W.Shimizu, T.Sugita, S.Murayama, T.Kanai, S.Minohara, M.Sudou, and F.Yatagai.
18. The irradiated volume dependency of early skin reaction after carbon beam irradiation.
H.Tatsuzaki, T.Okumura, H.Takahashi, M.Miyakawa, T.Kanai, S.Minohara, M.Sudou, and F.Yatagai.
19. The effects of carbon beam on hemopoietic system in mice.
A.Tsuboi, E.Kojima, and K.Tanaka.
20. Response of mouse intestine after fractionated doses of accelerated carbon-ion with spread-out Bragg peak.
K.Fukutsu, T.Kanai, Y.Furusawa, T.Aruga, S.Murayama, S.Hori, S.Minohara, S.Koike, F.Yatagai, and K.Ando.

21. Dose response relations in acute cell death of pancreatic islets after whole body irradiation of golden hamster with ^{60}Co gamma, 70 MeV proton and 135 MeV/u carbon beams.
S.Tsubouchi, K.Fukutsu., H.Itsukaichi, M.Murakami, K.Kasai, Y.Furusawa, T.Kanai, S.Koike, K.Ando, H.Ohara, F.Yatagai, and E.Kano.
22. Effects of accelerated carbon-ion on the induction of dominant lethality in the teleost fish, Oryzias latipes.
Y.Hyodo-Taguchi, T.Kanai, S.Minohara, and Y.Furusawa.

VI. GENE EXPRESSION
23. Apoptosis in thymocytes and lymphoma cells induced by neutrons and X-rays.
H.Ohyama, S.Koike, and K.Ando.
24. Irradiation increases manganese superoxide dysmutase gene in human fibroblasts: Possible mechanisms for its accumlatation.
M.Akashi, M.Hachiya, S.Shimizu, Y.Osawa, and G.Suzuki.

Errata
Initial recombination in a parallel plate ionization chamber exposed to heavy-ion beams.
T.Kanai, M.Sudou, S.Minohara, and F.Yatagai.

Biological and physical proporsals for a heavy-ion clinical trial

Tatsuaki Kanai and Bio-Phys. Group of RIKEN Ring Cyclotron Users

ABSTRACT

Based on biological and physical properties of monoenergetic heavy-ion beams, a range modulator was designed to make a biologically flat spread-out Bragg peak for V79 cells. The responses of V79, HSG, crypt cells of the mouse jejunum and other many biological systems were examined for the spread-out Bragg peak. The response of the cells for the range modulated beam was able to be expected from the responses for the monoenergetic beam. We also found that responses of cell killing ability of V79, HSG and crypt cell for the neutron irradiation were almost equivalent to those for the carbon beam which had a dose averaged LET of 65 keV/μm. For the first clinical trial of the heavy-ion radiotherapy with HIMAC beams[1], we proposed to use carbon 290 MeV/u and to start with an irradiation schedule of neutron therapy.

INTRODUCTION

In the 2nd workshop on "Physical and Biological Research with Heavy ions", we reported on the physical characteristics of the carbon and neon beams, accelerated by RIKEN ring cyclotron[2], which were used for the preparatory studies of heavy-ion therapy[3,4]. We also discussed on how to design a pspread-out Bragg peak with the heavy-ion beams.[3] The tested range modulator was successfully designed in making a biologically flat spread-out Bragg peak for V79 cells. It was proved that it is possible to expect cell survivals irradiated with the range modulated beam when LET dependence of the survival fractions for the monoenergetic beam is known. For the real radiation therapy using heavy-ion beams, we have to choose a kind of heavy ions, energy of the beam, schedule of the fractionation, and the size of dose of single and total irradiations for the treatment. Concerning these method of heavy-ion radiotherapy, we don't have sufficient biological and physical data to optimize the therapeutic results. Fortunately, there are many experiences of radiation therapies using the neutron beam which is regarded as one of the high LET radiations.

In this paper, we have shown physical and biological backgrounds for the first clinical trial of the heavy-ion radiotherapy, which make the best use of 20-year experiences of the neutron therapy at NIRS (National Institute of Radiological Sciences).

Design of Spread-Out Bragg Peak

In the heavy-ion radiotherapy, to sterilize cells uniformly in the target volume is directly related to reducing injuries of the healthy tissues at the entrance part of the heavy-ion path. We have to put additional doses to the normal tissues in order to irradiate a sufficient dose to a cold spot in the target volume if the uniform sterilization in the target volume is not realized. Then it is very important to make a spread-out Bragg peak in which cells are uniformly killed. In order to establish a method to make the spread-out Bragg peak, we choose V79 cells as a probe of the biological response of the heavy-ions[5]. The spread-out Bragg peak is realized by using a range modulator, which superpose shifted dose distributions of monoenergetic beams. The superposing ratio should be determined so as to make a suitable spread-out Bragg peak.

In order to design the spread-out Bragg peak, it is necessary to find a rule for an estimation of the biological responses of the superposed beam from those of the original beams. Lam formulated the relationship of the RBEs(Relative Biological Effectiveness) of the mixed beam and RBEs of the original beams as follows[6];

$$(RBE)_{mix} = f_1(RBE)_1 + f_2(RBE)_2$$

$$f_i = d_i / D$$

where $(RBE)_1$, $(RBE)_2$ and $(RBE)_{mix}$ are the RBE of radiations 1, 2 and the mixed beam, respectively. The mixed beam is the radiation field which radiation 1 and 2 are mixed with doses of d_1 and d_2, respectively. D is the total dose of the mixed beam, that is, $D=d_1+d_2$. Then, f_1 and f_2 are the dose fractions of each radiation.

Zaider and Rossi also developed a formalism for the mixed beam using the dual radiation action theory[7].

$$\alpha_{mix} = f_1\alpha_1 + f_2\alpha_2$$

$$\beta_{mix} = f_1\beta_1 + f_2\beta_2$$

α and β are coefficients of linear and quadratic terms of the survival curve of the LQ model, respectively. Results of the survival curves for the mixed beam calculated by the two methods were very similar. We examined these formula for the mixed beam using heavy-ion beams of

carbon and helium-3 or helium-4 accelerated by NIRS cyclotron.

The range modulator consists of sectoral absorbers of various thickness and forms like a propeller. The rotating propeller is inserted in the beam course. The ratio of the central angle of the each sector is the superposed ratio of the shifted Bragg curve for the spread-out Bragg peak. RBE at depth x for the range modulated beam is calculated by Lam formula as follows.

$(RBE)_{RM}(x) =$

$\{\Sigma r_j d(x + s_j)RBE(x + s_j)\} / \{\Sigma r_j d(x + s_j)\}$

where r_j is the superposed ratio of the j-th shifted Bragg curve, d(x) is the depth dose distribution of the monoenergetic beam, s_j is the water equivalent length of the j-th absorber of the range modulator, which corresponds to the shift length of the monoenergetic Bragg curve. $(RBE)_{RM}(x)$ and RBE(x) are the RBE of the range modulated beam and monoenergetic beam at depth x. Photon equivalent dose (or biological dose, D_{bio}) for the physical dose $D_{phy}(x)$ of the range modulated beam can be defined following the definition of RBE.

$D_{bio}(x) = D_{phy}(x)\ (RBE)_{RM}(x)$

$D_{phy}(x) = \Sigma\ r_j d(x + s_j)$

Therefore, the superposed ratio r_j of the range modulator should be determined so as that the biological dose is constant in the spread-out Bragg peak. r_j can be calculated by an iteration method.

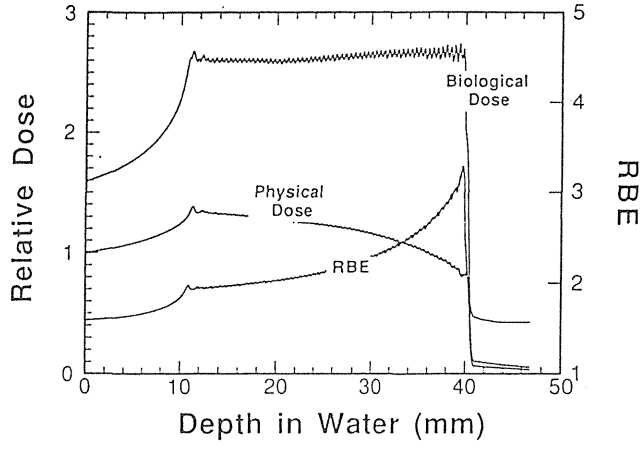

Fig. 1. Calculated physical and biological dose distributions and RBE for the spread-out Bragg peak of 135 MeV/u carbon beam. The spread-out Bragg peak was designed so that 10 % survival levels of V79 cells were flat in the peak region.

In this discussion about the biological dose of the range modulated beam using the concept of RBE, it is necessary to indicate survival level. Generally speaking, the value of RBE depends on the survival level.

The range modulator for 135 MeV/u carbon beam was installed at the biological irradiation course in RIKEN ring cyclotron facility[8] in order to establish the method of making the spread-out Bragg peaks in the heavy-ion therapy. The range modulator was designed which makes a spread-out Bragg peak of a 3 cm width in a 4 cm penetration in water. Biological dose at 10 % survival level of V79 Chinese hamstar cells is planned to be flat in the spread-out Bragg peak.

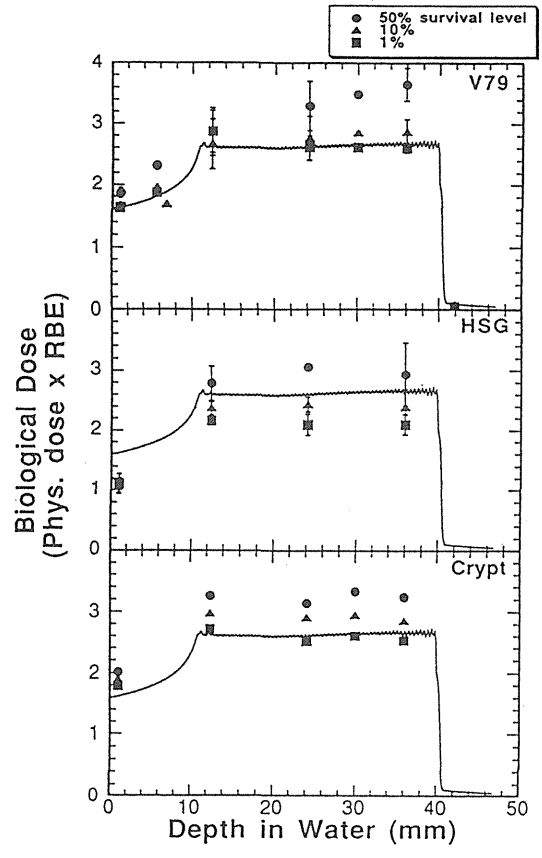

Fig. 2. Experimental results of biological dose distributions of 1, 10 and 50 % survival levels of V79 (upper), HSG(middle) and crypt(lower) cells.

Figure 1 shows calculation of the physical and biological dose and RBE distribution for the range modulated beam. The physical dose in the spread-out Bragg peak decreases as increasing depth in water. On the contrary, RBE increases as increasing depth in water.

As discussed in the 2nd workshop on "Physical and Biological Research with Heavy ions", the spread-out Bragg peak had successfully flat response for 10 % survival level of V79 cell line. Biological responses for the range modulated beam were also examined by quite

different biological species using the same range modulator. Fig. 2 shows experimental results of biological dose distributions of V79, HSG and crypt cells for the range modulated beam. As shown in Fig. 2, the biological dose of HSG and crypt cell were reasonably flat in the spread-out Bragg peak. The biological dose were lower than the calculated curve for the HSG cells and higher for the crypt cells. This is because the absolute values of RBE is lower than that of V79 for HSG and higher for crypt cells. Because of small shoulder size of the survival curves for HSG and crypt cells, the biological dose of 50 % survival level were still flat in the spread-out Bragg peak.

Neutron Equivalent Carbon Beam

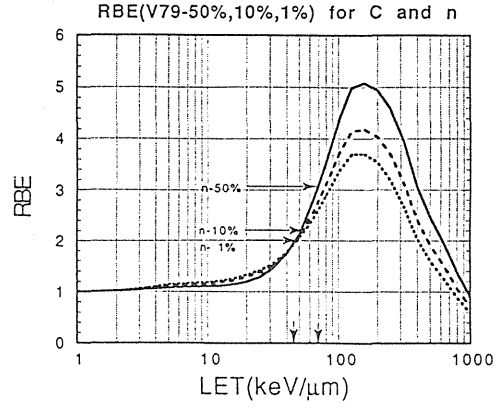

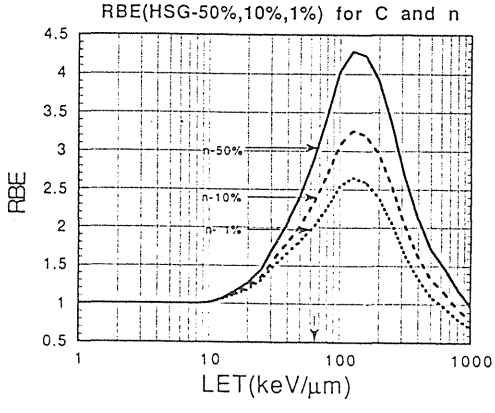

Fig. 3 LET dependency of RBE for colony formation of V79 and HSG cells. The arrows in the graph show the RBEs for the NIRS neutron beam.

In order to apply 20-year experiences of neutron radiotherapy at NIRS to the heavy-ion radiation therapy, we compared the effects of the neutron irradiation on cell survival with those of carbon irradiations. Fig. 3 shows LET dependency of RBE for colony formation of V79 and HSG cells. Solid, dashed and dotted curves in the figure indicate RBE of 50 %, 10 % and 1 % survival level, respectively. Arrows in the figure show RBE of 50 %, 10 % and 1 % survival levels for the V79 and HSG cells irradiated with NIRS neutron beam. As shown in Fig. 3, neutron RBEs of these survival levels coincided with RBE of carbon beam at the dose averaged LET of around 65 keV/μm. Then it can be said that neutron beam is nearly equivalent to 65 keV/μm carbon beam.

Ms. Fukutsu et al. have discussed on effects of fractionated irradiations of spread-out carbon beam and neutrons on crypt cells of the mouse jejunum in this workshop[9]. The survival curves of the crypt cells for neutron irradiations coincided with the survival curves for the irradiations of proximal peak of the range modulated carbon beam in both cases of the single and the fractionated irradiations. The dose averaged LET of the proximal peak of the spread-out Bragg peak is about 65 keV/μm. Even though the biological effects for the range modulated beam, which has the dose averaged LET of 65 keV/μm, should be slightly different from those for the monoenergetic beam of the same LET, these results of the effects of single and fractionated irradiations on the crypt cells have supported the assumptions that the NIRS neutron beam is nearly equivalent to 65 keV/μm carbon beam.

Simulation of High Energy Heavy-Ion Beams

In order to treat patients with heavy-ion beams, it is necessary to expect the effects of the fractionated irradiations at the survival levels of about 10^{-9}. However, at the present time, we don't have sufficient biological data for the above studies. Then, it is very reasonable to apply the 20-year experiences of radiation therapy with high LET neutron beams to our heavy-ion radiation therapy. As discussed in the previous section, the biological effects of the neutron beam at NIRS is very similar to the effects of the 65 keV/μm carbon beams. Then we have calculated depth dose distribution and LET distributions of monoenergetic beams of carbon and neon including the fragmentation effects, using a preliminary version of a code under development by L.Sihver and T.Kanai[10]. Spread-out Bragg peaks of 6 cm width were designed realizing flat biological dose for V79 cells. Physical and biological depth dose distributions were calculated for the range modulated beams of carbon and neon. Dose averaged LET for the SOBP beams were also calculated. Fig. 4 shows the results of the dose averaged LET for the

SOBP beams of carbon and neon beams. LET of the neon beam in the SOBP was over 80 keV/μm. LET at the entrance position in the depth dose distribution was 40 keV/μm. On the other hand, LET of the carbon beam in the SOBP was over 45 keV/μm and the LET at the entrance position was around 15 keV/μm. Then the biological effects of the carbon beams are expected to be similar to the effects with this high energy carbon beam. Severer response is expected for the neon irradiations than for the neutron irradiations. Fig. 5 shows the biological dose and LET distributions for the carbon SOBP beam of 6 cm width, which is obtained by modulating 290 MeV/u beam. It can be said that the beam quality at the entrance is similar to photon and is similar to neutron at the SOBP.

From the above bio-physical research with the heavy-ion beams, we have recommended to start clinical trials of the heavy-ion radiotherapy with carbon beams. Proposal of the first clinical trial is as follows;

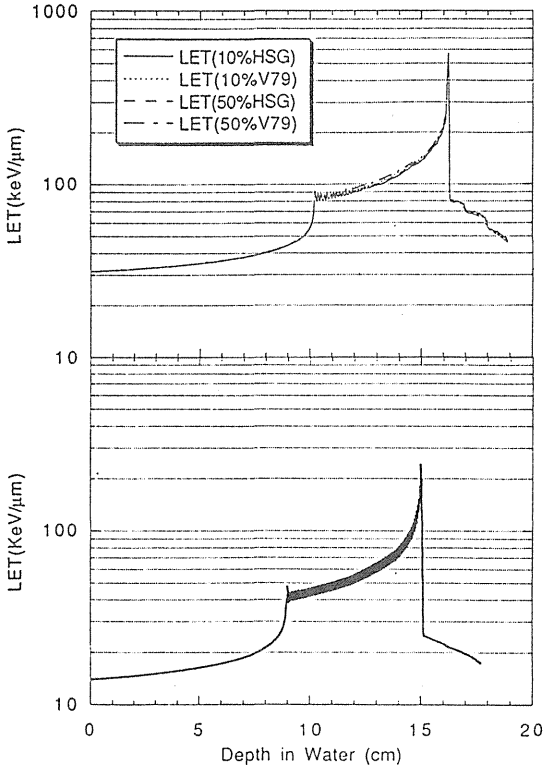

Fig. 4. Dose averaged LET of the range modulated beam of carbon(upper panel) and neon(lower panel) beams. Width of the spread-out Bragg peak was 6 cm.

(1) The first ion is carbon. The energy is 290 MeV/u beam, which have 16 cm range in water.

(2) In order to design the spread-out Bragg peak, responses of a virtual cell should be supposed to represent various kind of tumour cells. Now, we think the response of the virtual cell is in between the HSG and V79 cell line.

(3) Treatment planning of the heavy-ion radiotherapy should be based on the relative biological dose distribution calculated with the response of the virtual cells.

(4) A treatment schedule of the neutron radiotherapy should be accepted for the carbon irradiation for the first trial.

(5) Fractionated dose or the total dose of the carbon beam should be followed by the physical dose of neutron beam. That is to say, the fractionated physical dose of the carbon SOBP beam at the position where the dose averaged LET is 65 keV/μm should be equal to the neutron fractionated dose.

(6) In order to optimize the heavy-ion radiation therapy, the irradiation dose should be escalated from the neutron equivalent dose. And the dose averaged LET should be also escalated to search more efficient heavy-ion radiation therapy.

(7) In order to have the optimum fraction size and fractionation schedule, biological response of the fractionated irradiations should be investigated.

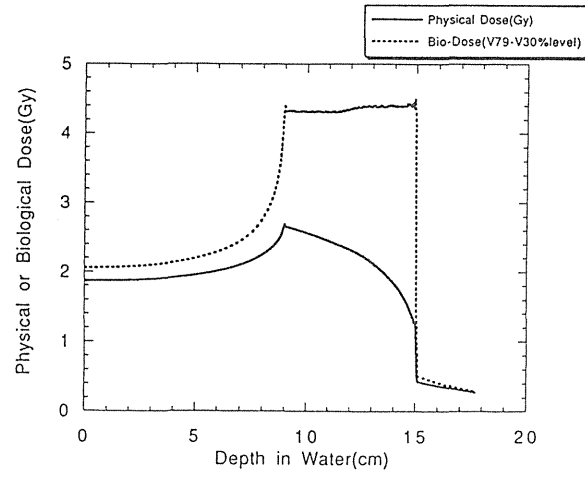

Fig. 5. Physical (solid) and biological (dashed) dose distributions of the carbon SOBP beam.

Conclusion

A heavy-ion irradiation system was designed and constructed at RIKEN ring cyclotron facility for preparatory studies of heavy-ion therapy. The range modulator was successfully designed to make a biologically flat spread-out Bragg peak for V79 cell line. We have found that response

of cell killing ability of V79, HSG and crypt cell to neutron irradiation are almost equivalent to carbon beam which has LET of 65 keV/μm. For the first clinical trial of the heavy-ion radiotherapy with HIMAC beams, we have proposed to use a beam of carbon 290 MeV/u and to start with an irradiation schedule of neutron therapy.

Bio-Phys. Group of RIKEN Ring Cyclotron Users

T.Kanai (NIRS) Y.Furusawa(NIRS)
K.Fukutsu(NIRS) H.Ohara(Okayama U)
K.Andou(NIRS) S.Koike(NIRS)
K.Eguchi-Kasai(NIRS) H.Itsukaichi(NIRS)
S.Minohara(NIRS) A.Fukumura(NIRS)
M.Sudou(NIRS) T.Kohno(NIRS)
S.Hori(NIRS) M.Iizuka(NIRS)
S. Murayama(NIRS) T.Aruga(NIRS)
A.Tsuboi(NIRS) E.Kojima(NIRS)
K.Tanaka(NIRS) Y.Taguchi(NIRS)
M.Murakami(NIRS) M.Suzuki(Nagasaki)
C.Muraiso(NIRS) S.Matsumoto(NIRS)
M.Furuse(NIRS) F.Soga(NIRS)
M.Watanabe(Nagasaki) Y.Kase(Nagasaki)
H.Tatsuzaki(Tsukuba) H.Itoh(Keio)
S.Yamashita(Saitama H) F.Yatagai(RIKEN)
N.Kubota(Yokohama C.U)

References

[1] Y.Hirao et al., HIMAC report (NIRS Publication), HIMAC-001, 1992.
[2] Y.Yano, in Proceedings of the 8th Symp. on Accelerator Science and Technology, 1991, p.10-12.
[3] T.Kanai et al., Proceedings of 2nd Workshop on Physical and Biological Research with Heavy ions, (Edited by K.Ando and T.Kanai), HIMAC report (NIRS Publication), HIMAC-003,1-3, 1992.
[4] T.Kanai et al., Radiation Research, 1993.
[5] Y.Furusawa, et al., in Proceedings of 2nd Workshop on Physical and Biological Research with Heavy ions, HIMAC report (NIRS Publication), HIMAC-003, 1992.
[6] G.K.Y.Lam, The survival response of a biological system to mixed radiations. Radiat. Res. 110, 232 - 243 (1987).
[7] Zaider and Rossi, Radiat. Res. 83, 1980, 732 - 739.
[8] T.Kanai, et al., HIMAC report (NIRS Publication), HIMAC-004, 1993.
[9] K.Fukutsu, et al., Seibutsu-bukai, Niti-I-Hou, 1993.
[10] L.Sihver and T.Kanai, to be published

Errata; LET dependency of the initial recombination written in "Beam Modulation for Heavy-ion Radiotherapy" in the 2nd workshop on "Physical and Biological Research with Heavy ions", HIMAC 003, 1-3, 1992. and in "Irradiation of 135 MeV/u carbon and neon beams for studies of radiation biology", HIMAC 004,p27,p28, 1993. should be corrected. The revised version of the LET dependence of the initial recombination will be described as follows. This paper is submitted to RIKEN accelerator report.

Initial Recombination in a Parallel Plate Ionization Chamber Exposed to Heavy-ion Beams

Tatsuaki Kanai, Michio Sudou, Shinichi Minohara, and Fumio Yatagai

We have installed an irradiation system at E5 room of the RIKEN Ring Cyclotron Facility for studies of radiation biology using heavy-ion beams. The biological and physical data are used to modify the heavy-ion beams for the heavy-ion radiation therapy.[1] In the biological studies and radiation therapies using heavy-ion beams, an accurate determination of the absorbed dose is essential. Dosimetry for the heavy-ion beams was described in a separate paper.[2] Fluence of the uniform irradiation field was measured by a plastic scintillator, and dose at the entrance position of the depth dose distribution was obtained by multiplication of the fluence by the stopping power of the heavy ions at the position. Then, the depth dose distribution was normalized by the dose at the entrance position. The depth dose distributions are usually measured by a parallel plate ionization chamber. As discussed in a previous paper,[2] initial recombination plays an important role in measuring the ionization current of an air-filled parallel plate ionization chamber. The ion collection efficiency in the parallel plate ionization chamber is not 100 % because of the initial recombination. The LET dependence of the ion collection efficiency was measured for several gases and differential W-values of the gases for the 135MeV/u carbon and neon ions were deduced.

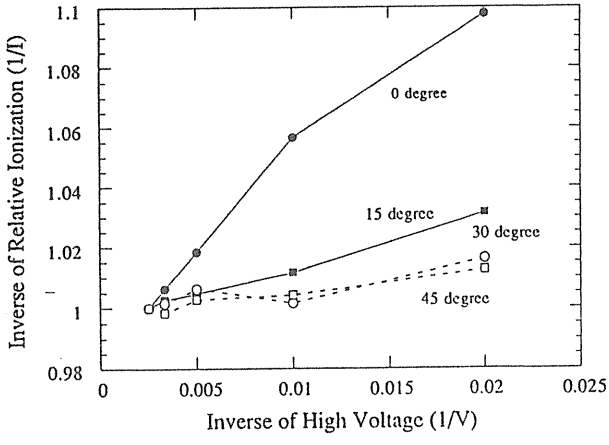

Fig. 1. Plots of the inverse of the ionization current against the inverse of the applied high voltage. Angle between the beam direction and the electric field was changed.

Two types of parallel plate ionization chamber were used for the measurements of the initial recombination. One has an entrance window of 2.5 μm thick aluminized polyester sheet and the other has an entrance window of 1 mm thick Lucite sheet. A signal electrode of 5 mm in diameter is surrounded by a guard ring that is against disturbance of electric field near the boundary of the signal electrode. A gap between the signal and the high voltage electrodes is 2 mm. Usual operating bias of the high voltage electrode is 400 V, which is 2000 V/cm electric field. The initial recombination of the parallel plate ionization chamber depends on an angle between the heavy-ion beam and the electric field of the chamber. The thin-window chamber was used for this angular dependence. Only air can be used as a gas of the cavity of the chamber. The gas in the thick-window chamber can be replaced. The recombination for several gases was measured by this thick-window chamber.

The chamber was irradiated by uniform heavy-ion beams at the irradiation site of the irradiation facility.[1] Ionization current was measured by an electrometer Keithley 617. The LETs of the heavy-ion beams were changed by changing absorber thickness of the irradiation facility.[1] Ionization currents of the parallel plate ionization chamber were measured by changing the voltage applied to the high voltage electrode. The inverses of the ionization current were plotted against the inverse of the applied high voltage. The data corresponding to $1/V < 0.01$, that is, $V > 100$, can be fitted by a straight line. Decrease of the ion collection efficiency at such a high electric field can be regarded as the decrease due to the initial recombination.

The differential W-values of air, nitrogen, argon, carbon dioxide, and tissue equivalent gas for 135MeV/u carbon and neon ions were measured by the same methods described in the previous report.[2] The ion currents were corrected by the recombination effect.

Figure 1 shows the angular dependence of the initial recombination. The slope in a region of $1/V < 0.01$ represents the initial recombination. When the beam was parallel to the electric field (0 degree in the figure), the slope was steepest. When the angle was over 30 degrees, the initial recombination could be neglected. Fig. 2 shows the results of LET dependence of the gradient of the slope at $V > 100$ for air. It can be said that the recombination depends only on the LET of the heavy-ion beams and increases roughly linearly with LET. The experimental data is now being analyzed using model calculation. For argon and nitrogen gases, the decreases of ion collection efficiency due to the initial recombination were not observed.

Table 1. summerizes the differential W-values of those gases for 135 MeV/u carbon and neon ions.

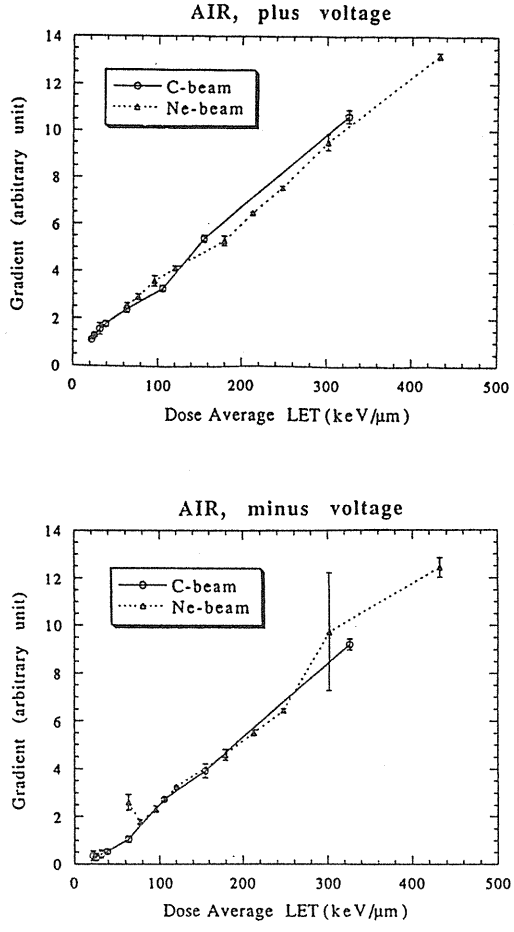

Fig. 2. Typical result of LET dependence of the slope of plots of the inverse of the ionization current against the inverse of the applied high voltage at V > 100. The upper and lower graphs show the results for ion and electron collection, respectively.

Table 1. Differential W-values for 135 MeV/u carbon and neon ions. The results in references [2) 3)] and [4)] are also written for comparison.

	C 135MeV/u	Ne 135 MeV/u	Photon/Electron[3)]
Air	33.5 eV	34.2 eV	33.85 eV
N_2	35.8 eV	36.6 eV	34.8 eV
Ar	23.6 eV	24.3 eV	23.8 ~ 26.4 eV
CO_2	21.4 eV	21.9 eV	33.0 eV
TEG	28.6 eV	29.3 eV	29.2 eV

	^{4}He 18.3 MeV/u[4)]
TEG	29.2 +/- 0.9 eV

	C 129.4 MeV/u	^{3}He 10.3 MeV/u	C 6.7 MeV/u [2)]
Air	33.7 +/- 0.9 eV	34.5 +/- 1.0 eV	36.5 eV +/- 1.0 eV

References

1) T.Kanai et al.: HIMAC report 004 (NIRS-M-91) NIRS publication, (1993).
2) T.Kanai et al.: Radiation Research ,135, 293-301(1993).
3) ICRU report 31 (International Commission on Radiation Units and Measurements, Washington), (1979).
4)T.Kanai and K.Kawachi: Radiation Research, 112, 426-435 (1987).

Effects of Object Size on a Function to Convert X-ray CT numbers into the Water Equivalent Path Length of Charged Particle Beam

S. Minohara, T. Kanai, M. Endo and K. Kawachi
Div. of Accelerator Research, National Institute of Radiological Sciences, Chiba, JAPAN

Introduction

The purpose of this study is to estimate the accuracy of X-ray CT method for determining the water equivalent path length of charged particle beam. For treatment planning of charged particle beams, a function to convert the CT number of X-ray CT image into water equivalent length is required. This function is used to calculate the dose distribution and to design the patient compensator. However, the CT number for a material varies with the method of imaging process of CT scanner, the object size and the degree of inhomogeneity. Such a variation of CT number decreases the accuracy of treatment planning. The converting function is experimentally determined by measurement for various materials. We report here effects of object size on converting function.

Method and Material

Table 1 shows the samples that we measured to determine the function to convert the X-ray CT number into water equivalent path length. The water equivalent length of proton beam (NIRS 70MeV/u) and carbon beam (RIKEN 135MeV/u) were measured by water column. The precision of water column is less than 0.05 mm. The Xray-CT(SHIMADZU CTS-10) data were taken in two cylindrical phantoms. One is 200 mm diameter and the other is 300 mm. Sample vials were symmetrically placed within the circumference. The sample vial is 20 mm diameter. The CT number of a sample is obtained by averaging CT numbers within 10 mm diameter of sample.

Result and Discussion

The difference in water equivalent path length between proton beam and carbon beam was less than 1%. The CT number measured at variable locations in a phantom had little difference.

Figure 1 shows calibration curves converting CT number to water equivalent path length. Linear curves are fit except the data of plastics (polypropylene, polyethylene, nylon, lucite, bakelite). Because these plastics aren't well analogous to human tissues that are characterized by a number of different atomic numbers and densities [1], [2]. The converting curve is divided into two regions. In each region, curves are shown linearly as follows,

Phantom of small size (200 mm)

$x<-43;\ y=1.035 + 1.065*10^{-3}x$

$x>-43;\ y=1.007 + 4.276*10^{-4}x$

Phantom of large size (300 mm)

$x<-49;\ y=1.05 + 1.075*10^{-3}x$

$x>-49;\ y=1.019 + 4.597*10^{-4x}$

where x ; CT number,

y ; water equivalent path length

In the region of low CT numbers, there are little difference in converting functions between the large phantom and the small phantom. However, in the region of high CT numbers, the water equivalent path length determined by 300 mm phantom was larger a few percentages than that determined by 200 mm phantom. The maximum difference of water equivalent length is about 6% for bone. This difference may not be ignored for the treatment planning of the region rich in bone. We must be careful about the field size of object and which calculation code we select to convert CT numbers.

References

[1] George T.Y Chen et al. ; Int. J. Oncol. Biol. Phys. 5, 1809-1819 (1979)

[2] A.A. Mustafa et al. ;Phys. Med. Biol. 28, 169-176 (1983)

Table 1. Materials used in investigating the relationship between CT number and water equivalent path length

Material		Physical density g/cm^3	Effective atomic number(*1) (calculated)	Relative electron density (calculated)	Water equivalent path length (measured) (*3) Carbon 135 MeV/u	Proton 70 MeV/u
Air		0.001	7.63	0.0009		
Lung equivalent (*2)		0.33	7.77	0.3169	0.312	0.313
Polypropylene(C_3H_6)n		0.91	5.44	0.9343	0.965	0.971
Polyethylene (C_2H_4)n		0.93	5.44	0.9549	0.990	0.993
Water H_2O		1.00	7.42	1.0000	1.000	1.000
Nylon ($C_6H_{11}NO$)n		1.16	6.13	1.1439	1.160	1.162
Lucite ($C_5H_8O_2$)		1.19	6.46	1.1511	1.162	1.165
Bakelite		1.34	6.18	1.2772	1.285	1.289
Bone equivalent (*2)		1.76	13.18	1.6361	1.570	1.556
Potassium phosphate K_2HPO_4 + H_2O	10%	1.079	9.04	1.0763	1.066	1.068
	20%	1.167	10.23	1.1515	1.137	1.138
	30%	1.265	11.20	1.2341	1.215	1.211
	40%	1.369	12.03	1.3206	1.300	1.293
Ethyl alcohol C_2H_5OH + H_2O	20%	0.947	7.23	0.9587	0.978	0.982
	40%	0.909	7.03	0.9233	0.958	0.957
	60%	0.867	6.81	0.8836	0.914	0.919
	80%	0.823	6.59	0.8415	0.874	0.877
	100%	0.781	6.35	0.8012	0.826	0.824

(*1) $Z=(\Sigma a_i . z_i^{2.94})^{1/2.94}$ a_i ; i-th elemental proportion by weight
(*2) Lung equivalent material (LP-430), Bone equivalent material (BE-103) ; Kyoto Kagaku Corp.
(*3) Carbon beam 135 MeV/u ; RIKEN ring-cyclotron, Proton beam 70 MeV/u ; NIRS cyclotron

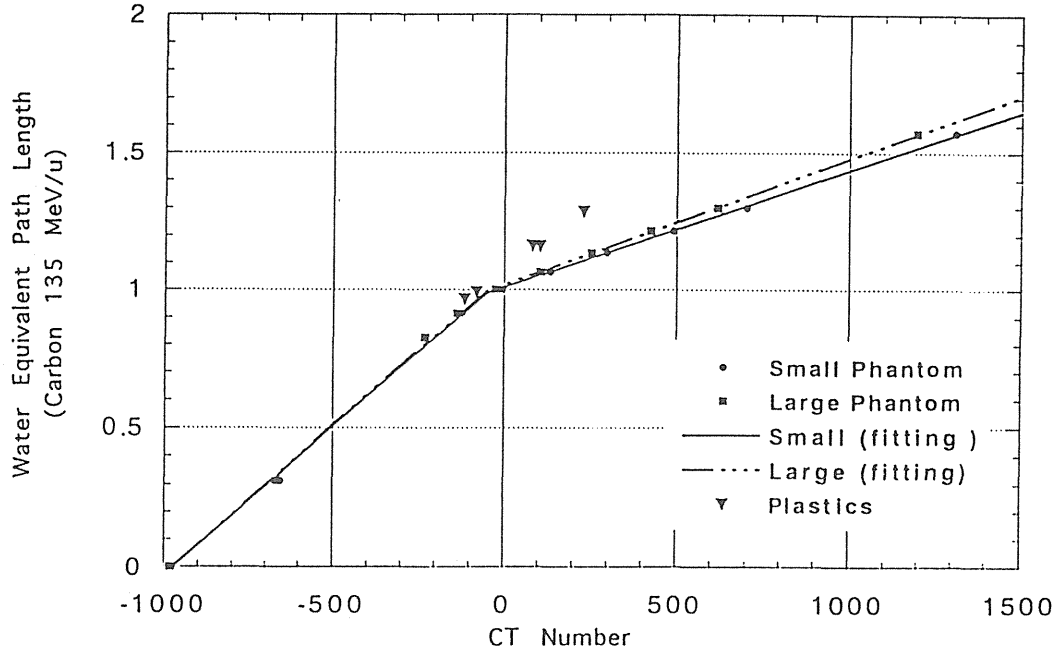

Fig.1 Calibration curves converting CT number to water equivalent pathe length

Secondary-electron Emission Monitor

Michio Sudou and Tatsuaki Kanai

National Institute of Radiological Sciences
4-9-1, Anagawa, Inage-Ku, Chiba-shi, Chiba 263, Japan

Abstract

Two sets of SEM of the same structure with different thickness of Al foils were tested by using 135 MeV/u heavy ion beams, C^{6+} and Ne^{10+}. The SEM in the HIMAC for other heavy ion beams of different energies is designed based on the output charge which can be estimated from this experimental result.

Introduction

Secondary-electron Emission Monitor (SEM) is popular as an intensity monitor in slow extracted beam lines of electron and proton accelerators. It has a unique characteristics of fast response, good linearity over many orders of magnitude and simple structure.

At NIRS, the particle radiotherapy is scheduled to start in 1994 with the heavy ion (He to Ar) beam of the energy from 100 MeV/u to 800 MeV/u. In order to use the high energy heavy ion beam to the radiotherapy, it is required to measure the fluence of the beam precisely to estimate the physical dose at the irradiation field. Such a requirement must be fulfilled even if the intensity of the beam extracted from HIMAC synchrotron is not ideally stable, especially when it has a steep spike structure.

We use a SEM as a dose monitor supplementary to the main dose monitor. For the main dose monitor we use a conventional parallel plate ionization chamber which shows a character of saturation arising from general recombination in case of an intense irradiation. Though a SEM has not such a character, it cannot supply an enough output current for the beam of low intensity. It is apparent that a SEM equipped with many electrodes can supply a large current output for the beam of low intensity. But it will result in the increase of material along the beam line and cause the deterioration of the beam quality. Therefore when a SEM is used as a dose monitor, it should satisfy two requirements ; it should have a wide range to measure the beam intensity, and the material on the beam line should be as little as possible. These requirements are mutually incompatible so that we must find a compromise in the design of SEM.

Although the SEM is used widely and the data on the efficiency (ε) for electron and proton beams are seen in the literature, reports on the high energy heavy ion beams covering the HIMAC region are few. They are only for light ions, p, d, and He^{2+}, and heavier ions in low energies of few MeV/u[1,2] and high energies of several GeV/u[3,4,5]. Therefore we constructed two sets of chamber of SEM and tested them with C^{6+} and Ne^{10+} beams of 135 MeV/u at RIKEN. The point of view in the test was to study the dependencies of the efficiency ε on the variation of the following quantities;

- the beam energy
- atomic number of the beam
- foil thickness of SEM
- high voltage of SEM
- gas pressure of SEM

Here the definition of the efficiency ε of SEM is given as follows;

$$\varepsilon = \frac{Q/(1.602 \times 10^{-19})}{(\text{no. of projectiles})} \qquad (1)$$

where Q is the charge measured in the SEM. This charge Q is the total current output from the SEM. For the comparison between the SEMs with different number of foils, the efficiency normalized by the number of surfaces of electrodes of SEM, ε/(surface), is later used in this paper.

Construction of test chambers

Two sets of test chamber of SEM were constructed at NIRS, which are shown in Figures 1 and 2. They have the same structure but have different thickness of foils ; one has 7 μm thick foils and another has 15 μm thick foils. The material of the foil is aluminum. The number of the foil is eleven for both sets, which corresponds to twenty as the number of surfaces of electrodes. At the operation the five foils were connected together and used as a collector electrode, and the other six foils were connected together and used as a potential electrode. The gap distance between neighboring foils are 8 mm. The effective area of the chamber is about ϕ20 mm.

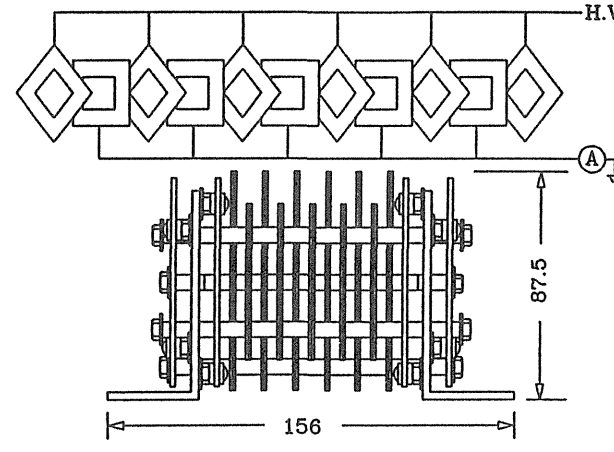

Fig. 1: The test chamber of SEM ; schematic (upper) and design (lower) illustrations.

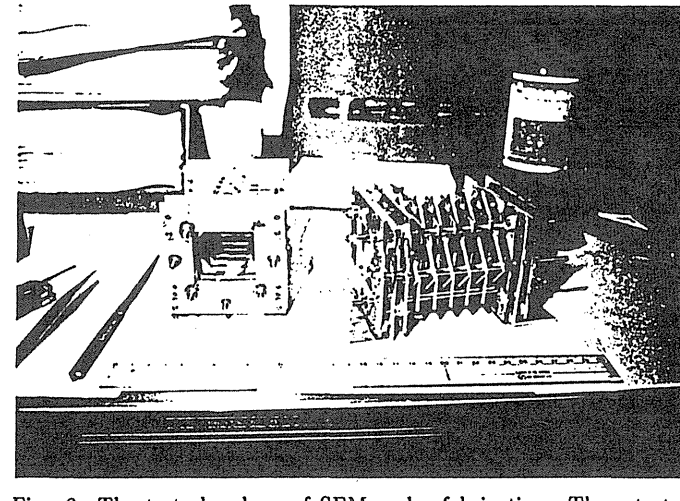

Fig. 2: The test chambers of SEM under fabrication. These test chambers are not equipped with aluminum foils.

Experimental Set Up

The test chambers of SEM were installed in a large scattering chamber in the E5B course of RIKEN Ring Cyclotron. Figure 3 shows a schematic diagram of the experimental set up. Figure 4 shows the scattering chamber and the test chambers of SEM. The operating pressure in the chamber was in the range of $4 \sim 8 \times 10^{-7}$ Torr throughout the experiment. The beam fluence was monitored by the beam monitor placed at the end of the course, which is a parallel plate ionization chamber. The output of the monitor was transformed by I/F converter with conversion efficiency of 102.4 pC/pulse and then counted by a scaler. The beam size was about $\phi 9 \sim 11$ mm at the places of SEMs. The output charge of a SEM was measured by an electrometer (Keithley 617). High voltage was fed to SEMs by a high voltage power supply (Ortec 665), and it was monitored by a multimeter (Sanwa FD-750C). The electrometer was connected to one of the two SEMs while the other was terminated with 50Ω. The beam intensity was kept almost the same at 10^8 pps for C^{6+} and Ne^{10+} beams.

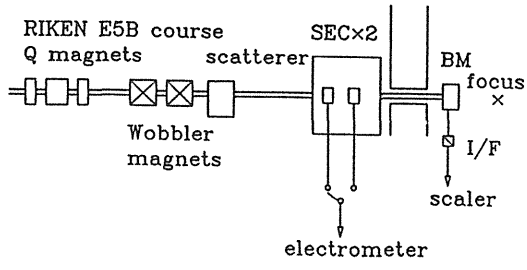

Fig. 3: The schematical diagram of the experimental set up.

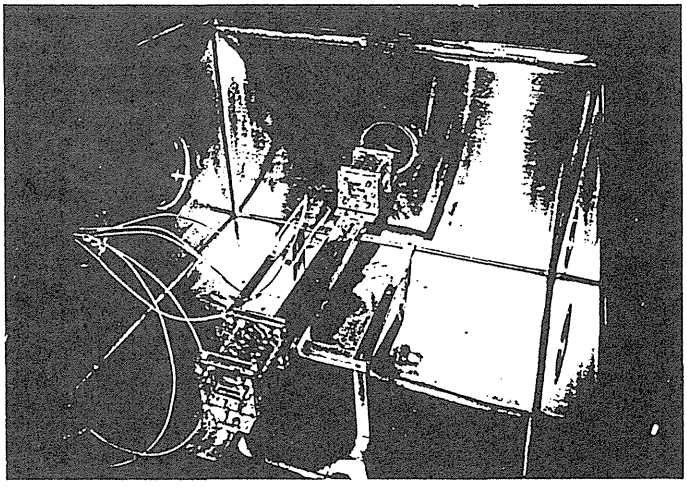

Fig. 4: The over view of the test chambers in the large scattering chamber in the E5B course of RIKEN Ring Cyclrotron.

Results

Figure 5 (a) and (b) shows the results of ε for the beams of 135 MeV/u C^{6+} and Ne^{10+}, respectively. Some characteristics are seen as follows ;

- ε makes peaks at about ± 20 V.
- ε changes abruptly between about -20V and +20V.
- ε changes rather slowly at the region higher and lower than about ± 100V.
- ε's of the aluminum foils of the thickness of 7 μm and 15 μm are almost the same.

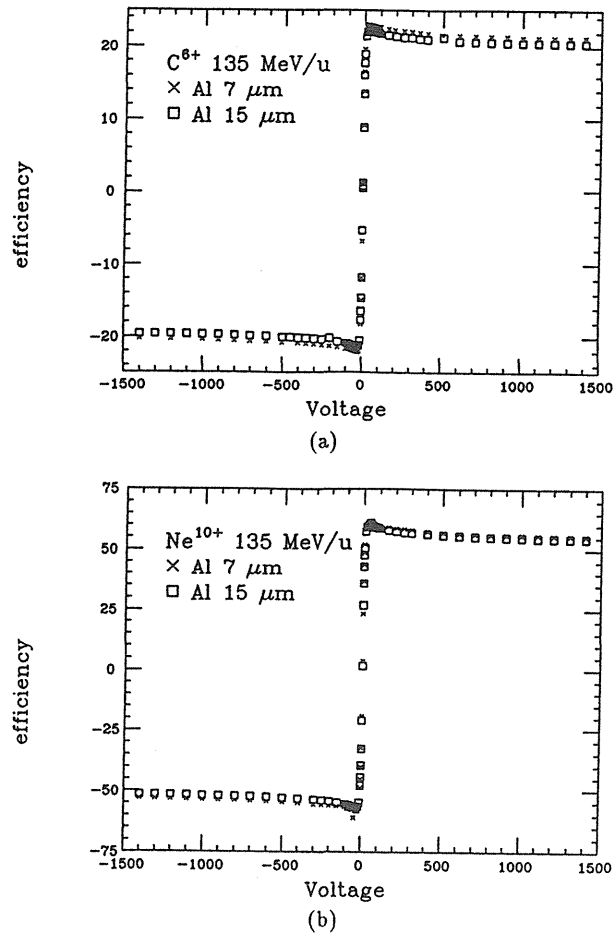

Fig. 5: The results of the efficiency ε of SEM for C^{6+} (a) and Ne^{10+} (b) beams of energy 135 MeV/u. Error bars are not shown which are lower than 3.2 %.

The ε's of the SEMs per surface of foil are tabulated in Table 1, which also gives the ratio ε/(surface)/STP, the efficiency per Stopping Power (STP) (keV/μm) of aluminum for the projectile. The ε/(surface)/STP in Table 1 were 0.023 ± 0.001 for the cases of the different thicknesses of the foils and different ions of the beam. The data shows that the yield of secondary electrons per number of surface is proportional to the energy loss of the beam in the material. If we assume that a certain part of the energy loss of any projectile in the foil are converted to produce the secondary electrons and their kinetic energies, we can estimate the ε/(surface)/STP for other projectiles with other energies, and also the output charge Q from SEM. Figure 6 the data of ε/(surface)/STP of several ions including protons and other heavy ions, where the ε/(surface)/STP data are plotted according to the atomic number of the ion ignoring the energy of the ion. A constant characteristics of ε/(surface)/STP in the ions except for proton and Argon can be seen, which supports our assumption.

Table 1: SEM efficiency at H.V.=+1400V

projectiles	thickness of Al	ε/(surface)	ε/(surface)/STP
C^{6+}	7 μm	1.1	0.024
	14 μm	1.0	0.023
Ne^{10+}	7 μm	2.8	0.023
	14 μm	2.7	0.022

Figure 7 shows the variation of of ε/(surface) for several ions and energies. The curves were drawn according to the values given by ε/(surface)/STP(= 0.023)×STP, where stopping powers (STP) were

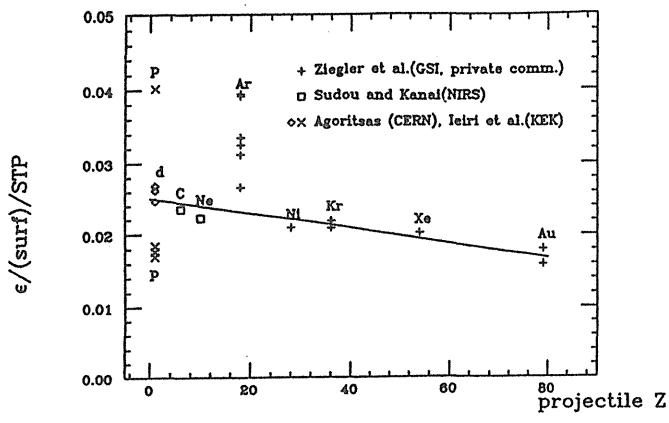

Fig. 6: ε/(surface)/STP for several ions. The data □'s are from this experiment. The data ×'s are those for protons of CERN[3] and KEK[5], the data ◇'s are those for deuterons of KEK[5], and the data +'s are those for several ions of GSI[4]. A line is drawn by the straight-line fit for the data excluding protons and Argons.

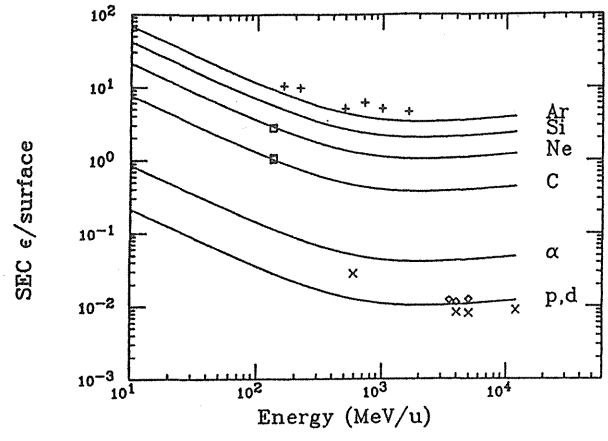

Fig. 7: ε/(surface) for several ions. The symbols are in the same definition of the figure 4, while the data of +'s include only Argon ions.

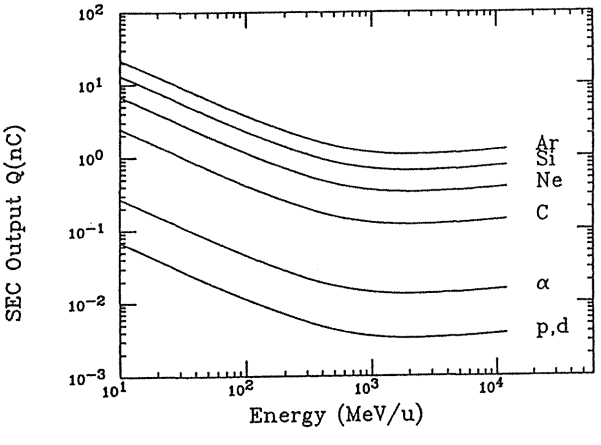

Fig. 8: The expected output charge Q of SEM for 10^8 projectiles.

calculated on the formula of Bethe[7]. We can estimate the output charge Q by using three parameters; the value of ε/(surface), the number of surfaces of SEM and the beam fluence. Our estimation of ε/(surface) for proton underestimates for the data of CERN[3] at 591 MeV, and overestimates for the data of KEK[5] at several GeV. The under- and over-estimations are also seen in the deuteron and Ar data. It suggests some dependence of ε on atomic number and/or energy, or some dependence on the surface condition of the foil.

Figure 8 shows such estimated output charges Q of our test chamber of SEM for the beam fluence of 10^8 particles. The number of 10^8 particles will be a typical value of beam intensity in the radiotherapy. It is seen that the SEM can produce measurable output charge by the fluence of 10^8 beam particles in the HIMAC.

We did not examine the dependence of ε on the gas pressure. The pressure changed from 8 to 4×10^{-7} Torr during this experiment.

The value of ε corresponds to an integral over the energy of the secondary electron. If we differentiate the ε with H.V. , we can yield an energy spectrum of the secondary electron. Figures 9 (a) and (b) show such energy spectra where the data of figure 3 were differentiated assuming the angular distribution[5] of a cosine dependence. It shows that the secondary electrons consist of large amount of slow electrons, lower than 10 eV, and the other faster electrons are few. Figures 10 (a) and (b) show those spectra of figure 9 in double logarithmic scale. We can see an inverse proportionality in the spectra, which can be a characteristic feature of the secondary electrons. We deduced the energy spectra assuming an isotropic shape on the angular distribution, which resulted in almost the same as above case. Similar result is also seen in the reference of Oda and Lyman[2].

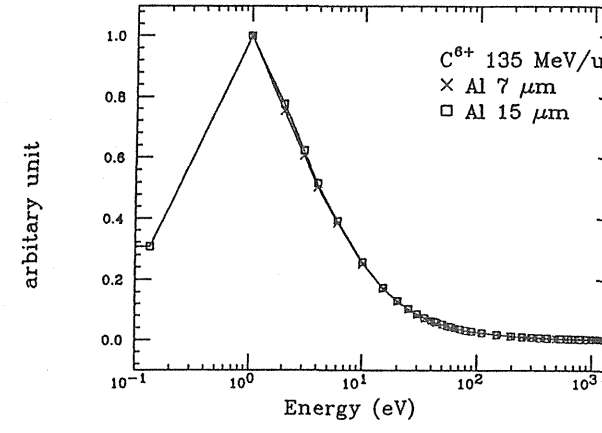

(a)

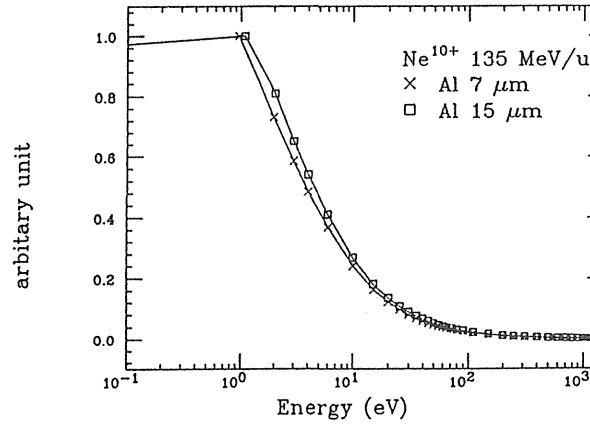

(b)

Fig. 9: The energy spectrum of the secondary electrons.

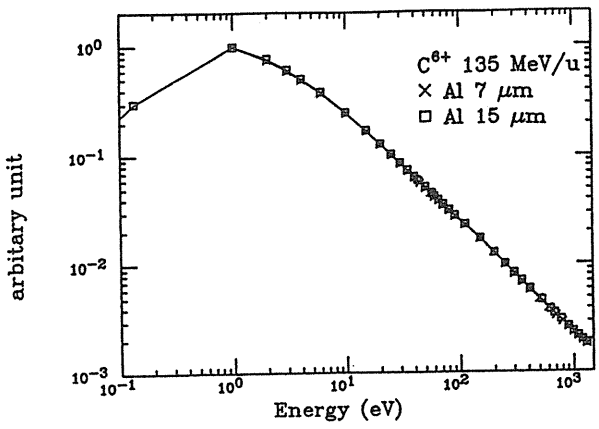

(a)

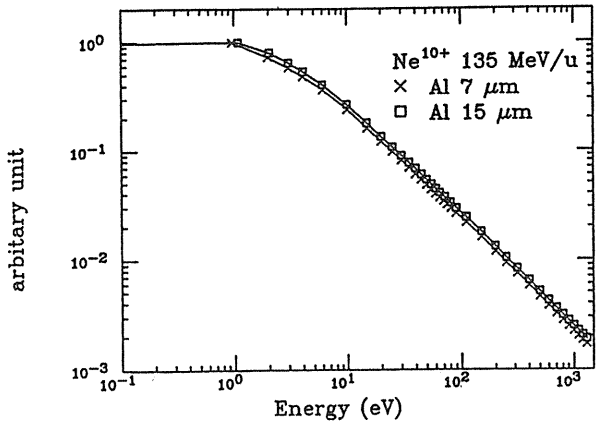

(b)

Fig. 10: The energy spectrum of the secondary electrons in double logarithmic scale.

Conclusion

We measured the efficiency of SEM equipped with 7 μm and 15 μm thickness of aluminum foil with C^{6+} and Ne^{10+} of energy 135 MeV/u. We assumed the efficiency ε of SEM depends on the stopping power of the projectile. On the assumption we estimated the ε/(surface) and the output charge Q of SEM for different projectiles and different energies. Energy spectra of the secondary electron was deduced from the data of the efficiency of SEM. It showed a characteristic feature of an inverse proportionality of the secondary electron. The under- and over-estimation of ε/(surface) for proton data shows a need for further study on the atomic number and/or energy dependence of ε or some dependence of the surface condition of the foil.

Design of SEM for HIMAC

The SEM for HIMAC as a dose monitor has been designed considering the stopping power dependence of output charge from the SEM. It was confirmed that there would be an enough output charge from the SEM to measure the dose of the beam for the radiotherapy. The main features of the SEM are as follows;

- SEM includes 6 collector electrodes and 7 potential electrodes.
- All electrodes are made of 7 μm thick aluminum foils.
- SEM has a wide sensitive area of ϕ166 mm.
- Electrodes are contained in a vacuum chamber electrically isolated.
- SEM should have a clean inside vacuum kept by an ion pump.

The SEM will be set between the main dose monitor and the flatness filter in the therapy room. It will be controlled by the irradiation control computer of the irradiation system. The SEM is now under fabrication and will be installed in September, 1993.

Acknowledgement

We wish to thank the staffs of RIKEN Ring Cyclotron for the helpful operation. The authors thank Dr.Yamanoi of KEK for discussions. The authors also thank Dr.Tomitani of NIRS and Nihon Seihaku Corp. for the precious materials supplied.

References

(1) R.Anne et al., IEEE Trans.Nucl.Sci.NS-24(1977)1754
(2) N.Oda and J.T. Lyman, Rad.Res.Suppl.7(1967)20
(3) V.Agoritsas, MPS/Int.CO 66-30
(4) C.Ziegler et al., GSI Scientific Report 1990,p291 and private communication
(5) M.Ieiri et al., Proc. of the 9th Symp. on Acc. Sci. and Tech., Tsukuba, Japan 1993,p477
(6) A.A.Schultz and M.A.Pomerantz, Phys.Rev.130(1963)2135
(7) Review of Particle Properties, Phys.Rev.D45(1992)II.14

Silicon Diodes as Detectors in Relative Dosimetry of Heavy Ions

Akifumi Fukumura[1)], Kazuo Hoshino[1)], Mitsue Takeshita[1)],
Tatsuaki Kanai[2)], Shinichi Minohara[2)] and Michio Sudou[2)]

[1)]Division of Physics and [2)]Division of Accelerator Research
National Institute of Radiological Sciences
9-1, Anagawa-4-chome, Inage-ku, Chiba-shi, 263, Japan

P-type silicon diodes are regarded as candidate detectors for in-vivo relative dosimetry for several reasons as follows[1]; (1) They have high spatial resolution because of miniature size. (2) They can be made water-proof. (3) They are operated with zero bias voltage. (4) They can be used in real-time measurements. (5) They are mechanically stable. These advantages would seem to make them quite useful for measuring steep Bragg Curves of heavy ions. They are, however, known to suffer from radiation damage. Before use as detectors in relative dosimetry of heavy ions, we should determine the characteristics of diodes.

We exposed p-type silicon diodes (commercially available from SCANDITRONICS AB) to 135 MeV/u C and Ne beams at the Bio-physics port[2] in RIKEN Ring Cyclotron facility. In front of the diodes we placed a water column of variable length to measure the Bragg Curves. The effects of radiation damage were investigated at both shallow and peak positions. Figure 1 shows the responses of diodes as a function of accumulated dose at the shallow position. The drop in relative sensitivity was only approximate one percent during irradiation up to 100 Gy in water. It was several percent even at the Bragg Peak region where the accelerated ions were stopped in the silicon diodes. These results mean that the effects of radiation damage are not too serious to prevent application of p-type silicon diodes to measurements of heavy ions. Figure 2 shows the sensitivity dependence of the diode on dose rate. It illustrates constant sensitivity for a range of therapeutic

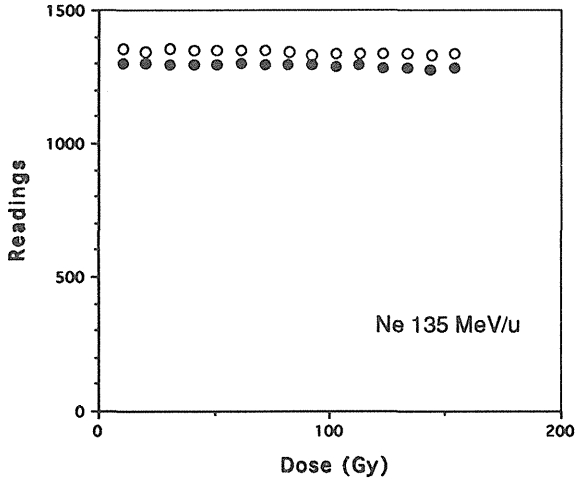

Fig. 1 The responses of the two diodes as a function of accumulated dose at shallow position for Ne beam.

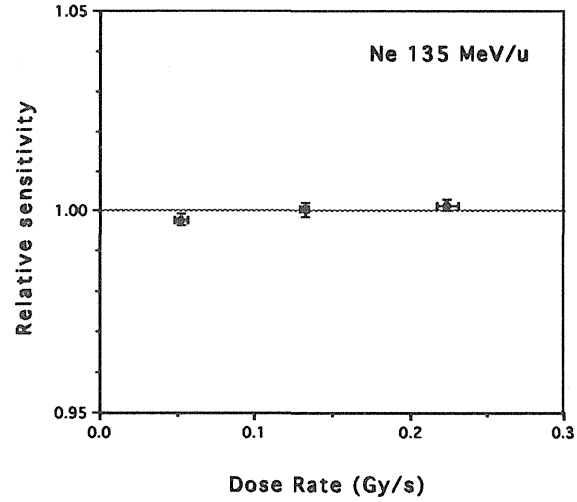

Fig. 2 The relative sensitivity of the diode as a fuction of dose rate for Ne beam.

dose rate. The reproducibility of the response had only about 0.2% in relative standard deviation for irradiation of the order of 1 Gy. Figure 3 shows sensitivity dependence on angle between axes of beam and of diode. We can easily find independence from angles up to 60 degrees at both shallow and peak positions. These results make it possible to apply the diodes as detectors in relative dosimetry of heavy ions.

Then we used these diodes to measure the depth dose curves as functions of depths in water for 135MeV/u C and Ne beams. Figure 4 shows results obtained with the diode and the parallel plate ionization chamber, which is operated with 400V and filled with air at atomospheric pressure. It also shows calculations based on the formulation by Litton et al.[3] for comparison. To deduce depth dose curves from relative ionization curves we assumed that differential W value was independent on the energy of ion beams. On this assumption we have regarded the relative ionization curves measured by the chamber as the depth-dose curves since we can neglect the dependence of the stopping power ratio between air and water upon energy above a few MeV/u. On the other hand, for the silicon diode we have made correction due to the energy dependence of that between silicon and water. In Fig.4 we can easily find the good agreements. This means there is a good possibility for p-type silicon diodes to be used as detectors in relative dosimetry of heavy ions. Beholding the vicinity of the peaks, we notice that there are slight disagreements. The calculations did not take into account momentum spread of the incident beams and dose contribution of fragments. That is the reason why Bragg peak is higher and narrower without tail in the calculation. The peaks measured by the diode are higher than that by the chamber for both beams. These results suggest that w-values of air increase as the energies of ions decrease and/or that there is a recombination of ion pairs around the peak region.

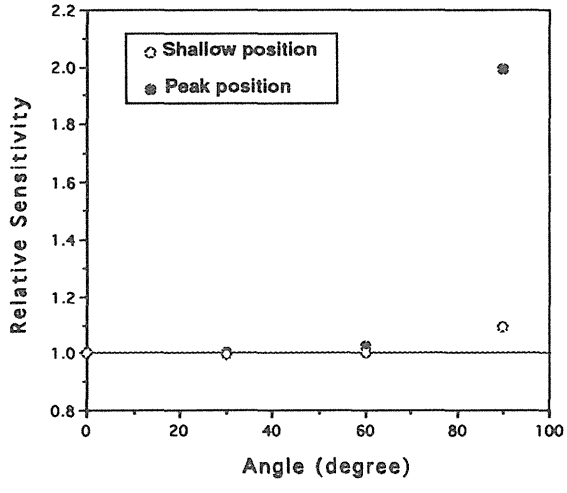

Fig.3 The relative sensitivity as a function of the angle between axes of Ne beam and of diode.

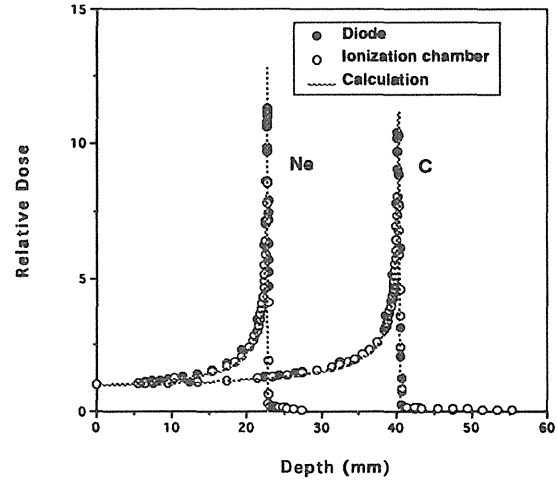

Fig.4 The depth dose distributions for 135 MeV/u Ne and C beams.

References

[1] G. Rikner, Doctoral thesis, Uppsala Univ. 1983

[2] T. Kanai et al., NIRS-M-91, HIMAC-004, NIRS Chiba, 1993

[3] G. M. Litton et al., UCRL-Report 17392, LBL Berkeley, 1968

Beam End Point Measurement with Positron Emitting Secondary Beams

T. Tomitani†, M. Kanazawa*, M. Sudo*, H. Soga*, T. Kanai*,
Y. Sato*, M. Inabe^, A. Yoshida# and Y. Watanabe#

Division of Physics† and Division of Accelerator Research*
National Institute of Radiological Sciences
9-1, Anagawa-4-Chome, Inage-Ku, Chiba-Shi, 263 Japan
and
Cyclotron Laboratory^ and Radiation Laboratory#
The Institute of Physical and Chemical Research (RIKEN)
2-1, Hirosawa, Wako-shi, 351-01, Japan

Abstract

Results of preliminary experiments on the measurements of end point distribution with positron emitting radioactive secondary beams along with a positron emission tomography are presented. Images of a test pattern engraved with two sets of characters of 2 mm line width could be reconstructed and the results are consistent with what were expected from the knowledge of range of the beam and characteristics of PET device. For imaging purpose, experiments indicate the importance of beam intensity correction.

Introduction

The accuracy of dose distribution in heavy ion therapy strongly depends on the range estimation of projectile ions in the target medium, which is a function of the electron density of the medium. Heavy ion range is estimated from the measured CT number by looking up a measured conversion table. Since CT number is a complex function of electron density and Z-number, there are some ambiguities in the conversion and some sorts of experimental checking means are needed. One approach is to measure auto-activity inside the object, which results from fragmentation reaction of primary beams and target nuclides.[1] This method essentially relies on the measurement of the end point of β^+ emitting fragments and is limited by the dose delivered by the primary beams, since yield of β^+ emitting fragments is a fraction of %. Dose limitation can be overcome by using β^+ emitting beams, provided that the intensity of β^+ emitting projectiles is ample enough. With the latter approach, dose can be reduced by at least two order. End point distribution can be measured by positron emission tomography(PET). Radioactive ion beams of wide range of nuclear species are available from the ring cyclotron at the Institute of Physical and Chemical Research. Preliminary experiments on the measurement of end point distribution of β^+ emitting beams were carried out with a small high resolution PET developed for animal studies. Some preliminary results are presented.

Radioactive Ion Beam

Radioactive ion beam facility at RIKEN was reported in ref. [2]. For preliminary experiments, ^{11}C beam was used whose half life is 20.34 min. and is appropriate for the present experiments. Beam yield is about 10^7 and is ample enough for the present experiments. Beam contaminants were measured with a spectrometer consisting of a ΔE counter and a time-of-flight telescope. Major contaminants were ^{9}Be and ^{12}C and are harmless to the experiments, since they are stable isotopes. Measured intensity of the contaminants is a few % of that of ^{11}C. Beam energy was measured with a range telescope. Beam profile was measured with a parallel plate avalanche counter(PPAC). During the experiments, beam intensity was monitored with a parallel plate ionization chamber calibrated with a PPAC by particle counting.

Experimental Setup

PET device consists of 128 Bismuth Germanate crystals of 4 mm wide by 10 mm high by 20 mm deep along with 64 gridded photomultipliers of 12.7mm square[3]. Measured spatial resolution inside the tomographic plane is 3 mm full width at half maximum (fwhm) at the center of the field of view tending to deteriorate towards the periphery and that along axial direction is 2.5 mm fwhm. Calculated system detection efficiency is about 0.5 %. Experimental setup is shown in fig. 1.

Polymethylmetacrylate ($C_6H_8O_5$, Lucite) block was used as a target material. Since PET consists of a single ring, scanning motion is needed to measure three-dimensional distribution of ^{11}C. To this end, target sample was moved rather than PET was displaced. The sample was driven by a ball screw system and a pulse motor controlled remotely by a micro-computer through GPIB coupled with optical fibers.

Lucite sample was engraved with two sets of characters, i.e., 'RIPS' and 'NIRS.' Character line width was set to 2 mm which is comparable to spatial resolution of PET and the depths of the character sets were set to 4 mm and 5 mm, respectively. Lucite sample is shown schematically in fig. 2.

Corrections

Detection efficiency of each detector pair of PET varies due to variation among crystals, energy threshold level, etc. Means to measure detector response was built in to the PET system. The response was measured with a ^{68}Ge-^{68}Ga source external to the object. Measured projection data are attenuated by self-absorption inside the object. Attenuation factors were measured in the same way except that the object

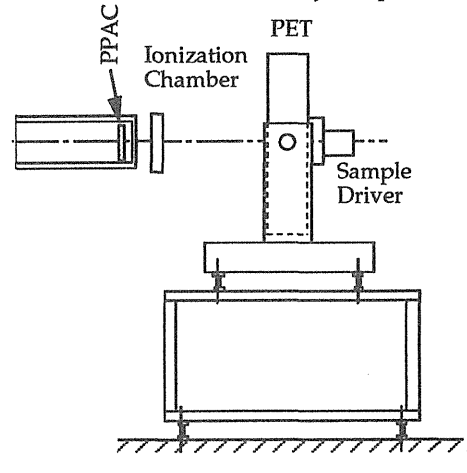

Fig. 1. Schematic drawing of experimental setup, where PET and PPAC indicate positron emission tomography and parallel plate avalanche counter, respectively.

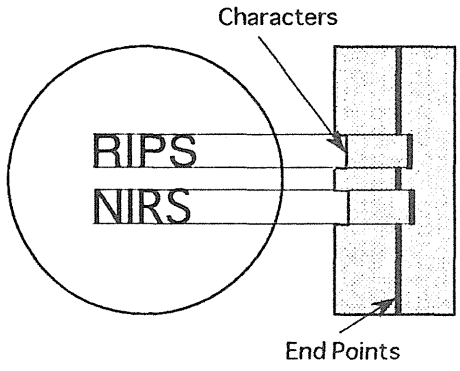

Fig. 2. Depth resolution test pattern made of Lucite engraved with two sets of characters.

was set in place. Measured attenuation factor was fitted to an analytical curve to reduce the effect of noise in the measured attenuation factors and the latter was used for correction.

To cover the pattern shown in fig. 2, RIPS secondary beam was broadened to 6 cm dia. by defocusing, however, beam was not uniform. Beam profile was measured directly with a PPAC and indirectly with PET with a flat disk target. The latter result is shown on the left hand side of fig. 3.

Results

One typical reconstructed ^{11}C distribution is shown on the right hand side of fig. 3, which was corrected for detector response and self-attenuation but not for beam non-uniformity. One can see the effect of beam non-uniformity. The ^{11}C distributions corrected for beam profile are shown in fig. 4. Since beam intensity at periphery of the field of view is weak, noise in the reconstructed image is enlarged enormously, hence images inside the region of 6 cm diameter are only shown.

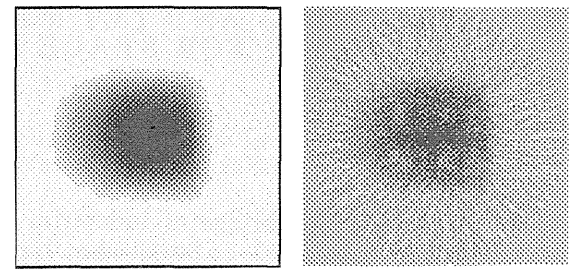

Fig. 3. Left: beam profile measured with a flat disk target and PET. Right: one example of ^{11}C end point distribution (not corrected for beam uniformity).

Discussions

End point distributions of ^{11}C were imaged successfully. Spatial resolution of end point measurement is limited to 3 mm cube due to that of PET. If we restrict ourselves to the determination of end point surface, then statistical estimation may be applied and precision of position resolution in depth direction could be improved, but this approach is left for future study.

References

1. T. Tomitani, M. Sudo, S. Minohara, T. Kohno, E. Takada, and T. Kanai: "Feasibility Study on the Application of Auto Activation of Heavy Ions to the Monitoring of the Dose Distribution," Proceedings of ICRO'93, O37-7, 1993.

2. T. Kubo, M. Ishihara, N. Inabe, H. Kumagai, I. Tanihata, K. Yoshida, T. Nakamura, H. Okuno, S. Shimoura and K.. Asahi: "The RIKEN radioactive beam facility," NIM B70:309-319, 1992.

3. T. Tomitani, N. Nohara, H. Murayama, M. Yamamoto and E. Tanaka: "Development of a High Resolution Positron CT for Animal Studies," IEEE Trans. on Nucl. Sci., NS-32:822-825, 1985.

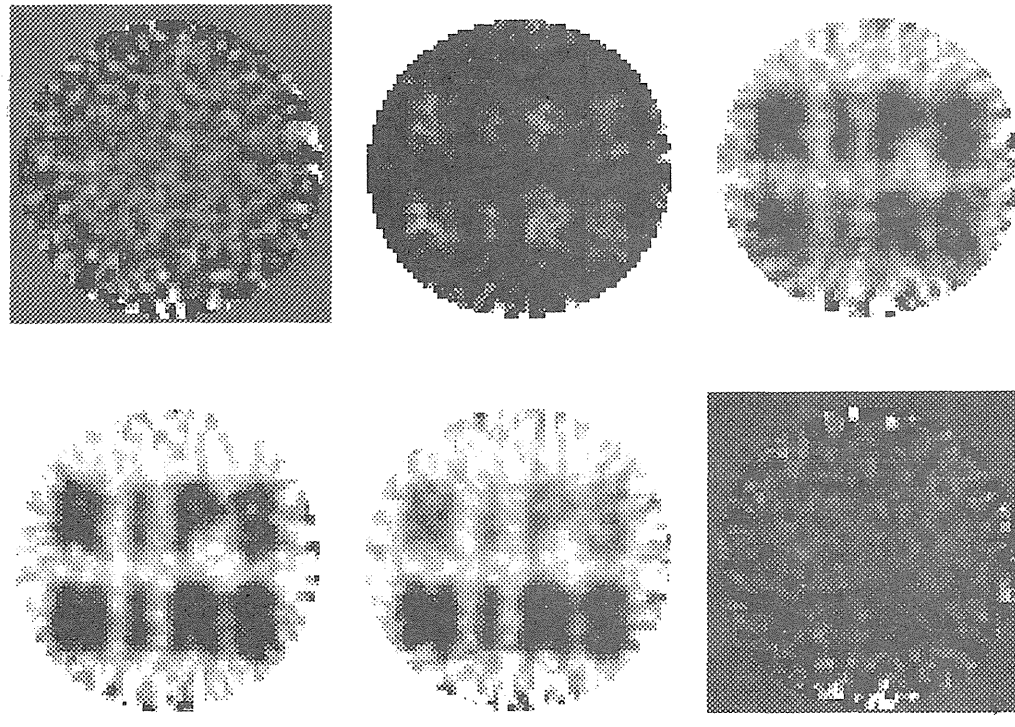

Fig. 4. Distribution of ^{11}C at various depths from the surface of Lucite block.
Upper left: 16 mm,
upper center: 21 mm,
upper right: 24 mm,
lower left: 25 mm,
lower center: 26 mm,
lower right 29 mm,
respectively. Character line width is 2 mm and character height is 14 mm.

TRACKING AND LET MEASUREMENTS OF COSMIC RAY NUCLEI FOR SPACE RADIOBIOLOGICAL STUDIES

K. Ogura[1], T. Doke[2], T.Hayashi[2], T. Kojima[1], M. Matsushima[1], S. Nagaoka[4], K. Nakano[3], T. Takahashi[3], H. Yamada[1] and F. Yatagai[3]

1.College of Industrial Technology, Nihon University
1-2-1, Izumi-cho, Narashino, Chiba 275, Japan
2.Science and Engineering Research Laboratory, Waseda University
17, Kikui-cho, Shinjuku, Tokyo 162, Japan
3.The Institute of Physical and Chemical Research (RIKEN)
2-1, Hirosawa, Wako, Saitama 350-01, Japan
4.National Space Development Agency of Japan (NASDA)
2-4-1, Hamamatsu-cho, Minato, Tokyo 105, Japan

ABSTRACT

During the IML-1 and FMPT Space Shuttle missions in 1992, CR-39 detectors were exposed to the cosmic radiation for space radiobiological studies. The precise determination of the distance between the center of the particle trajectory and the individual biological objects around it was performed by referring to the laser grid marks which were printed on the surface of CR-39 detector. We describe such an experimental method and results. Integral LET-spectra and absorbed doses of cosmic ray nuclei with LET above 4 keV/μm are also reported.

INTRODUCTION

In the complex radiation field in space, the so-called HZE (high Z and high energy) particles are of special concern to the space radiobiological studies. Since a single HZE particle produces a highly localized damage of temporal concentration of energy deposition along particle's trajectory, it may cause severe effects to living cells. So far, a number of experiments on the biological response to cosmic HZE particles was carried out on board U.S. or U.S.S.R. space missions. These are well summarized in a recent review paper[1]. Plastic nuclear track detectors are commonly used for the dosimetries of cosmic ray nuclei for such a space radiobiological study.

During the First International Microgravity Laboratory (IML-1) and the First Material Processing Test (FMPT) mission in 1992, Japanese Radiation Monitoring Container & Dosimeters (RMCD) accommodating biological samples and CR-39 track detectors were exposed to cosmic radiations for about 7 days each, while the space shuttle Discovery and Endeavour stayed in the orbits at about 300 km altitude with the inclination of 57° , respectively. After the mission, particle tracks in CR-39 detectors were investigated and traced through the detector stacks. Then the intersection points of the particles' trajectories through the biological layers in the stack were estimated. Absorbed dose rates and dose-equivalent rates inside of the RMCD were also estimated by using the measured LET-spectra of cosmic ray nuclei recorded on CR-39 detectors.

TRACKING RESULTS OF HZE PARTICLES

CR-39 plates doped with 0.01% of antioxidant, Naugard 445, were manufactured by Fukuvi Chemical Industry Co., Ltd., and have a size of 100 × 100 mm^2 and 1 mm in thickness. For the laser marking after the space mission, CR-39 plates, C-3 and C-4 in Fig. 1, were dyed brown beforehand to be opaque to 355 nm of UV, the third harmonics of a YAG laser. *B. subtilis* spores were fixed with a 5% poly-vinyl alcohol solution in five specific areas of C-3 and C-4 plates. After the fixing of spores, these plates were sandwiched between the other four CR-39 plates, C-1, C-2, C-5 and C-6, and assembled into a stack, then nine holes were drilled through the stack as shown in Fig.1. Five holes were provided as a reference of the coordinates among the detector plates.

After the mission, the stack was disassembled and the CR-39 detectors both above and below the biological layers were etched in 7N-NaOH solution at 70℃ for 37 hrs. For the HZE particle track we determined the geometrical parameters of the etch cone opening of the surface of detector, i.e. the center of coordinates, minor and major axes, d and D, and azimuthal orientation of the major axis, ϕ, by using video image processing. The incidence zenith angle of the particle, θ, is also given by

$$\cos\theta = (4B^2+d^2)[16B^2D^2+(4B^2- d^2)^2]^{-1/2},$$

where B was measured in advance and is the thickness of etched layer from the single surface of the detector. In this manner detection and localization of HZE particle tracks of the individual detectors (C-1, C-2, C-5 and C-6 in Fig. 1) were carried out and the 3-dimensional reconstruction of individual particle trajectories was done as described in detail elsewhere[2]. By using the fitted or extrapolated straight line being representative of particle trajectory, now it is possible to estimate the points of passage of the individual particles through the surfaces of detectors, C-3 and C-4, onto which spores were fixed.

By using a UV laser beam of several tens of μJ per pulse, reference grid marks covering an area of 1 ~ 2 mm^2 around the estimated coordinates of intersection points of the individual particles' trajectories were printed on the surface of C-3 and C-4 detectors, on which spores have been fixing. Laser marks were printed at a rate of 10 dots per 100 μm and single dot was about 2 μm in diameter. After the laser marking, microphotographs were taken in order to confirm the positions of spores in relation to the reference grid marks, and then the spores were covered with a nutrient agar film. Photographs of same sections of the detector were taken again to check the outgrowth of the spores at different steps of the incubation at 37℃ for about 15 hours (Fig.2 a). After removal of the spores from the detectors, CR-39 detectors were etched lightly in 10-N KOH solution at 90℃ for 15 ~ 40 minutes, thereby the etch pits of high LET particles were revealed but the laser marks did not so enlarged. Then photographs of the tracks were taken to determine the positions of etch pits in relation to the laser marks as shown in Fig.2 (b).

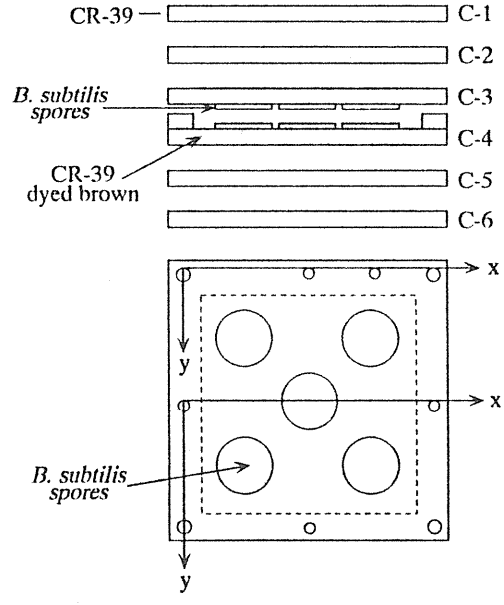

Fig.1. Schematic diagram of a stack for space flight experiment and the relations between the reference holes and detector-coordinates.

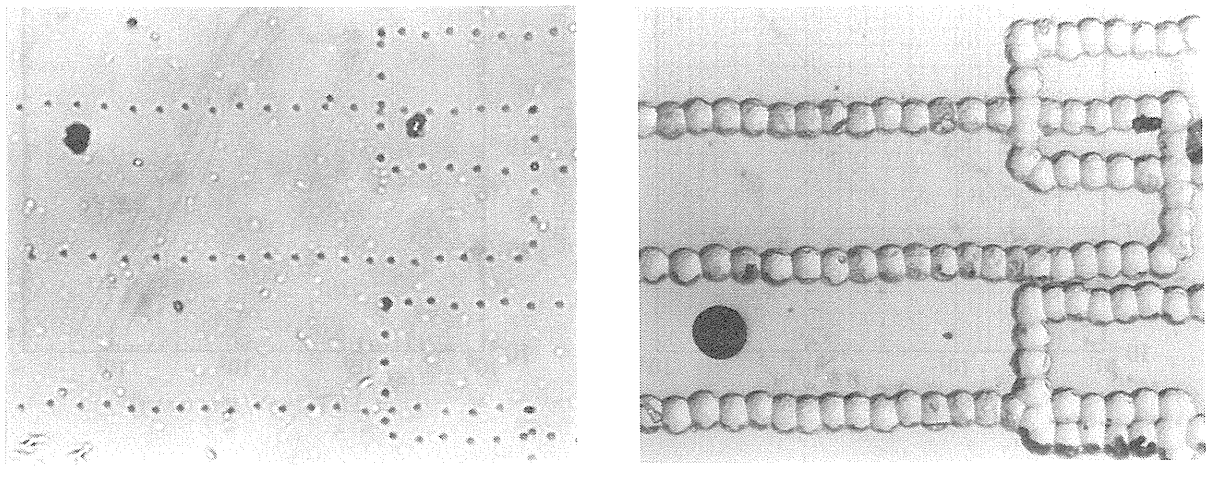

(a) (b)

Fig. 2. (a) Laser marks (dark dots) and *B.subtilis* spores (light spots) fixed on the CR-39 detector.
(b) Laser marks and an etch pit of HZE particle.

For measuring the impact parameters, i.e. the distance between the center of the particle trajectory and spores around it, only the necessary sections of the photographs were specially enlarged further. By referring to the laser grid marks, the impact parameters were investigated with its enlarged pictures of an object magnified to a scale of more than 1000 times the natural size. This can be determined the impact parameter with an accuracy better than 0.5 μm and occasionally read to 0.2 μm[3].

In the stacks consisted of the track detectors, it is generally impossible to determine the trajectories of HZE cosmic particles with an accuracy better than 1 μm due to the following causes: 1) the non-uniformity in the thickness of an individual detector plate, 2) an inevitable bending and/or distortion of the plate during the fabrication of the stacks, and 3) an irreversible swelling of the plate during the etching. We have developed the method to determine the impact parameters precisely by means of the laser marks printing on the detector surfaces. The laser grid marks are printed around the individual particles' crossing points with the detector surface covering an area of 1~2 mm^2. Therefore the reconstruction of the particle trajectories with an accuracy less than 100~200 μm is sufficient for this purpose. This method has also the advantage of making it possible to identify the outgrowth of spores directly on the detectors and to precisely localize their positions relative to a single particle track through the intermedium of the laser grid marks.

LET SPECTRA AND ABSORBED DOSE

For the cosmic ray LET-spectra measurements, we analyzed several CR-39 plates putted on the different place in Spacelab of IML-1 and FMPT missions. By using the response curve of the detector (Fig.3), LET_{200eV}-value in CR-39 for individual particles was computed from the reduced etch rate ratio , V_T/V_B-1 , which is given by

$$V_T/V_B-1 = [16B^2D^2/(4B^2- d^2)^2+1]^{1/2} -1,$$

where V_T and V_B are the track etch rate and the bulk etch rate respectively. The measured data of LET_{200eV} in CR-39 were converted to the total energy loss LET_∞ in water. In Fig.4 we present some examples of measured integral LET-spectra for the FMPT mission in September 1992. Inside of the RMCD, D-A and D-B detectors were placed behind the shielding of 2.8 g/cm^2 and 5.6 g/cm^2 of CR-39, respectively. The effective detection threshold of LET_∞ -values in water was reduced down to ~ 4 keV/μm due to the high sensitivity of our CR-39 detector.

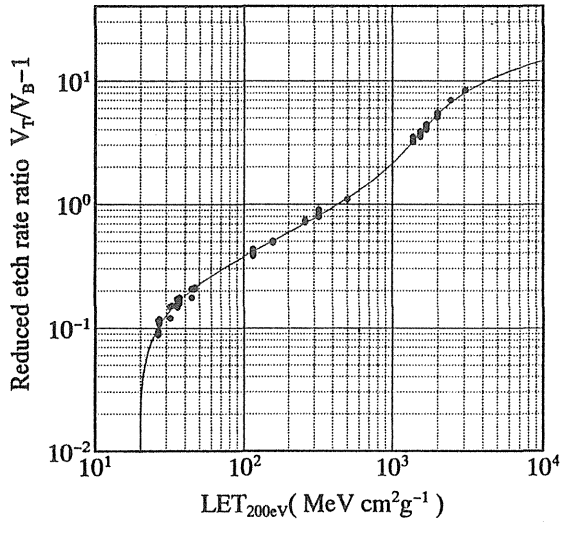

Fig. 3. Response curve of the detector : reduced etch rate ratio vs. LET_{200eV} in CR-39. This curve was calibrated by the irradiations of H, C, N, Ne and Ar ions from the accelerators.

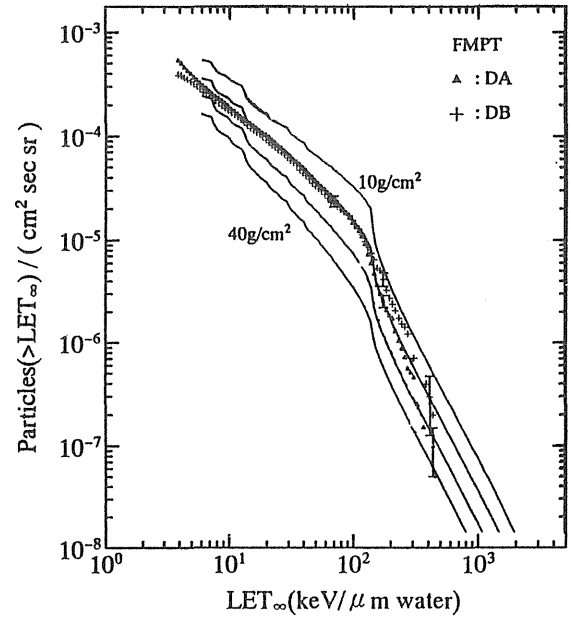

Fig. 4. Observed integral LET-spectra inside of the RMCD on FMPT and calculated spectra (solid lines) behind shieldings of 10, 20, 30 and 40g/cm^2 of CR-39 (Wiegel et al., 1988).

For comparison of LET-spectra, Fig.4 additionally shows calculated LET-spectra behind shieldings of 10, 20, 30 and 40 g/cm^2 of CR-39. These model spectra were calculated by the group of Siegen University for the orbit of the German Spacelab Mission D1 in October 1985[4]. Mission D1 the space shuttle Columbia stayed for 7 days in a circular orbit at 324 km altitude with an inclination of 57° . This is almost the same mission parameters as FMPT mission. Taking account of the data of neutron monitor[5] and the intensities of protons observed in space[6], the influence of solar modulation for galactic cosmic rays can

be considered as almost the same magnitude at the period of both missions, D1 and FMPT. Therefore the calculated LET-spectra for D1 mission can be used to compare our spectra with theoretical one. As seen in Fig.4, our spectra are very similar to the calculated spectra over the entire LET range. Moreover, the position of the shoulder of spectrum due to the minimum ionizing iron ions appeared around 130 keV/μm and agrees well with model predictions. From Fig.4 we can also estimate that the total amount of the effective shieldings of the D-A and D-B detectors were approximately 20 g/cm^2 of CR-39.

The absorbed dose rates for cosmic ray nuclei with LET above 4 keV/μm in water were deduced from the measured LET-distributions in the detectors. The dose-equivalent rates were computed in the same fashion as the absorbed dose rates by weighting the LET dependent quality factor QF(LET). QF(LET) proposed by the ICRP (1986)[7] was used in our calculations. For an example, dosimetry results inside of the RMCD on FMPT mission are summarized in Table 1.

Table 1. Dosimetry results inside of the RMCD on FMPT

Detector	Number of tracks	Minimum value of LET_∞ (keV / μm)	Absorbed dose rate (mrad / day)	Dose-equivalent rate (mrem / day)	Effective quality factor $\overline{QF}$
DA	3207	3.9	0.777 ± 0.017	5.60 ± 0.22	7.2
DB	1368	3.9	0.692 ± 0.024	5.68 ± 0.35	8.2

The effective quality factor $\overline{QF}$, which is defined by the ratio of dose-equivalent to absorbed dose, is 7~8 for cosmic ray nuclei recorded inside of the RMCD on FMPT mission. The average dose rate and dose-equivalent rate observed inside of the RMCD on IML-1 mission in January 1992 were 0.603 ± 0.023 mrad/day and 4.17 ± 0.31 mrem/day, respectively. Such a discrepancy of dose rates between IML-1 and FMPT missions may mainly be due to the difference of the magnitude of solar modulation for galactic cosmic rays. While, the effective quality factor QF for IML-1 is almost equal to the value for FMPT.

ACKNOWLEDGMENTS

We are grateful to NASA and NASDA for supporting us through this study. We are greatly indebted to Drs. T. Kanai, Y. Furusawa, National Institute of Radiological Sciences, and the staffs of RIKEN for providing and kindly helping with the heavy ions exposures at RIKEN Ring Cyclotron. We wish to thank Drs. M. Yoshida and M. Asano of JAERI, Takasaki for the proton exposure at the TIARA Cyclotron.

REFERENCES

1) G. Horneck, Nucl. Tracks Radiat. Meas., 20, 185, 1992.
2) K. Ogura et al., Nucl. Tracks Radiat. Meas., Special Volume (in press).
3) T. Takahashi et al., Jpn. J. Appl. Phys., 27, 2181, 1988.
4) B. Wiegel et al., in Terrestrial Space Radiation and Its Biological Effects, P. D. McCormack et al., ed. (Plenum Press) 795, 1988.
5) R. A. Mewaldt et al., Proc. 23rd ICRC (Calgary) 3, 404, 1993.
6) Z. Fujii and F.B. McDonald, ibid., 477, 1993.
7) ICRU Rep. 40, 1986.

TRACK STRUCTURE OF HEAVY IONS AND INACTIVAYION MODEL FOR MICROORGANISMS

T. Takahashi, F. Yatagai and M. Suzuki
RIKEN (Inst. Phys. Chem. Res.), Wako-shi, Saitama 351-01, Japan

In a recent paper, Katz and Zachariah[1] analyzed experimental inactivation cross sections for *E. coli* mutants B, B/r and B_{S-1}[2,3] by the theory of Butts and Katz[4], where radiosensitivity parameter E_0 is assumed to be equal to D_{37}^{γ}, the γ-ray dose for 37% survival of the microorganism. In their theory, probability of inactivation is given by:

$$P = 1 - exp(-\overline{D}(r)/E_0), \qquad (1)$$

where $\overline{D}(r)$ is the average dose at the target, whose center is at a distance r from the ion's path. The inactivation cross section is approximately calculated by the following equation:

$$S = 2\pi \int_0^R rPdr, \qquad (2)$$

where R is the maximum radial penetration of δ-electrons. For *E. coli* B (D_{37}^{γ} = 46 Gy), with target radius a of 0.5 μm, their calculated cross section lies within 25% of the experimental data except for B and Ar ions at 0.057c (c = velocity of light in vacuum). For *E. coli* B/r (D_{37}^{γ} = 36.5 Gy), their calculations were within 30% of the experimental values except for O and Ne ion bombardments. For *E. coli* B_{S-1} (D_{37}^{γ} = 12.6 Gy), their calculations were within 39% of the experimental values with the exception of He ion bombardments. They also analyzed our experimental inactivation cross sections for for *E. coli* K-12 mutants[5] and *E. coli* B_{S-1} and B/r.[6] Their calculated cross sections were within 0.1 to 47% of the experimental values for *E. coli* K-12 AB2470 (*rec* B) and JC1553 (*rec* A). However, for *E. coli* K-12 AB1157 (*rec*$^+$, *uvr*$^+$) and *E. coli* B/r, their calculations were within 0% to 70% of the experimental values. It means they were unable to get a consistent fit for both strains. In the above analysis, Katz and Zachariah[1] used Waligorski, Hamm and Katz's radial dose distribution function[7] assuming target radius of 0.5 μm.

In our paper[5,6] we got a better fit by assuming πa^2 = 0.57μm^2 for JC1553, πa^2 = 0.65μm^2 for AB2470, πa^2 = 0.50 μm^2 for B_{S-1} and πa^2 = 0.44 μm^2 for B/r. On the other hand, we were unable to get a reasonable fit for *E. coli* K-12 AB1157 (D_{37}^{γ} = 118 Gy) by Butts and Katz's theory in its original form. In the case of radioresistant microorganisms with high D_{37}^{γ}, as described in ref. 5, it seems necessary to assume that radiosensitivity parameter E_0 is LET dependent and inactivation cross section is shown as follows:

$$S = 2\pi \left(\int_0^a P_{in} r dr + \int_a^R P_{\delta} r dr \right). \qquad (3)$$

Here, P_{in}=1-$exp(-\overline{D}(r)/E_{in})$ is the probability of inactivation when the ion impinges upon and goes through the target ($r<a$) and P_{δ}=1-$exp(-\overline{D}(r)/E_{\delta})$ is the probability of inactivation when the ion passes by the target and the trajectories of its δ-electrons come into the target ($r>a$). This implies that the radiosensitivity of AB1157 for the LET region of the heavy ion's core $1/E_{in}$ is higher than the radiosensitivity for that of δ-electrons $1/E_{\delta}$. By the modified Katz's theory mentioned above, we have also succeeded in explaining the inactivation cross section of *B. subtilis* spore.[8] In Fig. 1, we showed result of our analysis for *E. coli* K-12 mutants based on Waligorski, Hamm and Katz's

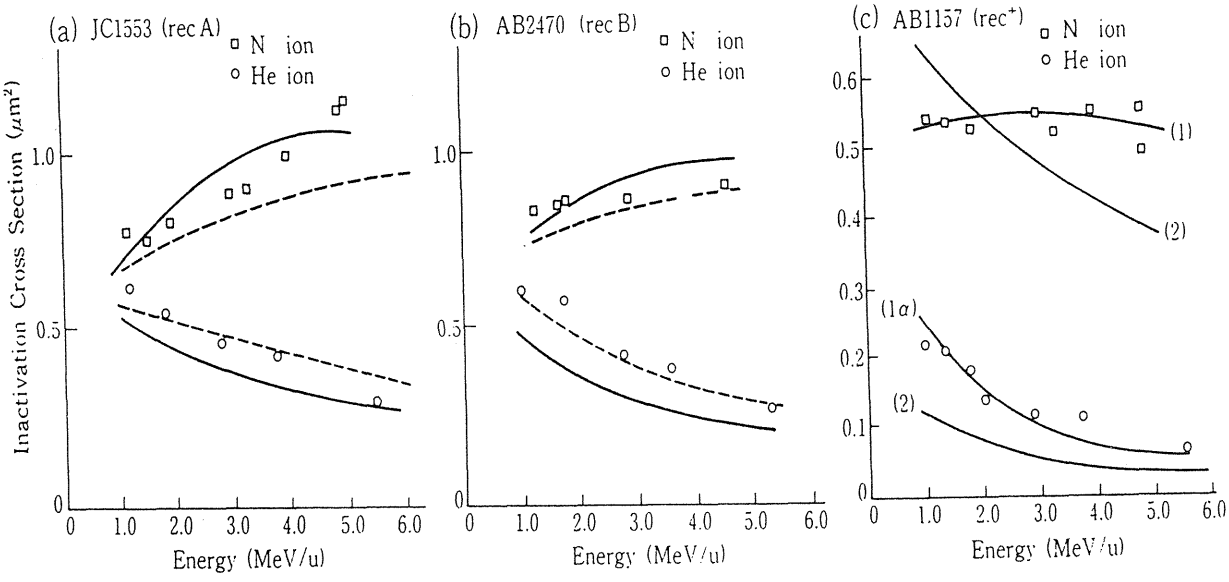

Fig. 1. (a) Inactivation cross sections as a function of energy of ions for *E. coli* K-12 JC1553 (rec A). Analysis was made by D_{WN} (solid line) and D_{TN} (dotted line). Here, D_{WN} and D_{TN} are the dose D_W and D_T normalized to the stopping power.

(b) Inactivation cross sections as a function of energy of ions for *E. coli* K-12 AB2470 (rec B). Analysis was made by D_{WN} (solid line) and D_{TN} (dotted line).

(c) Inactivation cross sections as a function of energy of ions for *E. coli* K-12 AB1157 (rec$^+$). Least squares analysis was made by D_{WN}. Line (1) was obtained from eq. (3) and line (1α) from eqs. (2) and (4), and the optimum geometrical cross section was found to be 0.495 μm^2. Line (2) was obtained from eqs. (1) and (2) and the optimum geometrical cross section was found to be 0.96 μm^2.

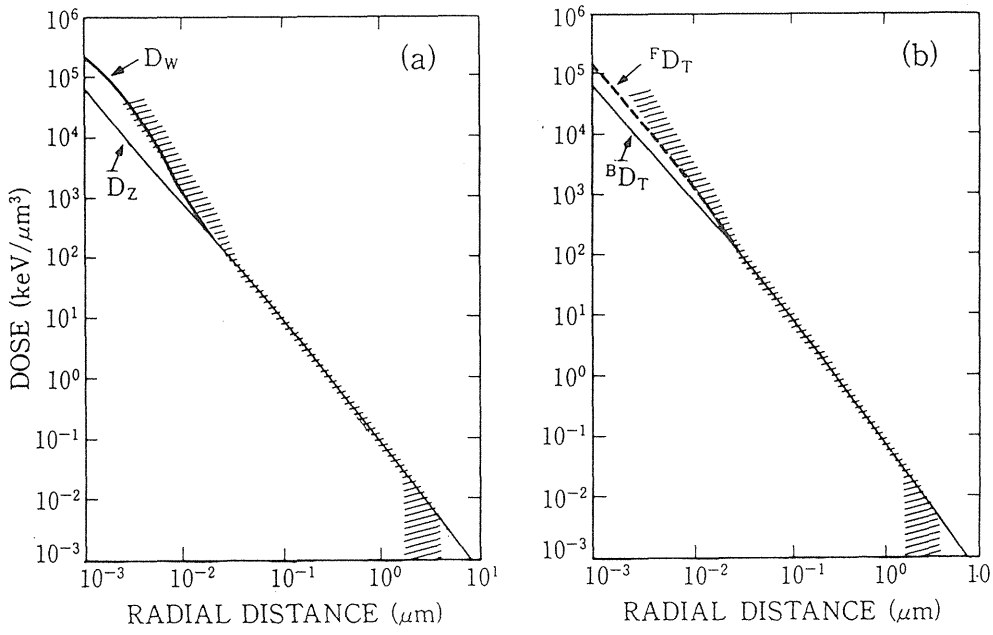

Fig. 2. Experimental and theoretical radial distribution of energy deposited around the path of 18.3 MeV/u He ion. The shaded area shows a 68% confidence band of Kanai and Kawachi's experiment[13] for tissue equivalent gas. The radial distances are at unit density. (a) D_W and D_Z[14] for 18.3 MeV/u He ion in water. (b) ^BD_T and ^FD_T for 18.3 MeV/u He ion in water. ^BD_T = D_T(bound) and ^FD_T = D_T(free) are calculated under the assumption that electrons in the medium are bound and free, respectively.

dose D_w as well as the radial dose distribution D_T. Here, D_T was calculated by essentially the same method as that given by Katz and Kobetich[9], but Tabata and Ito's energy deposition algorithm for electrons[10, 11] was used as described in our previous paper[6] (Fig. 2). If E_0 is a function of LET, it is possible to express E_0 approximately by the following equation:

$$E_0(L) = D_{37}^{\gamma}/(a+bL), \quad L < L_C. \qquad (4)$$

Here, a and b are constants and L_C is cutoff LET[12].

Since the quantity $\bar{D}(r)$ plays an essential role in evaluating the inactivation cross section as the above consideration indicates, it should be ideal if there exists any instruments which can measure $\bar{D}(r)$ directly for individual ionization tracks produced by the heavy ions. In this respect, a proportional scintillation chamber coupled to an image-intensifier-associated CCD camera has been constructed as a promissing candidate at RIKEN, and is currently under test in various aspects by using heavy ion beams available at RIKEN Ring Cyclotron Facility.

REFERENCES

1. R. Katz and R. Zachariah: *Radiat. Res.* 134, 261 (1993).
2. Yu.G. Grigotiev *et.al.*: *radiobiology(USSR)*, 5, 245 (1971).
3. R.H. Haynes: *Radiat. Res.* suppl. 6, 1 (1966).
4. J.J. Butts and R. Katz: *Radiat. Res.* 30, 855 (1967).
5. T. Takahashi, F. Yatagai and K. Izumo: *Adv. Space Res.* 12, No. 2, 65 (1992)
6. T. Takahashi, F. Yatagai, S. Konno, T. Katayama and I. Kaneko, *Adv. space Res.* 6, No. 11, 117 (1986)
7. M.P.R. Waligorski, R.N. Hamm and R. Katz: *Nucl. Tracks Radiat. Meas.* 11, 309 (1986)
8. T. Takahashi, F. Yatagai and S. Kitayama: *Adv. Space Res.* 3, No. 8, 95 (1983)
9. R. Katz and E.J. Kobetich: *Nucl. Instrum. Methods* 71, 226 (1969).
10. T. Tabata and R. Ito: *Nuclear Science and Engineering* 53, 226 (1974)
11. T. Tabata and R. Ito, *Jpn. J. Appl. Phys.* 20, 249 (1981)
12. J.L. Bateman et. al.: *Radiat. Res.* 15 694 (1961).
13. T. Kanai and K. Kawachi: *Radiat. Res.* 112 426 (1987).
14. C. Zhang et. al.: *Radiat. Protect. Dos.* 13 215 (1985).

Microscopical Investigation of Cellular Effects of 135 MeV/amu Carbon along the path of the Beam.

Masako Furuse, Fuminori Soga and Shinji Matsumoto

National Institute of Radiological Sciences
Anagawa 4-9-1, Inage-ku, Chiba 263, Japan

Introduction

Differences in the biological effects are normally described by the concept of RBE. RBE values, however, depend on not only LET along the trajectory but also on complicated parameters such as distribution of the energy deposition due to differences in the spreading of the secondary electrons perpendicularly to the beam axis. Precise knowledge is needed about the energy deposition mechanism along the beam path. We are interested in using a biological dosimeter of microorganisms, which is possible to compare directly biological effects such as survival level. We tested the yeast cell survival rate for this purpose with a carbon beam at 135 MeV/amu from Riken ring cyclotron. The haploid cells of a wild type and a radiation sensitive strain were used. Yeast, a simple eukaryote, has been used as a test organism especially in studies of the relationship between DNA double-strand breaks and cell killing. This organism has various merits in radiation biological studies. There are ploidy stages of haploid and diploid in different radiation sensitivities, and various types of radiation sensitive strains. In addition, the budding stage is known as a state radioresistant to ionizing radiation like the diploid cells. The resistance has been interpreted to be due to the action of an enzymatic repair mechanism which requires duplicated but unsegregated DNA as a substrate and to be further enhanced by the checking mechanism of cell cycle progression.

Materials and Methods

Two strains of haploid yeast of Saccharomyces cerevisiae in this investigation are a wild type, S288C, and a radiation sensitive mutant, M3691-9B (rad 52-1). The mutant is reported to be deficient in double-strand break repair. An apparatus was used, in which five holes were drilled in a block of Lucite (acrylic resin) at the depths of 0.585, 3.276, 3.861, 3.978 and 4.095 g/cm2 from the surface, corresponding to the positions of the surface (hereafter, position 1), before the Bragg peak (2), at the peak (3), just after the top of the peak and just after the range of the primary peak (5). The microtubes containing packed cells were inserted into each hole. The survival rates were determined by counting visible colonies on YEPD agar plates.

Results

Survival data of wild and sensitive strain at stationary and log phase were obtained. The data were expressed in the incident fluence of the beam, in order to get a direct comparison of survival level along the path. The ratio of dose to fluence along the path was determined by separate experiments using Lucite absorber plates and an ion chamber. The values were used for the RBE estimation. The survival curves of the wild type at stationary phase have a biphasic pattern which is a combination of a straight line initially and the following concave curve. In Fig. 1, the curves at the positions of 1 and 2 show typically this combination. The former of the single hit must be due to the cells without budding and the latter of the multi-hit response due to the cells with budding. It has been confirmed that the resistant population originates from the budding cells. Percentages obtained by extrapolation of the survival curves in multi-hit response to y axis were in good agreement with budding population percentage counted under a microscope. We estimated two kinds of inactivation rates from the exponential parts in the initial and the final slopes of the survival curves assuming a single and a multi hit responses.

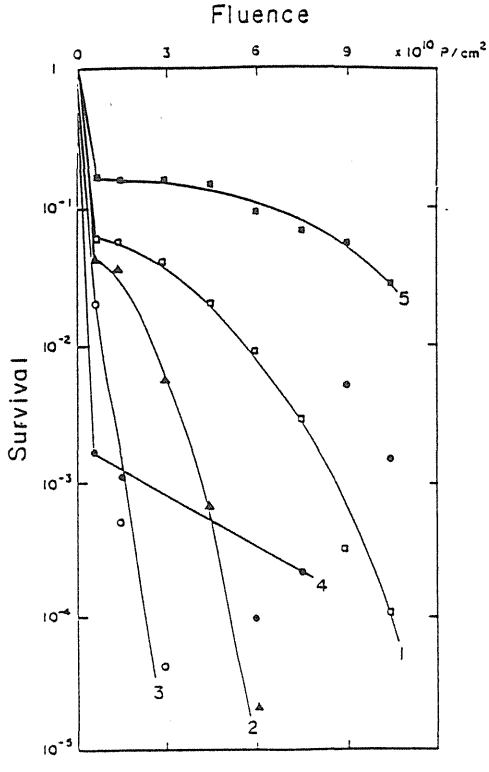

Fig.1. Survival curves of the wild type yeast at the depths of (1)0.585, (2)3.276, (3)3.861, (4)3.978 and (5)4.095g/cm2 in a Lucite block after irradiation of the carbon beam from Riken ring cyclotron.

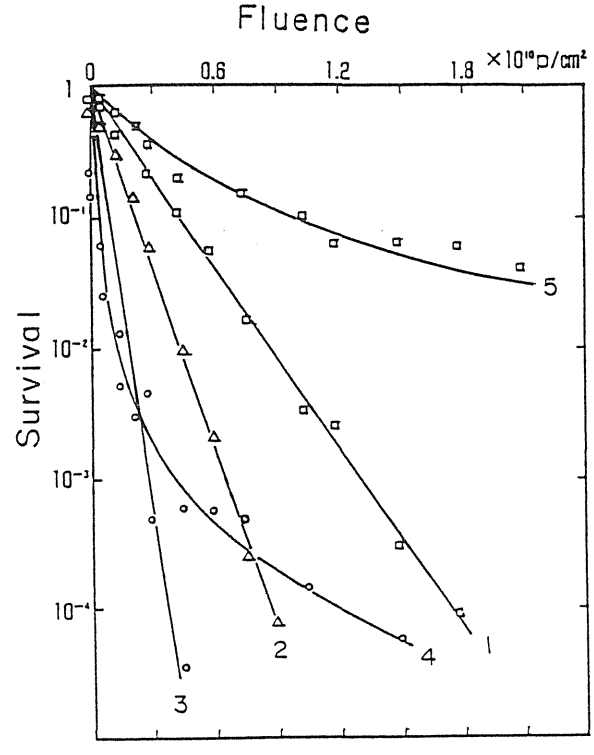

Fig.2. Survival curves of the radiation sensitive yeast at the depths as in the caption of Fig.1.

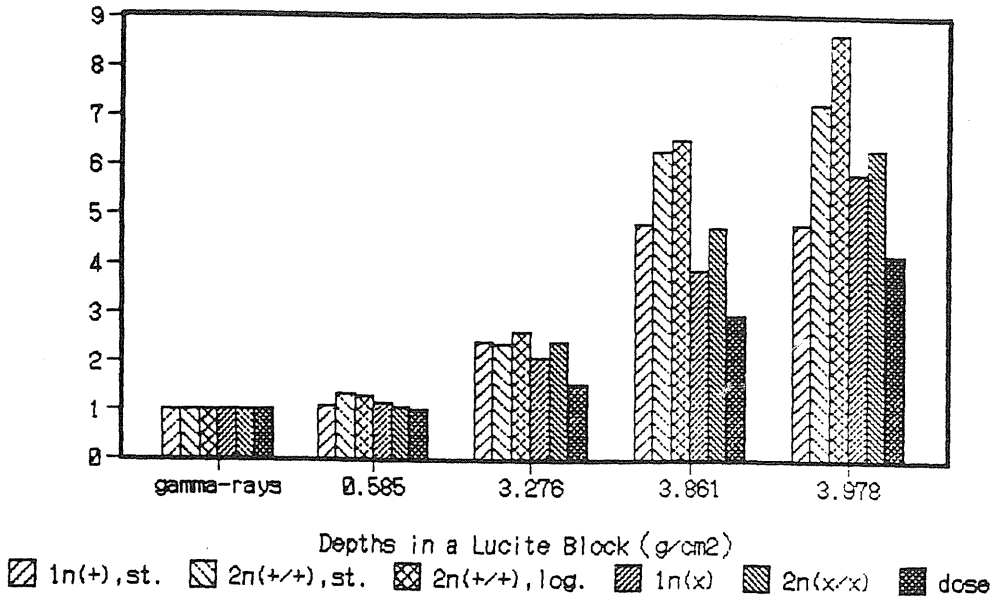

Fig.3. Reciprocal fluences at 10% survival of the yeast cells at log and stationary phases. The reciprocal fluences are normalized at the position 1. The columns from the left indicate 1n wild at stationary, 2n wild at stationary, 2n wild at log, 1n sensitive at stationary and 2n wild at stationary.

Similarly, survival curves of the radiation sensitive strain for stationary and early log phase were obtained at the same positions. The curves at stationary phase are shown in Fig.2. The survival curves, even at the surface position of 1, were almost expressed in straight lines with small shoulders. The discrimination in the survival between the haploid and the diploid was not possible. This contrasts with the extensive concave parts of the curves for the wild types. This reflected the deficiency in the recombinational repair.

The sensitivities along the path were compared with the sensitivity at the surface position among the same run and shown in Fig. 3. The comparisons among different runs were not possible due to different waiting time before the usable timing of the accelerator. The fluence at 10% survival level was used as an indication of the sensitivity for the evaluation. For the evaluation in diploid phase, the values were obtained as the fluences which decreased the survival to 10% from the percentages of the budding populations. The RBE values were estimated based on the sensitivity at the surface position and the evaluated doses. The RBE values increased with the increase of the position in depth until the 3. Among them, the higher RBE were observed in the diploid phases, indicating inefficiency in the damage repair using the diploid chromosome of the wild type strain. The inactivation ratios at the 5 may be usable for estimation of the secondary particle effects.

Difference in the LET-RBE and -OER response to Heavy-Ions Revealed by Accelerated Ions and Cell Strains.

Y. FURUSAWA[1], K. FUKUTSU[2], H. ITSUKAICHI[2], K. EGUCHI-KASAI[2], H. OHARA[3], F. YATAGAI[4], and T. KANAI[1];

[1]Division of Accelaretor and Engineering, [2]Division of Radiation Hazards, National Institute of Radiological Sciences, Chiba 263, [3]Faculty of Education and Arts, Okayama Univ., Okayama 700, and [4]Institute of Physical and Chemical Research, Saitama 351-01, Japan

ABSTRACT: There is some possibility of different radiobiological effectiveneses according to the types of accelerated ions but using the same LET (linear energy transfer) beam. We determined the difference in terms of the RBE (relative biological effectiveness) and OER (oxygen enhancement ratio) using ^{3}He, ^{12}C and ^{20}Ne ion-beams upon HSG cells at the same LET. The D_{10} values at the same LET were largest for the ^{3}He ion-beam, middle for the ^{12}C ion-beam and smallest for the ^{20}Ne ion beam in the lower LET region (<100 keV/μm). With an increase in the LET for the ^{3}He ion-beam the OER values rapidly decreased compared with the other ion-beams. The LET-RBE curves for ^{3}He and ^{20}Ne ion-beams upon HSG cells were shifted to a lower LET region compared with V79 cells.

INTRODUCTION

The relative biological effectiveness (RBE) is thought to be given by a simple function of the linear energy transfer (LET), which is described as a linear-dimensional energy-deposit density. The three-dimensional energy-deposit density is different according to types of accelerated ions when their LETs are the same, because of the difference in velocities and electric charges of the accelerated ions. The cross sections between the ions and energy-absorbing materials, such as living cells, are different based on the target sizes of the irradiated cells, the truck structure of the accelerated ions, the target-truck distance, and so on. Thus, the biological effectiveness to the same LET ion beams may vary according to the types of ions and cells. The differences in the biological effectiveness were previously reported (Furusawa *et al.* 1992) in terms of the cell-killing efficiency on Chinese Hamster V79 cells by ions. To obtain the difference between the cell strains, we exposed another cell strain of HSG (human salivary grand tumor cell) to several types of ion-beams having various LETs. We clarified the difference in the RBE as well as the oxygen enhancement ratio (OER) between the cell strains by the same ion, but different LET.

MATERIALS & METHODS

We exposed exponentially growing Chinese Hamster V79 cells and Human Salivary Grand Tumor (HSG) cells to accelerated ^{3}He ^{12}C, and ^{20}Ne ion-beams. The details concerning of the beam characteristics and energy and/or LET ranges used, as well as the dosimetry, were reported previously (Furusawa *et al.* 1992, Kanai *et al.* 1993). Briefly, the exposures were carried out at the NIRS cyclotron (^{3}He- and ^{12}C- ions, 12 MeV/u) and the RIKEN ring cyclotron (^{12}C- and ^{20}Ne-ion, 135 MeV/u) facilities. We could expose the cells with an average LET ranging roughly from 20 to 90 (^{3}He), from 30 to 430 (^{12}C), and from 60 to 570 (^{20}Ne) keV/μm. For cell exposure to those ion-beams, custom-made gaseous-control irradiation chambers as well as custom-made glass dishes for cell growing were used as the irradiation apparatus.

HSG cells were pre-cultured, harvested with trypsinization, and seeded in the central area (2 cm in diameter) of the dishes to be 50,000 cells/cm^2. For all of the cell cultures and treatment, an MEM medium containing 10% FBS and antibiotics were used (for V79 cells, see Furusawa *et al.* 1992). The dishes were cultured for about 1.5-2 days at 37°C in 5 % CO_2 containing an air incubator. Excess medium (0.5 ml/dish) was added into the dishes; they were then transfered into the irradiation chamber before heavy-ion beam exposure. For aerobic exposure, the dishes were transferred to a chamber; inside the chamber they were first flushed with air containing 5 % CO_2, after which exposures immediately started. Under hypoxic exposure, the cells in the dishes with the medium in the chambers were flushed for more than one hour before ion-beam exposure at a rate of 500 ml/min of pure-N_2 gas containing 5% pure-CO_2 gas. The hypoxic gas was also flushed during the exposures at a rate of 200 ml/min. At the time of the exposure, cells on the dishes were transfered from the chamber, washed twice with the medium, harvested by trypsinization, diluted with the medium, seeded on a 6 cm plastic dish filled with 5 ml of medium, and then incubated for 12 days. The survivor measurements were carried out within 2-3 hours after the heavy-ion beam exposure.

RESULTS & DISCUSSION

The cell-killing efficiencies of HSG and V79 cells were measured with various LET beams of ^{3}He, ^{12}C and ^{20}Ne ions under both aerobic and hypoxic exposure conditions. The survival curves of V79 cells for lower LET beams had large shoulders (4 Gy as D_q, at 20 keV/μm for aerobic condition), and that of HSG cells had small shoulders (1 Gy for ^{3}He-ion and 2 Gy for ^{12}C-ion, at 20 keV/μm for aerobic condition); the shoulders were reduced by an increment of the LET. The survival curves under both the aerobic and hypoxic conditions were analogous for the same LET beam. The survival curve parameters were numerically determined by using the Linear Quadratic Model as a fitting method, rather than the theoretical model of the survival fraction; the D_{10}s (dose required to reduce the survival to 10%) were obtained for each experiments. In this report, the cell survivals are discussed based only on D_{10}, since D_{10} was the most stable parameter for our experiments. The RBE and OER values for each ion-beam were plotted against the LET of the exposed ion-beam. D_{10} to 200 kVp X-rays, as standard radiation, was defined as 8.1 Gy for V79 cells and 4.1 Gy for HSG cells.

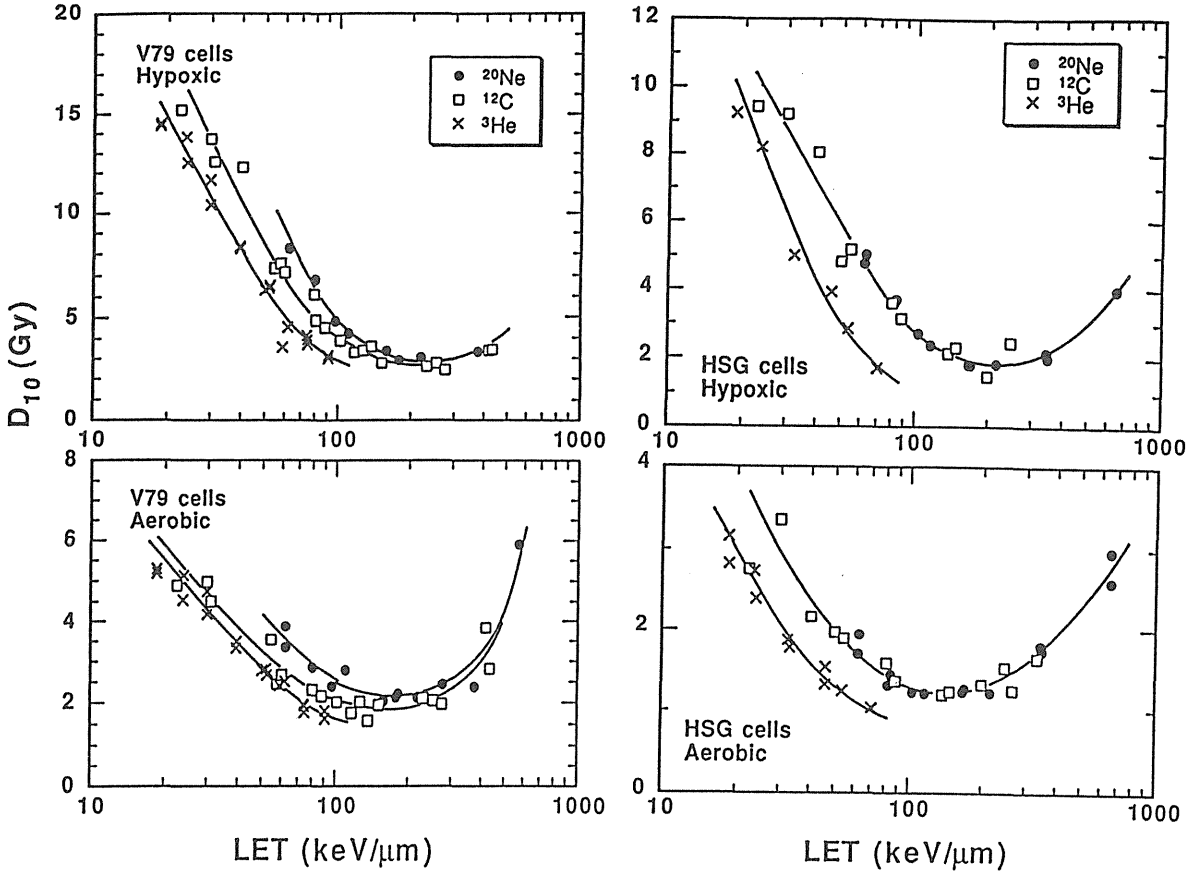

<Fig 1.> LET-D_{10} relationship of V79 and HSG cells under both hypoxic and aerobic conditions for ^{3}He, ^{12}C, and ^{20}Ne ion-beams.

Summaries of the D_{10} vs. LET for HSG and V79 cells under both aerobic and hypoxic conditions are shown in Figure 1. The D_{10} values were, for all cases, reduced with increments of LET to a minimum at about 100-300 keV/μm, and then increased in a much higher LET region. The LET-D_{10} curves for the V79 cells were separated for ^{3}He-, ^{12}C- and ^{20}Ne-ions. From the figures in the middle (30-90 keV/μm) LET region, the lowest D_{10}s at the same LET radiation were found by the ^{3}He-ion rather than other ion-beams. The minimum value of D_{10} was, however, not found for the ^{3}He-ion. Because of the LET range, what we could examine was not sufficient for finding the minimum D_{10} for the ^{3}He-ion. The D_{10} were middle for the ^{12}C-ions and highest for the ^{20}Ne-ions at the same LET, as described previously (Furusawa *et al.* 1992). Analogous figures were found for HSG cells. The curves produced by the ^{3}He-ion for the HSG cells were lower than those by the other ions as well as the V79 cells. In the curves for HSG cells by the ^{12}C-ion and ^{20}Ne-ions, it was hard to find any difference between each other. The reason for this is hard to explain; it may be caused by a difference in the target size of these two cell strains. This difference by exposed ions and cell strains is summarized as an expression of RBE in figure 2 by using some data from the ^{3}He-ion and ^{20}Ne-ion beam experiments. In the figure, not only the difference produced by the ions described above, but a difference due to the cell strains could also be found. The RBE curves

of V79 cells for ^{3}He-ions were shifted to a much higher LET region compared with that of the HSG cells. The same figures could also be found for the ^{20}Ne-ions.

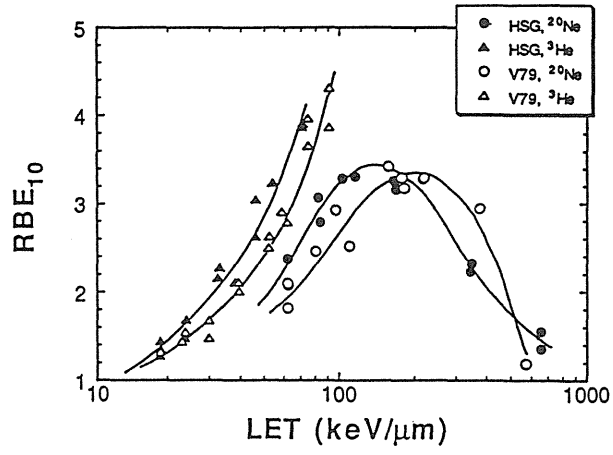

<Fig.2> Difference in the LET-RBE relationship between V79 and HSG cells for ^{3}He and ^{20}Ne ion-beams.

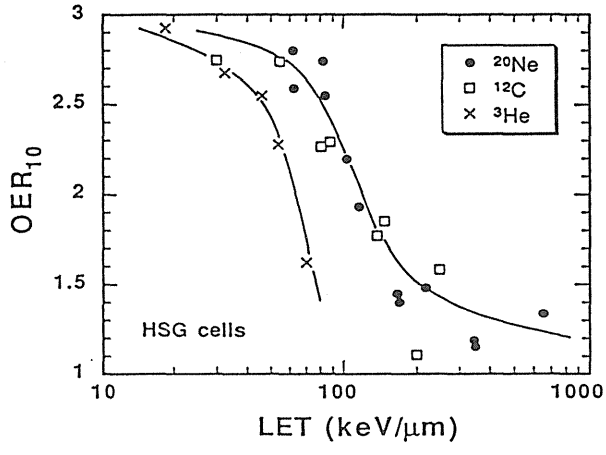

<Fig.3> LET-OER relationship of HSG cells for ^{3}He, ^{12}C, and ^{20}Ne ion-beams.

From the survival parameter of D_{10} under both aerobic and hypoxic conditions, the oxygen enhancement ratios (OER) were obtained (Fig.3). The OER decreased monotonously from 3 to 1.2 with an increase of LET; also, the decrement in OER started at a significantly lower LET region by the ^{3}He-ion than the other ion-beams. When an ^{3}He-ion beam was used for cell exposure, a low OER was clearly found for the same LET beams of around 20-90 keV/μm for HSG cells, and a sharp decrement of OER vs. LET was found for HSG cells compared with that for V79 cells (Furusawa *et al.* 1992). However, no differences were found for HSG cells when using ^{12}C- and ^{20}Ne-ions.

REFERENCES

Furusawa *et al.* Biological effectiveness by the same LET heavy-ion species with the same LET. *Prosc. 2nd Workshop on Phys. Biol. Res. Heavy Ion.* Eds. K. Ando and T. Kanai, **HIMAC-003**, 11-13, Natl. Inst. Radiol. Sci., Chiba (1992).

Kanai *et al.* Dosimetry and measured differential W values of air for heavy ions. *Radiat. Res.* **135**, 293-301 (1993).

Response of Plateau-Phase Cultures and Multicellular Spheroids of Human Osteosarcoma Cells to Carbon Beam Irradiation

Nobuo Kubota[1], Masae Kakehi[1], Sho Matsubara[1], Fumio Yatagai[2], Tatsuaki Kanai[3], and Tetsuo Inada[4]

[1]Dept. of Radiology, Yokohama City University School of Medicine, 3-9 Fukuura, Kanazawa-ku, Yokohama 236

[2]The Institute of Physical and Chemical Reserach, Wako, Saitama 351

[3]National Institute of Radiological Sciences, Chiba 260

[4]University of Tsukuba, Tsukuba 305

INTRODUCTION

The possible therapeutic advances in achieving local tumor control using high LET radiation therapy is major area of interest to clinical radiation oncologists and radiobiologists. These include an improved depth-dose distribution as well as a greater relative biological effectiveness (RBE) and greater reduction of oxygen enhancement ratio (OER). In addition, the type of damage produced by charged particles is reported to be less amenable to repair (1). Mammalian cells repair radiation damage by two known phenomena: Sublethal damage (SLD) repair and potentially lethal damage (PLD) repair. Repair modification of SLD with increasing LET has been investigated extensively, but repair modification of PLD with increasing LET has been investigated only to a limited extent. The results of these PLD repair experiments, in contrast to the severely reduced repair of SLD, are uncertain and discrepant. Because recovery from PLD might significantly contribute to the ultimate therapeutic response of a solid tumor, we have investigated the ability of plateau phase osteosarcoma cells to recover from PLD after irradiation with RIKEN ring cyclotron accelerated carbon ions in the spread-out Bragg peak (SOBP) region.

Multicellular spheroids grown in tissue culture display many of the properties of solid tumors in vivo and thus can be considered as an in vitro tumor model. We also measured relationship of dose and cure probability for spheroids of osteosarcoma cells after irradiation with carbon beam in the SOBP.

MATERIALS AND METHODS

Cell line and culture

MG-63 human osteosarcoma cell line was used for this study. The cell line was cultured in α−MEM supplemented with 20 mM HEPES, 10% FCS, and antibiotics.

Plateau phase cells were prepared by plating $5x10^5$ cells in 25 cm^2 flask and incubating for 5 days without an intervening change of medium. Spheroid growth was initiated by inoculating $1x10^6$ cells in 10 ml into Petri dishes coated with 1% agar. Three days after initiation of speroid growth, cell aggregates were transferred into spiner flasks inside an CO_2 incubator (2). Spheroids were irradiated at a diameter of 150-160 μm (3).

Cell survival and spheroid cure

Cell survival was measured by standard colony-formation techniques. For PLDR experiment, plateau phase cells were trypsinized at various postirradiation times. For spheroid cure experiments, about 50 spheroids were directly placed on a Petri dish 24 hours after irradiation and incubated for 3 weeks. Spheroid cure was judged by the absence of growth during the observation period.

Irradiation

Carbon-12 (135 MeV/n) accelerated by a ring cyclotron at RIKEN were used for this study. Both plateau phase MG-63 cells and spheroids were irradiated with carbon beam at several positions in the SOBP made by a range modulator. The physical characteristics have been described in detail (4).

RESULTS AND DISCUSSION

Cell survival was measured for plateau phase MG-63 cells at various depths (entrance, proximal, midpoint, and distal) in the SOBP of carbon beam. Dose-response curves measured by 24 hr delayed plating are given in Fig. 1.

From the survival curves RBE values calculated at 0.1 survival level were 1.70, 2.48, 2.70, and 3.22 at entrance, proximal, midpoint, and distal within the SOBP, respectively. Corresponding RBE values at 0.01 survival level were 1.54, 1.92, 2.08, 2.46.

Results of repair of PLD of plateau phase MG-63 cells at various depths in the SOBP of carbon beam and γ-rays are shown in Fig. 2. After γ-ray exposure, there was an increase in survival with time. The repair ratio, measured by the ratio of cell survival after 24 hr to 0 hr, was about 7.0. After carbon beam irradiation, recovery was found to be reduced, and the ratios were 6.1, 3.2,

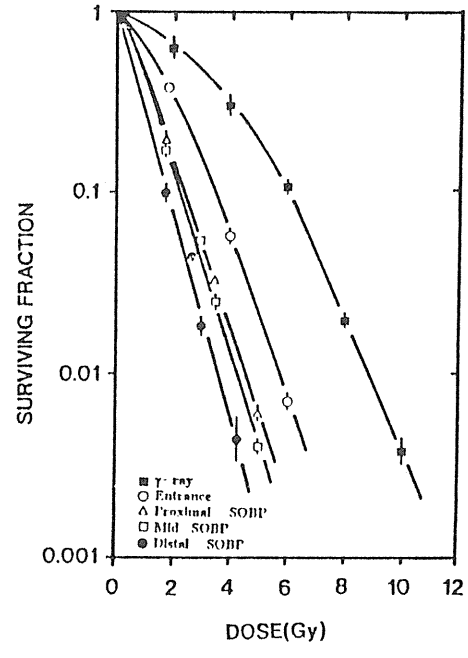

Fig. 1. Cell survival by 24 hr delayed plating of plateau phase MG-63 cells after carbon beam and γ- ray irradiation.

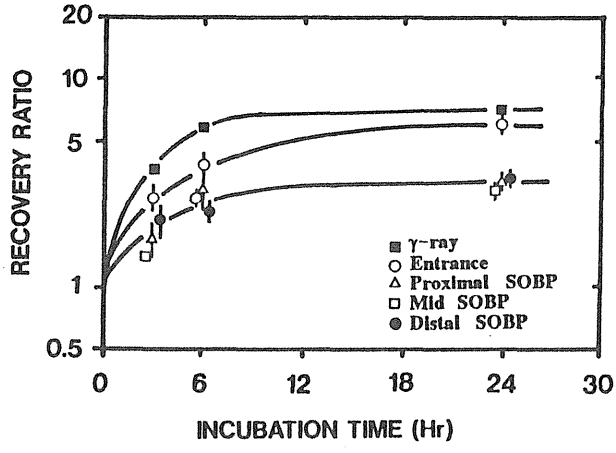

Fig. 2. Cell survival of plateau phse MG-63 cells plotted as afunction of time after irradiation with γ- rays and carbon beam with SOBP.

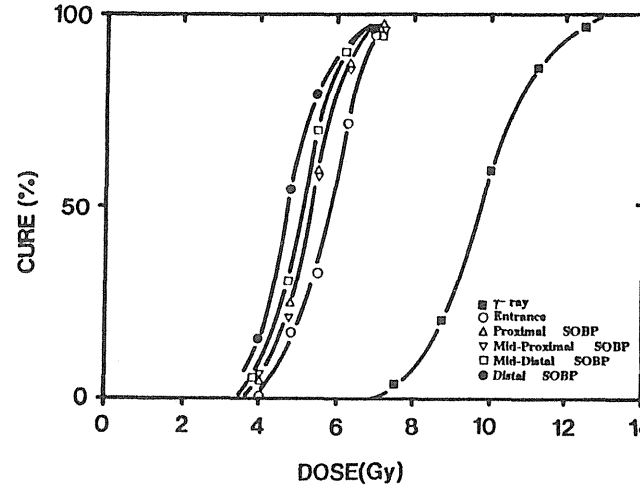

Fig. 3. Spheroid cure curves after irradiation with carbon beam with SOBP and γ- rays.

3.0, and 3.4 at the entrance, proximal, midpoint, and distal within the SOBP, respectively. Thus, our results clearly demonstrated that there was still detectable PLD repair when plateau phase MG-63 cells were exposed to carbon beam.

The spheroids of MG-63 cells received single doses of carbon beam with SOBP. Fig. 3 shows the relationship of dose and cure probability for spheroids at various depths in the SOBP of carbon beam and γ-rays. SCD_{50} after irradiation with γ-rays and carbon beam at entrance, proximal, midpoint, mid-distal, and distal in the SOBP were 9.85, 5.80, 5.30, 5.35, 5.15, and 4.70 Gy, respectively. Resultant RBEs were 1.70, 1.86, 1.84, 1.91, and 2.10 for entrance, proximal, midpoint, mid-distal, and distal peak, respectively.

REFERENCES

1) Shipley, W. U., Stanley, j. A., and Courteney, V. D. (1975) Cancer Res. 35, 932-938.

2) Kubota, N., Kakehi, M., and Inada, T. (1993) Int. J. Radiat. Oncol. Biol. Phys. 25, 491-497.

3) Kubota, N., Kakehi, M., Matsubara, S., Koike, S., and Ando, K. submitted.

4) Kanai, T., et al. (1992) Proceedings of the Second Workshop on Physical and Biological Research with heavy Ions. 1-3.

RBEs of Various Human Monolayer Cells Irradiated with Carbon Beams

Hisao Ito [1], Shoji Yamashita [1], Iku Nishiguchi [1], Naoyuki Shigematsu [1], Wei-jei Ka [1], Atsushi Kubo [1], Fumio Yatagai [2] and Tatsuaki Kanai [3]

1 Department of Radiology, Keio University, School of Medicine.
2 Department of Cell Biology, The Institute of Physical and Chemical Research.
3 Division of Accelerator Research, National Institute of Radiological Sciences.

(Introduction) The effect of the heavy particle irradiation on cell survival is different from that of the X-ray irradiation. In Japan, heavy particle irradiation will be applied to cancer patients in the near future. Many biological and physical experiments are going on to make necessary arrangements for clinical trials. Most biological studies are performed with mice and rodent cells. However, radiation effects of X-ray on human cells are something different from those on rodent cells, for example, smaller initial shoulders and smaller Do values for human cells. This study was performed to determine the RBEs of carbon beam irradiation on various human monolayer tumor cells in vitro.

(Materials and Methods) Thirteen human tumor cell lines were used in this study (detailed in Table 1). They were maintained in F10 medium supplemented with 10% fetal calf serum by transfering cells into new vessels once a week. For irradiation experiments, a series of cell cultures were prepared in flasks (numc 52094) for RIKEN's beams. The flasks for irradiation by RIKEN Ring Cyclotron were filled up with serum containing medium and sealed tight to avoid harmful change of pH in the medium by air, being allowed for the temporal transport from a home laboratory to a place of irradiation experiment (RIKEN)(1 hour). During round trip transportation between home lab. and RIKEN, all culture flasks were kept in a ice-cooled box. The plating efficiencies of the cells were not changed by this transportation system. The cells were irradiated either with 135 MeV/n carbon beams from the RIKEN Ring Cyclotron or 200 KVp X-rays in my laboratory. After irradiation the cells in flasks were treated with 0.1% of trypsin solution for dispersion, suspended in seum containing medium and counted. Then known number of cells were replated into 4 new assay dishes and incubated to allow colonial growth of surviving cells for 8-10 days at 37 C in the humidified atmosphere of 95% of air and 5% CO2 gas. The resulting colonies of surviving cells were fixed with 0.2% crystal violet in 95% alcohol and counted to determine the cell survivals in the ratio of that of the unirradiated controls. A dose reponse of cell survivals was also established for several kinds of LETs with carbon beams to determine the mathematical parameters of cell inactivation. The curve fitting was made by multitarget model for Do, n and Dq.

Carbon beams used for biolgical experiments wre usually characterized by specified range of LET, because change of LET values has already been known to bring about dependent change in biological effect. RBE is defined as the ratio of dose required for a given level of radiation effect between reference and test radiation. For a convenience, dose for Do or dose to give cells 10% survivals has been used for RBE estimation as the comparison fo radiation qualities. RBE can be determined easily if the dose relationship

of biological effects v.s. radiation dose is established. In this sutdy, we have used 200 KVp X-rays as a reference radiation.

(Results and Discussion) Figure 1 showed the survival curves of two cell lines (TE5 & A43.1) irradiated with 200 KVp X-ray and various LETs of carbon beams. These cells had the similar n values (1.7 vs 1.5) but different radiosensitivities (Do : 1.38Gy vs 2.43Gy) for X-ray. When these were irradiated with carbon beams, the survival curves became steeper and do values decreased with increment of LETs in both cell lines. The initial shoulder of TE5 survival curve disappeared at lower LET of 20 KeV/um. On the other hand, A43.1 cells showed the initial shoulder even at higher LETof 80 KeV/um. RBEs were calculated at the 10% survival level. The TE5 cells irradiated with 20KeV/um carbon beams showed RBE of 2.54, and the A43.1 cells, 1.70. This result suggested that the radiation effects of carbon beams on human tumor cells were different between cell lines. The Do, n values and RBE at 10% survival level of several human tumor cells were shown in Table 1. RBE values irradiated with LET of 20 KeV/um showed 1.31 - 2.54, and those with 80 KeV/um, 2.24 - 4.07. Nine cell lines were established from adenocarcinoma and 4 from squamous cell carcinoma. There was no relationship between histology of tumor and RBE. If RBEs determined from in vitro experiments could be applied to clinical radiotherapy, it is very difficult to determine the average single RBE value even for the some LET value in heavy particle therapy, because the RBEs were different from one cell line to the others. However, the estimated RBE value is necessary to perform the clinical trials, and it might be convenient if we can expect it from our past experiences of X-ray radiotherapy. Figure 2 showed the relationship between RBEs for 20 or 80 KeV/um carbon beams and Do or n values calculated from the survival curves with 200 KVp X-rays. There was a slight tendency that cells with smaller Do values has larger RBE, but this was not statis-

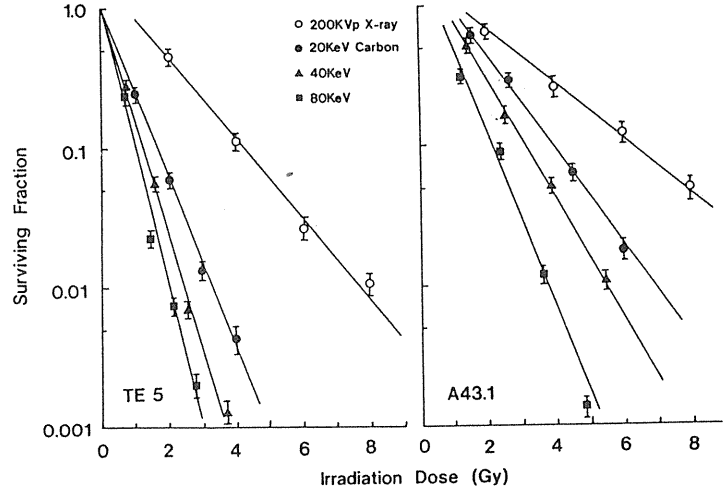

Fig. 1. Survival curves of TE5 and A43.1 cells.

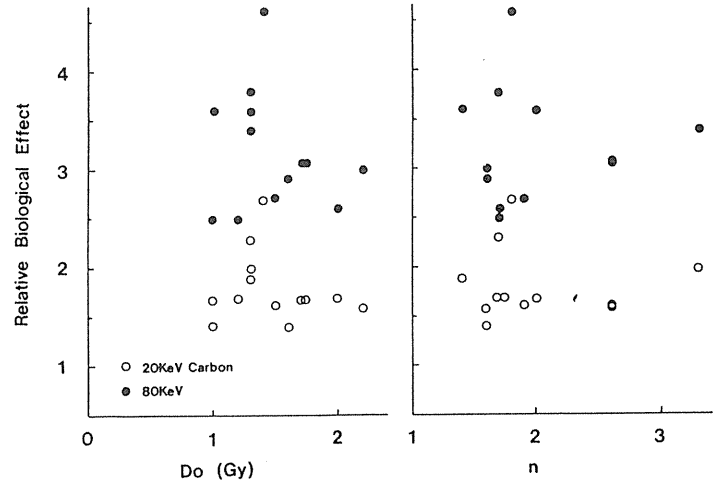

Fig. 2. Relationship between RBE for 20 and 80 KeV/um carbon beams and Do (right panel) and n (left panel) values for 200 KVp X-ray.

tically significant. The analysis of relationship between RBE and n values showed the similar result as that between RBE and Do, that is, not significnat. We could not estimate RBEs of humna tumor cells with carbon beam irradiation from the radiosensitivities of cells with 200 KVp X-ray, but it might be necessary to look for some indicators to conjecture those to succeed the heavy particle therapy.

Table 1. Do, n values and RBE of each cell line.

Cell	Irradiation	Do(Gy)	n	RBE 0.1 S.F.
HeLa	200KVp Xray	1.87	1.35	
(cervix adeno)	20KeV Carb.	1.30	1.2	1.49
	80	0.78	1.6	2.24
SKGIIIB	200KVp Xray	1.37	2.6	
(cervix squamous)	20KeV Carb.	0.75	1.5	1.94
	80	0.59	1.0	3.47
SNGM	200KVp Xray	1.33	1.6	
(endometrium adeno)	20KeV Carb.	0.60	1.25	2.31
	80	0.43	1.0	4.06
SNGII	200KVp Xray	1.23	1.8	
(endometrium adeno)	20KeV Carb.	0.73	2.0	1.61
	80	0.57	1.0	2.56
HEC	200KVp Xray	0.95	1.35	
(endometrium adeno)	20KeV Carb.	0.68	1.0	1.55
	80	0.42	1.0	2.70
RMGII	200KVp Xray	1.75	2.1	
(ovarian mucinous)	20KeV Carb.	1.12	1.3	1.89
	80	0.67	1.2	3.23
RMG I	200KVp Xray	1.63	2.5	
(ovarian mucinous)	20KeV Carb.	1.23	1.3	1.77
	80	0.78	1.0	3.04
RMUG	200KVp Xray	1.60	1.3	
(ovarian mucinous)	20KeV Carb.	1.03	1.8	1.31
	80	0.60	1.0	2.92
RTSG	200KVp Xray	1.33	1.7	
(ovarian adeno)	20KeV Carb.	0.73	1.7	1.6
	80KeV	0.48	1.6	2.45
A431	200KVp Xray	2.43	1.5	
(esophagus squamous)	20KeV Carb.	1.37	1.7	1.70
	80	0.75	1.8	3.01
TE1	200KVp Xray	1.40	1.4	
(esophagus squamous)	20KeV Carb.	0.88	1.0	1.86
	80	0.43	1.0	3.67
TE5	200KVp Xray	1.38	1.7	
(esophagus squamous)	20KeV Carb.	0.73	1.0	2.54
	80	0.47	1.0	4.07
TE2	200KVp Xray	1.03	2.0	
(esophagus squamous)	20KeVCarb.	0.63	1.8	1.73
	80	0.40	1.0	3.75

CHROMOSOME ABERRATIONS INDUCED BY 135 MeV OF CARBON AND NEON BEAMS BY RRC.

Hiroshi OHARA[1],Masako MINAMIHISAMATU[2],Tatsuaki KANAI[2],Kiyomi EGUCHI-KASAI[2], Hiromi ITSUKAICHI[2],Kumiko FUKUTSU[2],Fumio YATAGAI[3], and Kohki SATO[2].
[1]Okayama Univ.,Gen. Edu.,Okayama,[2]NIRS, Chiba,[3]Inst. Phys. & Chem.,Wako.

Introduction : Radiation-induced chromosome aberrations can be a indicator of radiation lesions in a irradiated cells.Many studies on chromosome aberrations induced by X- and γ-rays have indicated that a dose response of aberrations can be fitted to a linear-quadratic equation,$Y=\alpha D+\beta D^2$ and becomes linear as LET of beams increases.Thus,main subject of this study was some quantification of chromosomal aberrations induced by 135 MeV/n of carbon and neon beams produced by RIKEN Ring Cyclotron (RRC), the operation of which increasingly became useful for the studies of heavy ion biology. The results will meet with some of radiobiological features connected to the specific actions of charged particles.

Materials & Method : Beam dosimetry was mainly carried out by using parallel plate ionization chamber counter, and its relative (calibration) dose and LET were determined at defferent depth to make up a Bragg curve. Variables of LET could be available if different thickness of aluminum foils was used as a absorber. 4 different LETs by 2 different ion beams were examined here.

Chromosome analysis was made by culturing whole blood irradiated with these two different ion beams.Fresh venous blood from a healthy male donor was used for the present study, and for each dose a irradiation chamber containing 3-5 ml of whole blood was positioned in the same place of beam dosimetry. Thus, 2-5 of cell cultures containing 1.0 mlwhole blood, 3.0 ml RPMI medium, 0.5 ml fetal calf serum,0.13 ml of phytohaemagglutinin for stimulation of lymphocytes were set up for each dose of experiments. After 49-51 hrs of culture time chromosome preparations were made up by staining Giemsa solutions. Chromosome analysis was carried out exclusively in first metaphase after exposure.

Results : Fig.1 showed 4 different curves of dose response for the production of dicentric and ring types of aberrations induced by carbon and neon beams as well with 4 different dose average LETs, which were determined for each experiments as 22.4 (●),41.5 (□),69.9 (▲) and 98.4 (■) KeV/μ,respectively. Only the lowest LET experiment showed upward concavity like those with protons, X- and γ-rays but other high LET groups showed transformation of dose response into linear particularly at initial phase under 4 Gy, during which region the aberration production rate becomes always higher as LET increases.A higher LET beam produces more aberrations if irradiation dose is the same.It was also the same to the fiding that high Z number of ion beams can produce much more

aberrant cells.These, however,three upper positioned high LET curves appear to level off beyond 5 Gy of exposures. In order to understand transformation of d ose response quantitatively dose-effect coefficeints and goodness of fit were examined if the dicentrics and rings data were fitted to the linear-quadratic model above described. Table showed the result of examination, where only the coefficient of linear part (α) increased as LET increased.An increase,however, in quadratic (two hit) type of aberrations is considered to be originally due to the increase of one hit breaks at G_1 pahse,since lymphocytes are invariably exposed to radiation before entering DNA synthesis of constituent chromosomes. Production of exchange (single hit) type of aberrations can not be expected. It is also noted that a dose response for quadratic type of acentric fragments including interstitial minute pairs increased as LET increased. Neon beams can produce much more fragment typpe of aberrations than carbon beams as irradiation dose increases. This means that ability of reunion between broken ends of chromosomes reduces as ionizing density of radiation increases.

Conclusion : Chromososme aberrations can be quantified as a indicator of radiation lesions and of beam passages in the case of high LET particle radiations. As LET of the beam increases, a dose response changes its form from curvilinear into linear with remarkable increase in quadratic types of aberrations, since none of exchange type could not be observed.If LET as well as Z-number of ion beams are higher, production rate in unrepaired type such as quadratic fragments becomes higher than in those repaired type such as dicentrics and rings when radiation dose is increased.A levelling off of dose response can be interpreted as due to an increase of interphase death in cells as radiation dose increases. The levelling off is apparently different from the qualities of ion beams. A high efficiency of neon beams in production of aberrations at first post irradiation metaphase may not necessarily reflect radiation damage to induce an interphase death of cells. The findings may indicate some of inhomogeneity of beam efficiency in high LET radiations.

References :

1. Kiefer,J.,1985,Cellular and subcellular effects of very heavy ions. Int.J. Radiat.Biol.48,873-892.
2. Geard,C.R.,1985, Charged particle ctogenetics:Effects of LET,fluence, and Particle separation on chromosome aberrations. Radiat.Res.104,S-112-S-121.
3. Ritter,S.,Kraft-Weyrather,W.,Scholz,M.,and Kraft,G.,1990,Influence of radiation quality on heavy ion induced chromosome aberrations in V79 cells. Radiation.Protection.Dosimetry 31,257-260.
4. Kiefer,J.,1992,Heavy ion effects on cells:chromosomal aberrations,mutations and neoplastic transformations. Radiat. Environ. Biophys. 31,279-288.

Table. Dose-coefficients and goodness of fit for dicentrics and rings data fitted to the linear-quadratic model $Y=aD+bD^2+c$. r=relative coefficient

Ions	LET (Kev/μ)	a ($10^{-1}Gy^{-1}$)	b ($10^{-2}Gy^{-1}$)	c (Gy^{-1})	r
carbons	22.4	1.14	6.33	0.239	0.917
carbons	41.5	7..6	-5.65	0.090	0.899
carbons	69.9	8.12	-2.45	-0.201	0.983
neons	98.4	14.48	-4,75	-0.512	0.998

Figure. Dose response curves fitted to linear quadratic model($Y=aD+bD^2+c$) in human lymphocytes irradiated with 135 MeV/n ofcarbon and neon beams at RIKEN.

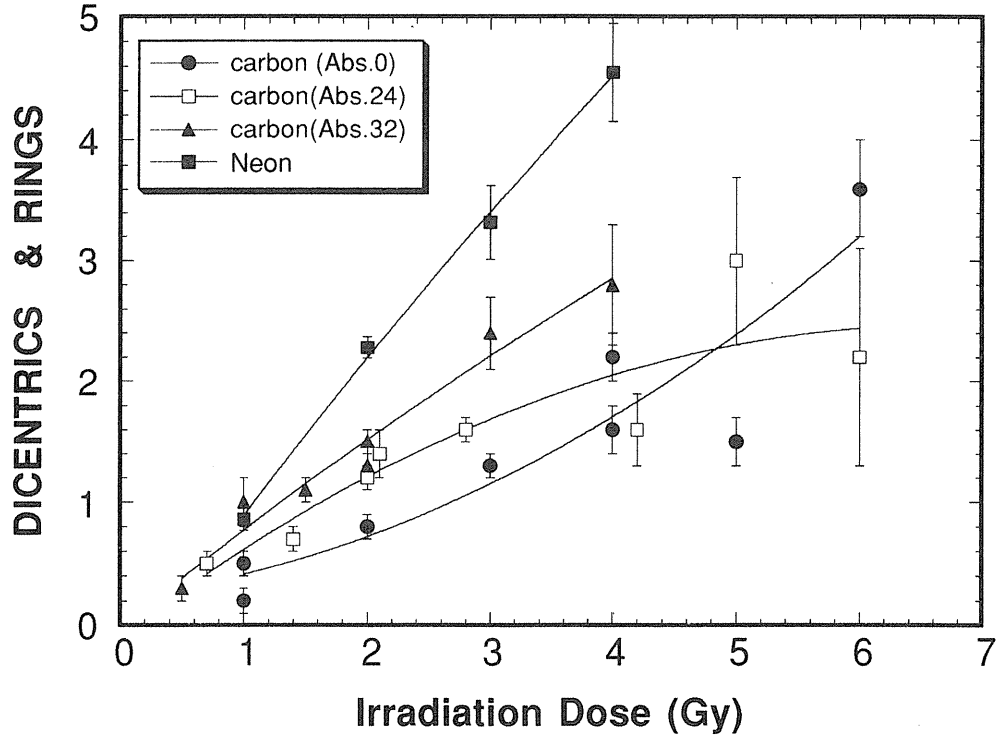

Sensitivity of ts85 Mutant Strain from Mouse FM3A Cells to Heavy Ions

Fumio Yatagai, Kazushiro Nakano, Tatsuaki Kanai*, Keiko Saito, Fumio Hanaoka

The Institute of Physical and Chemical Research, Wako, Saitama351-01

*) National Institute of Radiological Sciences, Anagawa, Chiba-shi 260

One of our interests in elucidating biological effects of heavy-ions is to get some insights into the induced DNA damages in mammalian cells. The cell cycle dependent change in the chromatin structure is generally believed to reflect one of the characteristics of the mammalian cells. In *Saccharomyces cerevisiae, RAD 9*-dependent response detects potentially lethal DNA damages and causes arrest of cells in G2 until such damage is repaired (1). The mutation in RAD 6, ubiquitin-conjugating enzyme E2, expresses the phenotype of G2 block through the lack of chromatin condensation. Interestingly, the *RAD 6* gene of *Saccharomyces cerevisiae* also plays a key role in postreplication repair of numerous chemical and physical DNA damages including UV- and X-ray induced lesions (2). The ts85 mutant strain from mouse FM3A , defective in ubiquitin-conjugating enzyme E1, represents the defects in the early step of chromatin condensation. The ts mutant cells as well as its wild-type were irradiated with ions of carbon and neon to study the contribution of this gene product to the repair of heavy-ion damages.

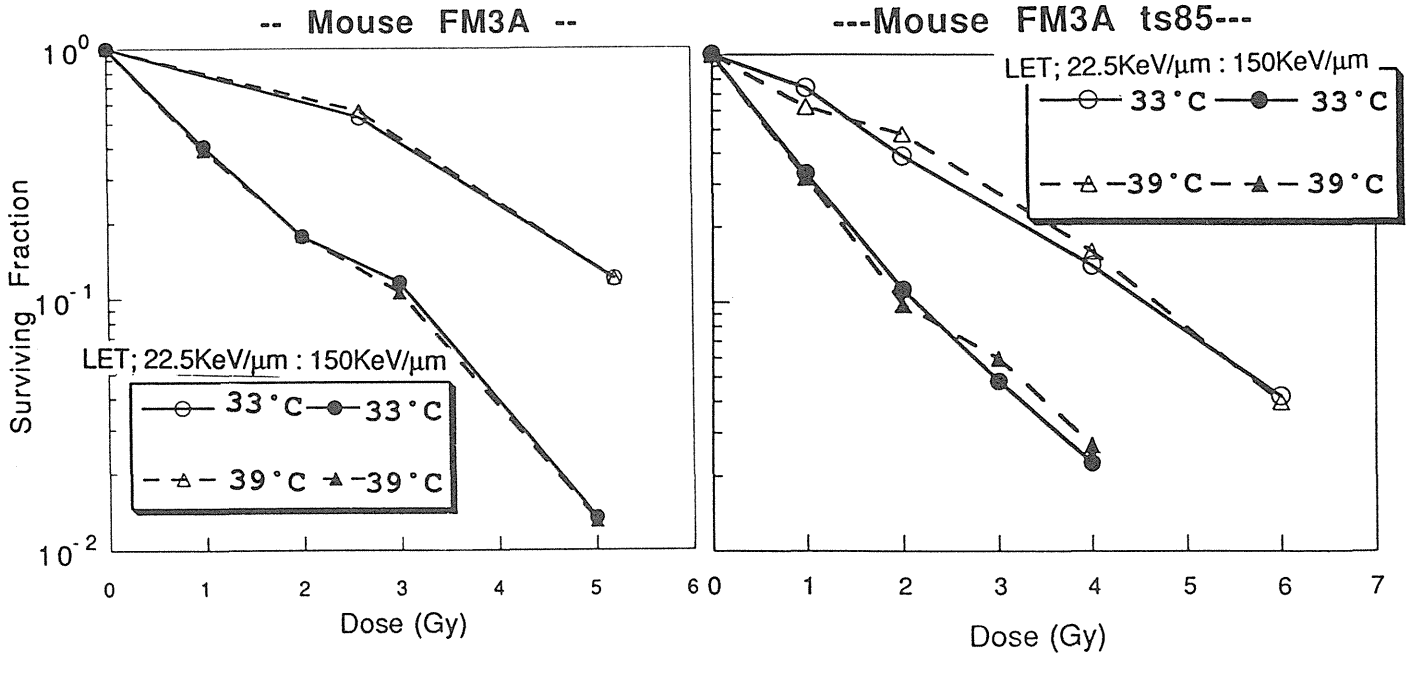

Fig.1 The survival curves of FM3A and its ts mutant ts85 cells for carbon ion .

The cells were cultured at 37°C in RPMI1640 medium and collected at the concentration of 3~5 X 10^5 cells/ml. They were resuspended at the cell density of 6 X 10^5 cells/ml with the same medium and exposed to C-ion or Ne-ion (135 MeV/n) accelerated by the RIKEN Ring Cyclotron. The irradiated cells were plated on the soft-agar and incubated at 39°C for 20 hours for the induction of ts phenotype. and then shifted down to 33°C. After continuing the incubation for approximately two weeks, the number of colonies were counted by the microscope. As the phenotypically non-expressed control, the plates were also incubated at 33°C without the above shifting up to 39°C. The survival curves obtained with C-ions, N-ions, and X-rays were shown in Figs. 1, 2, and 3, respectively.

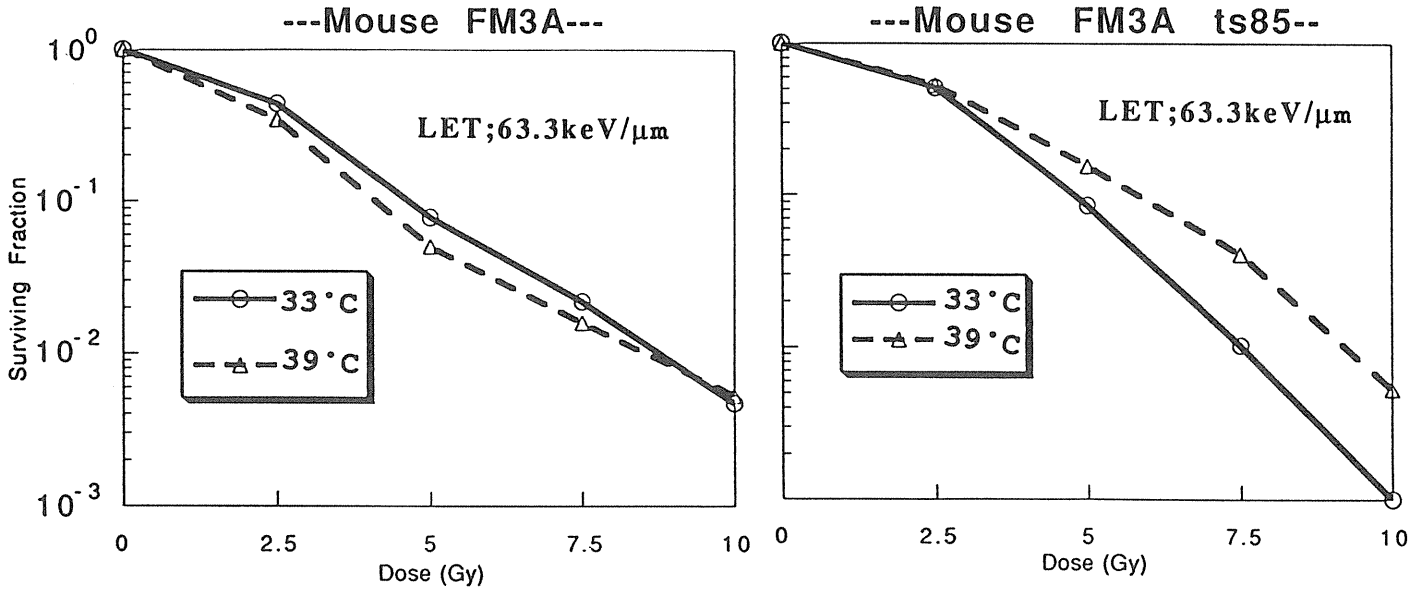

Fig.2 The survival curves of FM3A and ts85 cells for neon ion .

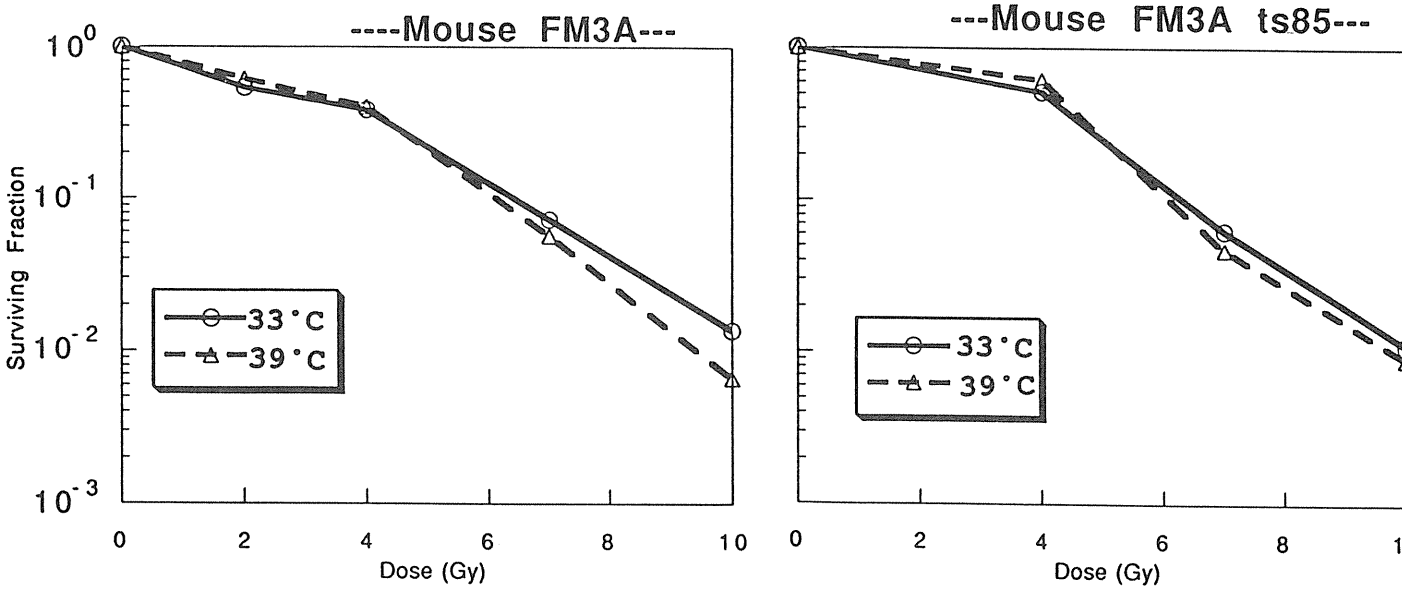

Fig.3 The survival curves of FM3A and ts85 cells for X-rays .

In contrast to UV-irradiation (data, not shown), the survival curves for ts85 mutant, irradiated with heavy ions and shifted up to 39℃ at the incubation, represent almost no sensitization compared to the curves of non-expressed cell, incubated at 33℃ following the irradiation (Figs. 1 and 2). This tendency seems to be not so much affected by the LET factor of heavy particles as far as we determined in this study. The tendency of LET-dependent sensitization by the temperature shift would be observed even with this sort of limited experiments if this mutant cell was sensitized by the δ-ray effect. In fact, this mutant cell irradiated with X-rays didn't show any sensitization (Fig. 3). Before getting the conclusion such as the function of ts85 mutation is, if not all, different from that of RAD6 in yeast, we have to check the detailed experimental conditions, for example, recovery of the lethal damage due to the delay in starting the incubation at 39℃, scavenging effect of the medium during the irradiation, etc.

The present experimental results also suggest that DNA damages are, at least, different from UV damages. At last we would like to refer that the methodology used for expressing the ts function was established by Dr. Hironobu Ikehata during his staying at our laboratory as a postdoctoral fellow.

REFERENCES

1) Weinert, T.A. and L.H. Hartwell (1988) *Science* **241** : 317-322.
2) Prakash, L. (1981) *Mol. Gen. Genet.* **184** : 471-478.

Enhancement of cell killing by split exposure of high LET heavy ion beams.

*Kiyomi EGUCHI-KASAI, *Hiromi ITSUKAICHI, *Masahiro MURAKAMI, *Kumiko FUKUTSU, **Yoshiya FURUSAWA, **Tatsuaki KANAI,*** Kazunori SHIMIZU, and *Koki Sato

*Div. Radiat. Hazards, **Div. Med. Phys., ***Hospital, Natl. Inst. Radiol. Sci., Chiba 263.

For cancer therapy by radiations, it is important to realize the effects of fractionated exposure. For X-rays, recovery from sublethal damage (SLDR) was known during cells were kept at 37°C for several hours between two separate exposures, and results in a reappearance of the shoulder of dose survival curves. With increasing LET of radiations, the shoulder decreases and SLDR decreased with increasing LET. In the high LET portion at the end of ion track, even an enhancement of cell killing (potentiation) was reported[1, 2]. As the cause of the potentiation, two possibilities are listed; they are (1) partial synchronization induced by the first dose by which cells are accumulated at a cell cycle position(s) sensitive to heavy ion exposure[1], and (2) interaction of damages individually induced by separate exposure[2]. In both hypothesis, it is postulated that the damages induced by particle beams with high LET are hardly reparable. We already showed the potentiation effect by split exposure of carbon ion beam at LET of above 140 keV/μm[3]. Here, we studied G_2 delay induced by first dose to know the population distribution at second irradiation. We also show the effect of caffeine which is known to release radiation induced G_2 block.

1. Potentiation by split dose

Asynchronous V79 cells were irradiated by X-rays (200 kV), ^{3}He (12 MeV/u, LET≈18.5 and 45.5 keV/μm) or carbon ion beam (12 MeV/n, LET≈250 keV/μm) and were kept at 37°C until next exposure up to 5 h. Recovery from sublethal damage (SLDR) was observed for the cells irradiated by X-rays ^{3}He ions of 18.5 keV/μm or 45.5 keV/μm (Fig. 1). Among these 3 radiations, extend of repair was smallest in ^{3}He ions with 45.5 keV/μm, biggest in X-rays. Therefore, extent of repair of SLD decreased with increasing LET of radiations. Whereas for cells irradiated by carbon ions, no recovery was observed, moreover the enhancement of cell killing was observed at 4 h interval (potentiation). Increasing the incubation time up to 5 h, bigger recovery in survival was observed for X-rays and ^{3}He, whereas bigger potentiation was observed for carbon ions. Extent of potentiation was smaller when cells were kept at room temperature until second dose than at 37°C(Fig. 2). At room temperature, cell cycle progression should slow down and the number of cells newly coming to G_2 phase after irradiation should decrease. Therefore this data may support the first hypothesis described above.

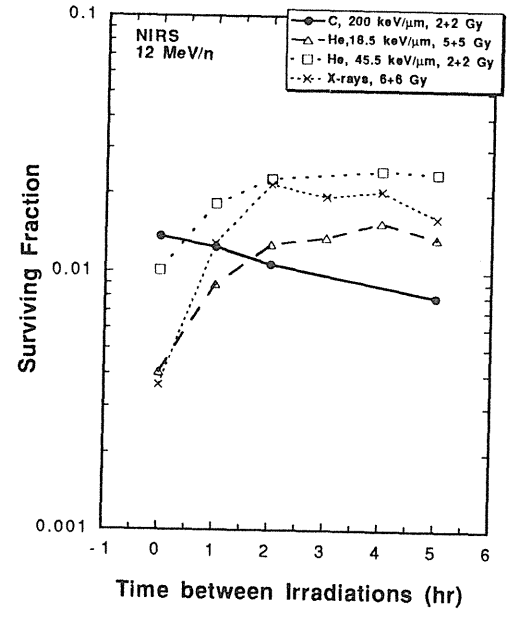

Figure 1 Time course of SLDR.

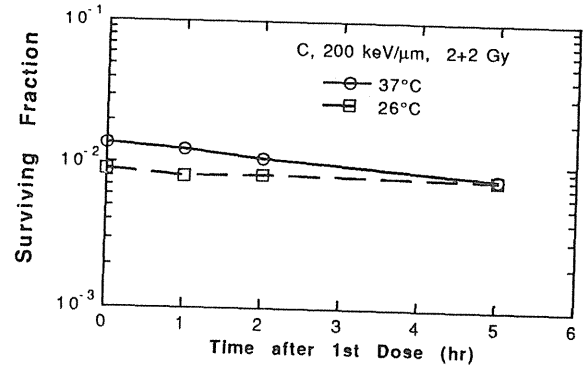

Figure 2 Time course of SLDR after carbon beam exposure.

2. Effect of caffeine

When 5 mM caffeine was added to the culture medium between the 2 doses of carbon ions, surviving fraction did not much change (Fig. 3a). Caffeine itself did not affect surviving fraction but reduced it when being added after irradiation. If this reduction is subtracted from decrease in split dose with caffeine, surviving fraction was almost same as single irradiation(Fig. 3b). These data also supported the first hypothesis. When caffeine was added after irradiation, decrease of surviving fraction for carbon ions is smaller than for X-rays.

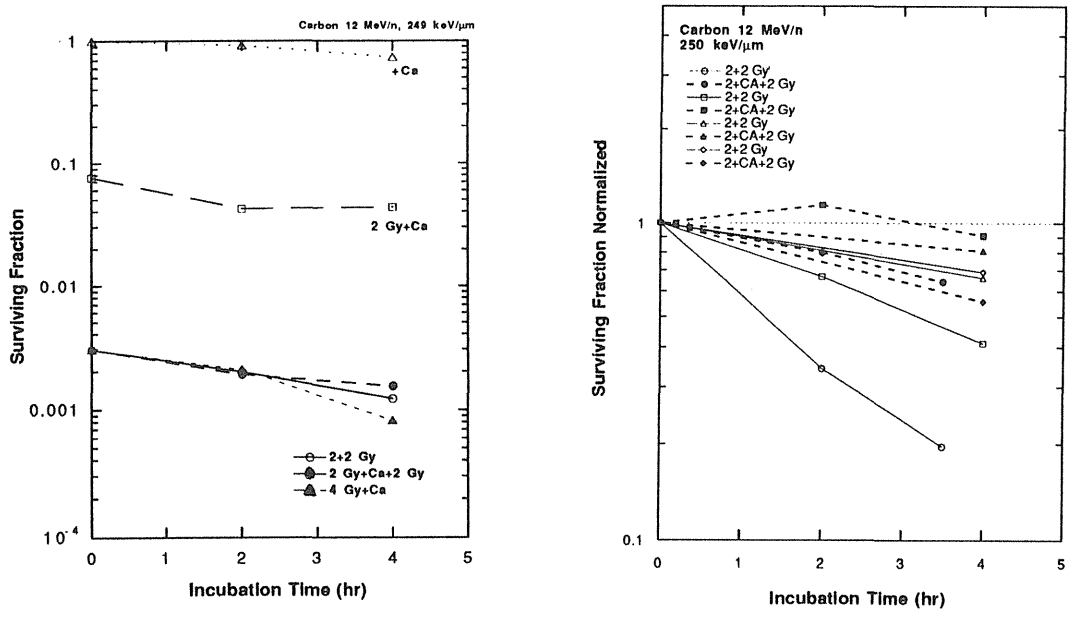

Figure 3 Effect of caffeine on cell survival. (a) Surviving fraction after 1st irradiation at time 0 with (●,o)or without (▲,□) 2nd dose. Caffeine was added at time 0 (Δ,▲,●,□). (b) Time course of potentiation with (closed symbols)or without (open symbols) caffeine. Different symbol came from different experiment. Data with caffeine were normalized to data treaded with caffeine following single dose.

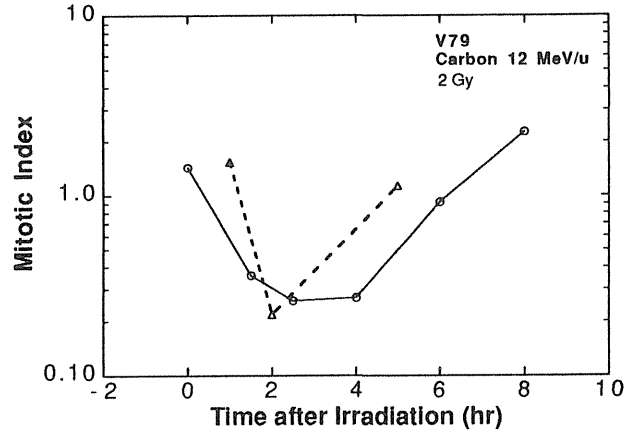

Figure 4 Change the mitotic index after irradiation by carbon ions. Different symbol came from different experiment.

3. G_2 delay

Mitotic Index (MI) was decreased until 3 to 4 h after an exposure by carbon ions of 2 Gy, and then increased to an original value at 6 h(Fig. 4). Caffeine released this G_2 delay. Preliminary FCM data also showed that more than 50% of the cells accumulated at a G_2/M phase at 4 h after irradiation(data not shown). It was reported that there is a difference in surviving fraction across the cell cycle, and cells in the M phase are sensitive even to high LET radiation[1, 2]. It can not be eliminated the interaction of damages. However the most of the potentiation might be caused by partial synchronization induced by the first dose. However this potentiation effect may take place even for low LET radiations, the increase of survival by SLDR is bigger than decrease by potentiation. For high LET carbon beams, SLDR should be very small or absent, only the effect of potentiation can be visible.

References

1. Kraft-Weyrather, W., *et al.*, *Fractionated irradiation with heavy ions at low energy.* GSI Report GSI-91-29, 1991. : p. C6.

2. Blakely, E.A., *et al.*, *Heavy-ion radiobiology: Cellular Studies,* in *Advances in Radiation Biology, Vol. II,* J.T. Lett, Editor. 1984, Academic Press: New York. p. 295-389.

3. Eguchi-Kasai, K., *et al.*, *Effects of split exposure of heavy ion beams at several positions of spread-out Bragg peak.* Proceedings of the second workshop on physical and biological research with heavy ions, 1992. **NIRS-M-90, HIMAC-003**: p. 14-15.

LET dependency of mutation induction at the HGPRT locus and molecular characterization of mutations in human cells irradiated with accelerated heavy ions

Masami WATANABE[1], Masao SUZUKI[1,2], Yoko KASE [1], Fumio YATAGAI[3], Tatsuaki KANAI[4] and Takeshi KATO[5]

1 Division of Radiation Biology, Department of Health Sciences, Nagasaki University, 1-14 Bunkyo-machi, Nagasaki 852, Japan; 2 Division of Radiation Biology, School of Medicine, Yokohama City University, 3-9 Fukuura, Kanazawa-ku, Yokohama 236, Japan; 3 The Institute of Physical and Chemical Research, 2-1 Hirosawa, Wako-shi, Saitama 351, Japan; 4 National Institute of Radiological Sciences, Chiba, Japan and 5 School of Medicine, Osaka University, Osaka 565, Japan.

HGPRT mutation, LET dependency, human cell

ABSTRACT: The incidence of mutation in cells irradiated with carbon ions was higher than that in cells irradiated with ^{137}Cs gamma-rays. The RBEs, compared to ^{137}Cs gamma-ray, were between 2.7-7.2 for carbon ions when it was compared at the same absorbed dose level and the highest value was 7.2 for 124 keV/μm carbon ions. DNA isolated from 201 independently derived mutants was examined by polymerase chain reaction (PCR). Primers for 8 exons of human *hprt* gene were used in a multiplex reaction to show rapidly whether the mutants carried deletions at these site. Few deletions were found among the spontaneous set, while 'total' gene deletions formed about half the mutants found after irradiation. At equilethal doses little difference in mutant spectrum was found for the gamma-ray set compared to heavy ion set. In the case of mutants induced by carbon ions, the proportion of complete deletion mutants was dependent on the LET of carbon ions. All mutants induced by 124 keV/μm carbon ions were total gene deletions, while all of mutants induced by 230 keV/μm carbon ions were not deletions. These results suggest that different LET radiation induce different mutation spectra and the present procedures will be useful for somatic mutagenesis studies.

1.INTRODUCTION

Several studies have focused on the molecular structure of radiation-induced mutations and have found that the most common lesion is a large deletion of genetic information(Thacker, 1986, Vrieling et al., 1985). However, only few studies have been reported in the literature determining how the molecular structure of radiation-induced mutations is affected by heavy ions. We previously reported that heavy ions were generally more effective in cell killing, chromosome aberration induction, mutation induction and neoplastic cell transformation induction than gamma-rays in SHE cells (Watanabe et al., 1991; Suzuki, K. et al., 1991; Suzuki, M. et al., 1989; 1992). It is clear from track structure studies that heavy ions can deposit large clusters of ionizations in DNA which may produce qualitatively different types of initial damage from those produced by the sparsely-ionizing X- or gamma-rays (Goodhead, 1988). It is considerable interest, therefore, to examine the nature of mutations induced by heavy ions in comparison to those induced by gamma-rays. In this study, we detected mutation induction at *hprt* locus in human cells irradiated with carbon ions with several LET (22, 39, 68, 75, 110 124, 148, and 230 keV/μm) and examined the

molecular characterization of mutations.

2.MATERIALS AND METHODS

2.1.Cells

Primary human embryo (HE) cells were isolated from embryonic abdomen tissue by mincing with scissors, which was then followed by a mild trypsinization at 37°C for 20 min in order to make a single cell suspension. The medium (Eagle's minimum essential) supplemented with 0.2mM serine, 0.2 mM aspartate, 1 mM pyruvate and 10% fetal calf serum, was previously described (Watanabe et al., 1992). Their cloning efficiency on plastic was over 80% for the passage 2 cells.

2.2.Irradiation

Cells were irradiated at confluence (about 90 % of cells were in G_1 or G_o phase) at room temperature(20°C). The carbon ions were generated by RIKEN ring cyclotron at the Institute of Physical and Chemical Research (RIKEN) and the cyclotron at National Institute of Radiological Science (NIRS). The details of the irradiation procedures and dosimetry have been described elsewhere (Suzuki, K. et al., 1989; Suzuki, M. et al., 1992). Briefly, the fluence of carbon ion beams was measured with a plastic scintillator and the value of LET was measured with a proportional counter filled with tissue equivalent gas. The energy of heavy ion beam were 135MeV/n (RRC) and 12 MeV/n (NIRS) for carbon ions and 135MeV/n(RRC) for neon ions. We changed LETs of beams by changing the Lucite absorber thickness. LET values at the sample position were estimated to be varied from 22 to 230 keV/μm. The dose rate was about 1 Gy/min in all beams. For comparison, we irradiated HE cells with ^{137}Cs gamma-rays at dose rate of 1.2Gy/min.

2.3. Mutant colony isolation

After irradiation, cells were grown in non-selective medium for 7 days, with subculturing as required and then placed into medium containing 40mM 6-thioguanine (Sigma) at $7.8x10^2$ cells/cm^2. The cells were incubated in a CO_2 incubator for 16-20 days and a mutant colony was randomly isolated from each set of dishes using a micropipette tip and small volume of complete medium. One mutant only was isolated from each culture to ensure independence of mutations. The isolated cells were cultured and stored in liquid nitrogen using the DMSO-freezing method.

2.4.DNA preparation and PCR reaction

The mutant cells were placed in a microfuge tube to which 5μl of 10% Nonidet P40 and 5μg of 2mg/ml protease K were added, and the volume made up to 100 μl with distilled water. After mixing, the tubes were then heated at 95°C for 5 min and centrifuged at 12 ,000 rpm for 5 min. The supernatant of each tube was removed and used in the PCR reaction. Eight sets primers were used in a multiplex reaction to amplify exons 2-9 on the *hprt* gene. 250 μg DNA was mixed with 7 primer pairs in a total volume of 50 μl containing 6.7mM $MgCl_2$, 16.6mM $(NH_4)_2SO_4$, 6.8μM EDTA, 5mM beta-melcaptethanol and 67 mM Tris HCl, pH8.8 and 5 mM each deoxyribonucleotide triphosphate. The mixture was heated at 95 °C for 5 min to denature DNA and annealed at 60°C for 15 min. Two units of *Tag* DNA polymerase (Promega Corporation) and 30 μl of mineral oil was added to the mixture. After preheating at 60°C for 15 min, the PCR reaction was performed 30 cycles of 94°C for 30 sec/60°C for 48 sec/70°C for 2min, followed by final extension at 70°C for 7 min with Perkin-Elmer Thermocycler. The PCR products were analyzed on 4% agarose gel electrophoresis in TBE buffer (89mM Tris HCl, 89mM boric acid, 2mM EDTA, pH 8.0) at 8.3 V/cm for 1 h at room temperature. The gel was stained with ethidium bromide.

3.RESULTS AND DISCUSSION

3.1. LET dependence for hprt mutation induction

Carbon beams were more effective for the induction of mutations at *hprt* locus in HE cells than gamma rays and the RBE relative to gamma rays increases with LET up to about 100-120 kev/μm and decreases at higher LETs. On the basis of our data, the RBEs, compared to ^{137}Cs gamma ray, were between 2.7-7.2 for carbon ions when it was compared at the same absorbed dose level and the highest value was 7.2 for 124 keV/μm carbon ions. It is worth noting that the RBE for mutation appears to peak at about 100-200 keV/μm. This LET dependency is coincident with those for induction of chromosome damage measured as PCC breaks and degree of lethal effects (Suzuki,M. et al., 1989; 1992), and morphological transformation (Suzuki, M. et al., 1989).

3.2.PCR analysis of spontaneous, gamma-ray and carbon-ion mutants

A total of 129 independently-derived mutants were analyzed. Table I summarizes the data collected on all the 6TG resistant cell lines. About 30% of spontaneous and gamma-ray induced mutants showed no change in the band migration pattern. Spontaneous mutants had no 'total' gene deletions, while almost 40% of the gamma-ray induced mutants did.

In the case of mutants induced by carbon ions, however, the proportion of 'total' gene deletion was dependent on the LET of carbon ions. Almost all mutants induced by 68 and 124 keV/μm carbon ions lacked any detectable *hprt* specific sequences and therefore were caused by deletions of the entire locus, while all mutants induced by 230 keV/μm carbon ions had no deletion. Also there was a larger proportion of partial gene deletions in the spontaneous and gamma-ray mutant set than among carbon ions mutants.

It is perhaps surprising that the 230 keV/μm carbon ions set have no deletions, given the biggest track structure among all of carbon ions used in this study. In addition the 68 and 124 keV/μm carbon ions are inducing deletions of all 8 exons. This result is inconsistent with the previous report (Aghamohammadi et al., 1992). They found that at equilethal doses, little difference in mutant spectrum was found for the X-ray induced mutants compared to the alpha-particle (121 kev/μm) induced mutants. However, it is not clear which component of energy deposition pattern from heavy ion tracks is responsible for mutation induction.

TABLE I MULTIPLES PCR OF *hprt* EXONS 2-9 IN SPONTANEOUS AND RADIATION-INDUCED MUTANTS

Treatment	Total mutants assayed	All 8 exons present	Partial exons deleted	Number of deleted exon[a]							All 8 exons deleted
				2	3	4	5	6	7-8	9	
none	18	5(28%)	10(56%)	1		1	7	6	8	8	3(17%)
gamma-rays	41	13(32%)	12(27%)	1	0	8	8	8	10	10	18(44%)
Carbon ions (kev/μm)											
39	16	8(50%)	4(25%)	2	1	1	2	2	1	1	4(25%)
68	14	0(0%)	0(0%)								14(100%)
124	41	3(7%)	0(0%)								38(93%)
230	32	32(100%)	0(0%)								0(0%)
Neon ions											
104	24	1(4%)	12(50%)	2	1	2	8	8	8	7	11(46%)
230	15	3(20%)	9(60%)			1	8	9	9	9	3(20%)

a) Many mutants loss of plural number of exons.

It may be that for mutation endpoint, which requires cell viability for recovery, only moderate clusters of energy deposition in DNA from carbon ions are responsible; these damage events may overlap in severity with damage from gamma-ray track ends, and so yield a similar mutations for mutational effectiveness of heavy ions than primary large clusters of energy deposition in DNA. Since large clusters of energy deposition from higher LET radiations may be dominantly lethal, it is likely that only low clusters of energy deposition from secondary electrons may be responsible for mutants induced by 230 keV/μm carbon ions.

So far in molecular studies, mutation spectra of different radiations have been examined mostly at single doses of X-rays may have different mutation spectra (Morgan et al., 1990; Whaley and Little, 1990). In the present study we reported that different LETs of heavy ions have different mutation spectra. Such phenomena require critical examination using large numbers of independently-isolated mutants; it is clear that the methods introduced in this report may be used to examine such aspects of comparative mutagenesis, also to examine biological meaning of track structure of heavy ions, where may mutants need to be assessed rapidly at the molecular level.

4.ACKNOWLEDGEMENTS

This work was supported by a Grant-in Aid from the Ministry of Education, Science, and Culture of Japan; by a Grant-in Aid from the Technology Agency of Japan.

5.REFERENCES

Aghamohammadi, S. Z., T. Morris, D. L. Stevens and J. Thacker (1992) *Mutation Res.*, **269**, 1-7.

Goodhead, D. T. (1988) *Health Phys.*, **55**, 231-240.

Morgan, T. L., E. W. Fleck, K. A. Poston, B. A. Denovan, C. N. Newman, B. J. F. Rossiter and J. H. Miller (1990) *Mutation Res.*, **232**, 171-182.

Suzuki, M. W., M. Watanabe, K. Suzuki, K.Nakano and I.Kaneko (1989) *Radiat. Res.*, **120**, 468-473.

Suzuki,K., M. Suzuki, K. Nakano, I. Kaneko and M.Watanabe (1990) *Int. J. Radiat. Biol.*, **58**, 781-789.

Suzuki, M., M.Watanabe, K.Suzuki, N. Nakano and K. Matsui (1992) *Int. J. Radiat. Biol.*, **62**, 581-586.

Thacker, J. (1986) *Mutation Res.*, **160**, 267-275.

Vrieling, H., J. W. I. M. Simons and A. A. Zeeland (1988) *Mutation Res.*, **198**, 107-113.

Watanabe, M., V. M. Maher and J. J. McCormick (1985) *Mutation Res.*, **146**, 533-547.

Watanabe, M., M. Suzuki, K. Suzuki and K. Watanabe (1991) *In vitro Toxicol.*, **4**, 93-100.

Watanabe, M. and K. Suzuki (1991) *Mutation Res.*, **249**, 71-80.

Whaley, J. M. and J. B. Little (1990) *Mutation Res.*, **198**, 107-113.

The effects of cell death and mutation induction irradiated with accelerated carbon ion beams with spread out Bragg peak.

Masao SUZUKI[1),2)], Masami WATANABE[2)], Yoko KASE[2)], Tatsuaki KANAI[3)], Fumio YATAGAI[4)], Takeshi KATO[5)] and Sho MATSUBARA[1)]

1) Yokohama City University, Yokohama 236
2) Nagasaki University, Nagasaki 852
3) National Institute of Radiological Sciences, Chiba 263
4) The Institute of Physical and Chemical Research, Wako 351
5) Osaka University, Osaka 530

1. Introduction

We have studied the LET dependence of cell death, mutation induction and chromatin damage in human embryo (HE) cells irradiated with monoenergetic carbon ion beams. The results showed that the effects of cell death, mutation induction and induction of non-repairable chromatin breaks were the same LET dependence. Carbon ion beams of 110 to 124keV/μm were the most effective of the effects. The spectrum of deletion pattern of exons in HPRT locus of carbon-ion-induced mutants was LET specific. Almost all the mutants induced by 124keV/μm beams showed deletion of the entire gene, while all mutants induced by 230keV/μm beams showed no deletion.

In this study we investigated the biological effects irradiated with carbon ion beams spread out Bragg peak (SOBP) to study the responsibility of biological effects by difference in the density distribution of carbon ion track and secondary electron. We also tried to accumulate biological data in carbon ion beams spread out of Bragg peak for radiotherapy.

2. Materials and Methods

2.1 Cell

Human embryonic (HE) fibroblast-like cells were used. HE cells was cultured in Eagle's minimum essential medium, supplemented with 0.2mM serine, 0.2mM aspartate, 1mM pyruvate and 10% fetal bovine serum in a 5% CO_2 incubator at 37^{0}C.

2.2 Irradiation

HE cells were inoculated into 25cm^2 plastic flasks at 8x10^5 cells per flask 2 days before irradiation. The cells were irradiated with carbon ion beams spread out of Bragg peak accelerated by the Riken Ring Cyclotron at the Institute of Physical and Chemical Research in Japan. The details of the irradiation procedures and dosimetry have been described elsewhere [1]. We irradiated HE cells at the entrance, proximal, middle and distal peak position in spread-out Bragg peak.

2.3 Cell survival and mutation assay

After irradiation, different number of HE cells were immediately plated onto 100mm plastic dishes to form 60 to 70 colonies per dish for cell survival assay. Residual cells were cultured in 75cm^2 plastic flasks at a density of 1.5 to 2.0x10^6 cells per flask and subculture was carried out three times at 5 to 6 day intervals to allow expression of mutation. After the expression period, 1x10^6 cells were plated onto 20 dishes containing MEM medium supplemented with 40μM 6-thioguanine (6TG). The frequency of mutation was determined as the number of 6TG-resistant colonies per 10^6 survivors.

2.4 Molecular characterization of HPRT mutants

Extracted DNA from 6TG resistant colony was mixed with 7 primer pairs of HPRT exons in 50μl of PCR reaction solution containing 67mM Tris HCl (pH8.8), 6.7mM $MgCl_2$, 16.6mM $(NH_4)_2SO_4$, 6.8μM EDTA, 5mM ß-melcaptethanol and 0.5mM each deoxyribonucleotide triphosphate. The mixture was heated at 95°C for 5min to denature the DNA which was then annealed at 60°C for 15min. Two units of Taq DNA polymerase and 30μl of mineral oil added. The PCR reaction was performed for 30 cycles at 94°C for 30sec / 60°C for 48sec / 70°C for 2min. The PCR products were analyzed by 4% agarose gel electrophoresis.

3. Results and Discussion

Figure 1 shows the dose-response curves for cell death irradiated with four different positions of spread-out Bragg peak and ^{137}Cs gamma rays. The RBE relative to gamma rays at 10% survival level was 1.5 at entrance, 1.9 at proximal, 2.0 at middle and 2.5 at distal position in spread-out Bragg peak. The effect of cell death increased with increasing average LET of spread-out beams. This effect is consistent with our data using monoenergetic carbon ion beams.

Figure 2 shows that the mutation frequencies of spread-out beams steeply increase at low doses compared with gamma rays. The RBE which calculated as 100 mutants per 10^6 survivors was 2.4 at entrance, 4.1 at proximal, 2.4 at middle and 2.7 at distal position.

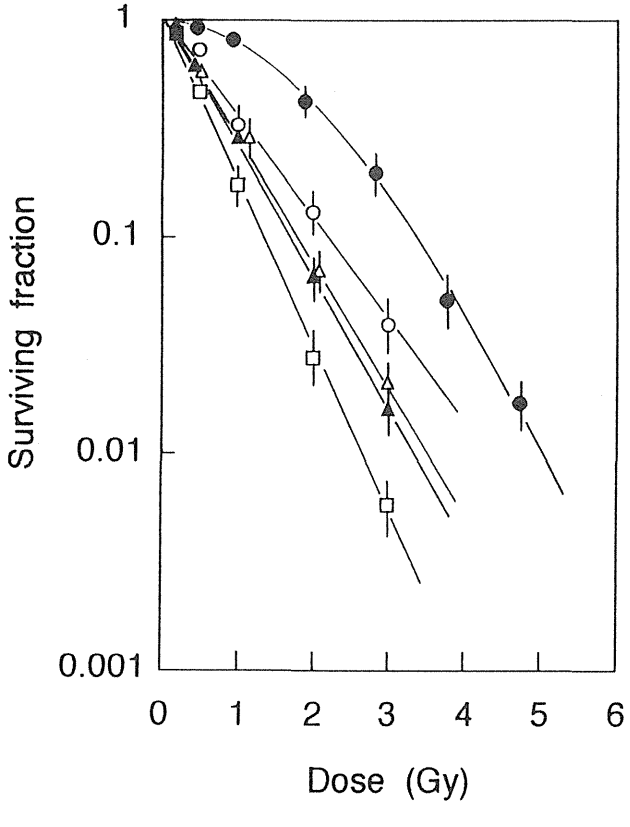

Figure 1. Effect of cell death irradiated at the entrance (○), proximal (△), middle (▲) and distal (□) position in SOBP beams. (●); ^{137}Cs gamma rays.

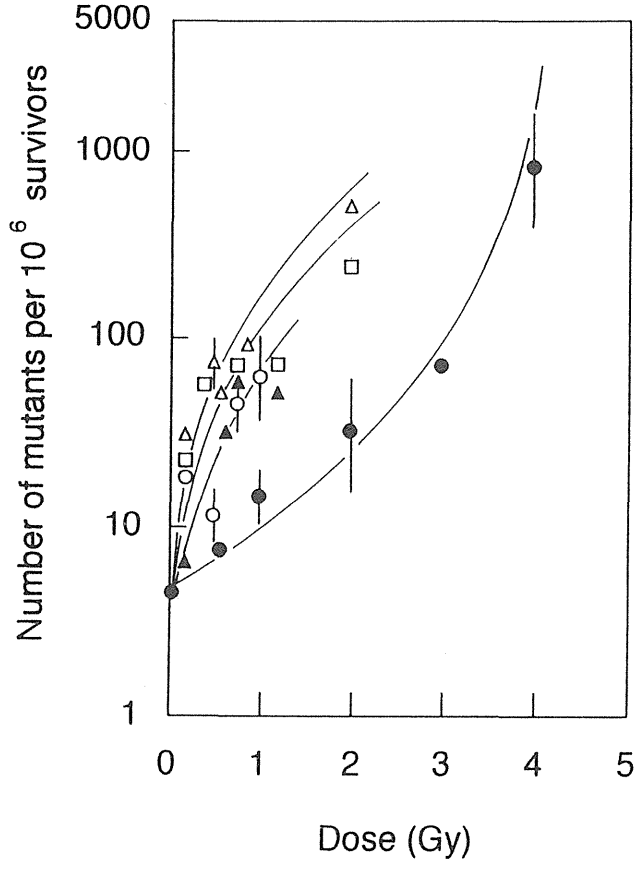

Figure 2. The dose repsonse curves of mutation induction irradiated with four different positions in SOBP beams.Symbols are the same in fig.1.

Figure 3 illustrates examples of various types of mutants analyzed by gel electrophoresis. Table 1 summarized the data obtained for all the 6TG-resistant mutants. About 75% of SOBP-entrance-induced mutants showed partial deletions in the band migration pattern of gel electrophoresis. On the other hand, 69% of SOBP-proximal-induced mutants showed all exons deleted pattern. The increase of all exons deleted mutants in proximal position (average LET ~ 80keV/μm) rather than in entrance position (average LET ~ 35keV/μm) is the same LET dependence with monoenergetic carbon ion beams.

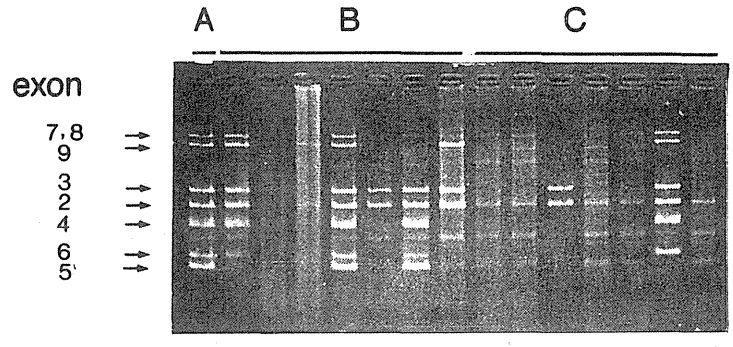

Figure 3. Photograph of gel electrophoresis with multiplex PCR products of 7 exons in the HPRT locus. A; control, B; mutants induced by the entrance position of SOBP beams, C; mutants induced by the proximal position of SOBP beams.

Table 1. Summary of the structure of the HPRT locus in spontaneous, ^{137}Cs gamma rays and carbon ions induced mutants.

Radiation	Total mutants assayed	Number of mutants								
		No alteration	All exons deleted	Partial deletion[a)]						
				total	exon 2	3	4	5	6	7,8	9
Spontaneous	8	2	2	4	1	0	0	1	0	2	2
^{137}Cs γ rays	41	13	18	11	1	0	8	8	8	10	10
C ions(entrance)	22	4	2	17	0	0	14	13	16	6	14
C ions(proximal)	39	1	27	11	0	0	5	5	11	5	5

a); Some mutants loss of plural number of exons

4. Reference

1. T.KANAI,S.MINOHARA,M.SUDOH,T.KOHNO, E.TAKADA, F.SOGA, K.KAWACHI Y. FURUSAWA, K. FUKUTSU, K. EGCHI-KASAI, H. ITSUKAICHI, H. OHARA and F.YATAGAI, Beam modulation for heavy ion radiotherapy. Proceedings of the Second Workshop on Physical and Biological Research with Heavy ions. 1-3 (1992).

Effects of High LET Radiation on Murine Skin and Tumors

Koichi Ando, Sachiko Koike, M.Iizuka, T.Aruga, N.Hori, W.Shimizu, T.Sugita, S.Murayama, T.Kanai, S.Minohara, M.Sudo and F.Yatagai *

Natl. Inst. Radiol. Sci., Chiba, and RIKEN * Wako, Japan

Physical characteristic of charged particle beams promise an excellent dose distribution by which a deep-seated tumor could be irradiated with Spread-Out-Bragg-Peak(SOBP) while its surrounding normal tissues would receive minimal doses. As we have already experienced cyclotron fast neutrons, and will use carbon beams in clinical trials, comparisons of biological effectiveness between carbons and neutrons are of great interest. We here investigated and reported effects of carbons, neons and neutrons on the skin and transplanted tumors in mice.

1. Skin

Right hind legs of C3H female mice were irradiated by 3 beams;i.e., (1)unmodulated carbon-12 and neon-20 which were accelerated by the RIKEN Ring Cyclotron at 135MeV/n, (2) cyclotron-produced fast neutorns(30 MeVd-Be) and (3) ^{137}Cs γ rays. Skin damage cause by irradiation was quantified by the tattoo method. Prior to irradiation, two spots of Indian ink were tattooed intradermally in the right hind legs. Distance between the two spots was measured by calipers, and a ratio of (distance in irradiated individuals) to (distance in pre-irradiated ones) gave percent skin shrinkage. **Fig.1** shows skin shrinkage 30days after carbon irradiation with single-and 8 fraction-doses. Equal doses were employed for the fractionated schedule which set an inter fractional internal of 12 hours. Reduction of skin damage was obvious for fractionated γ rays while no sparing effect was detected for fractionated 100keV/μm carbons. Relations between LET and RBE were determined using single doses of carbons and neons. LETs of carbons were 22,43 ,72 and 100keV/μm while those of neons were 74,100, 174 and 232 keV/μm. **Fig.2** shows bell-shaped curves for the LET-RBE relationship, and maximal RBEs at LETs ranging from 100keV/μm to 150keV/μm. RBEs also depended on level of skin damage: RBEs were small for sever damage or for large doses.

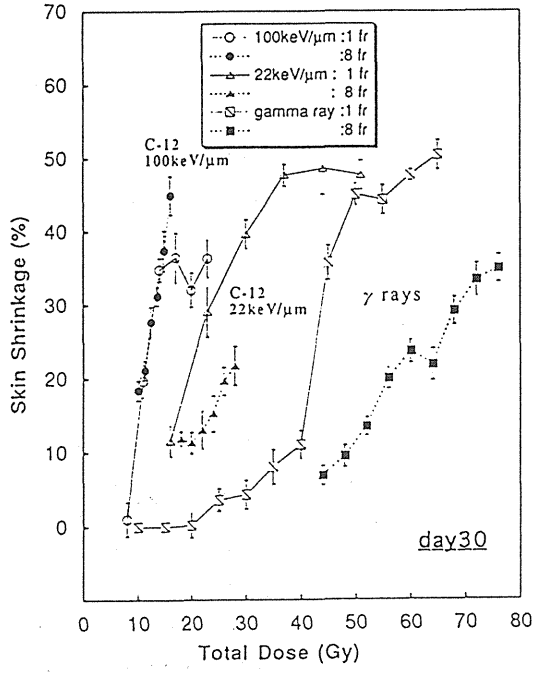

Fig.1 Early Skin Shrinkage after Single and 8-fractionated Doses of Unmodulated Carbon-12

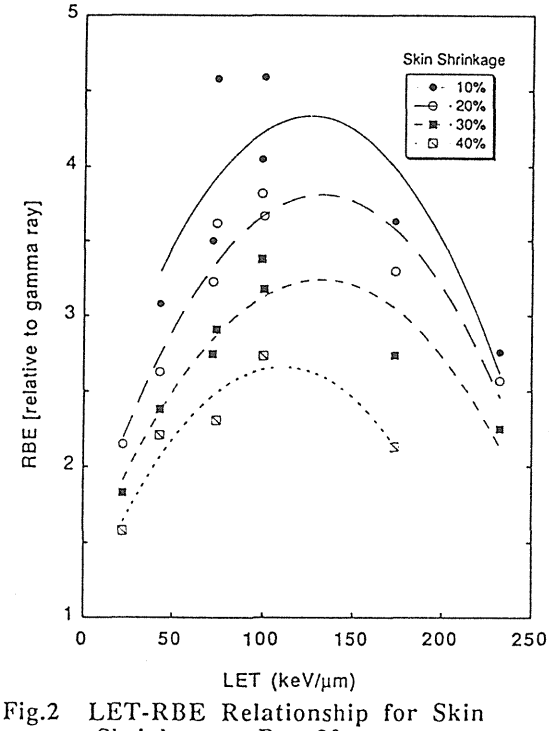

Fig.2 LET-RBE Relationship for Skin Shrinkage at Day 30. Data for unmodulated carbons (LET=22, 43, 72 and 100 keV/μm) and unmodulated neons (LET=74,100, 174 and 232 keV/μm) were included.

RBEs of carbons for skin reaction were investigated and compared with those for skin shrinkage. Hair of the right hind legs were removed by epilatory 7-11 days before irradiation. Skin reaction induced by radiation was scored by a modified Aizawa's method(1); minimal reaction received a score of 0.5 and maximal reaction did 5.0. Scoring started from Day 7, and was conducted every other day till Day 35. Mean scores were obtained by averaging data at Day 9 through Day 30. **Fig.3** shows dose- responses of skin reaction after single dose of Carbons, fast neutrons and γ rays. Carbons beams of 100keV/μ m was the the most effective radiation qualities, followed by 72keV/μ m, 43keV/μ m and 22keV/μ m in order. Maximal skin scores for 100keV/μ m and 72keV/μ m of carbons were lower than those for 43keV/μ m and 22keV/μ m of carbons; the saturation of damage or dose independence was also found in skin shrinkage (See Fig.1)(2,3). Fast neutrons showed a dose response similar to 43keV/μ m and 22keV/μ m of carbons, even though neutrons showed a steeper curve than carbons. RBEs for skin shrinkage were compared with those for skin reaction (**Fig.4**). An isoeffect for skin shrinkage used here was 25% while that for skin reaction was 2.5. RBEs of carbons increased with LET for either endpoints. Skin reaction showed a larger LET dependence than skin shrinkage.

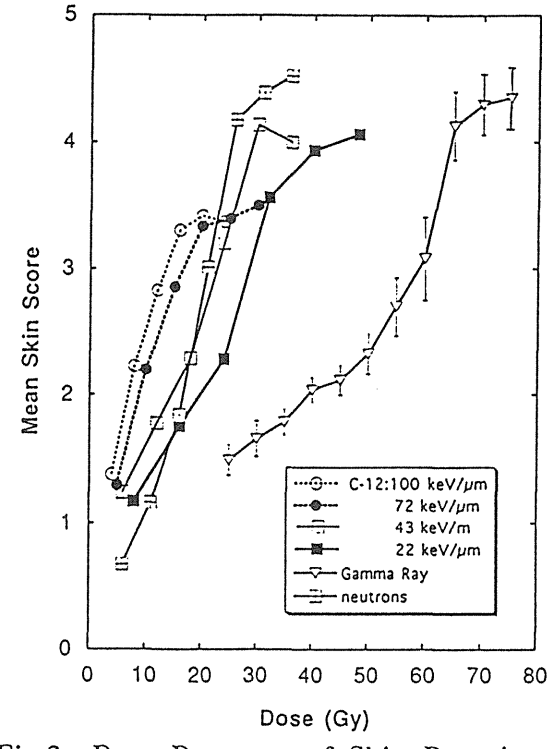

Fig.3 Dose Response of Skin Reaction after Carbon-12, Neutrons and Gamma Rays

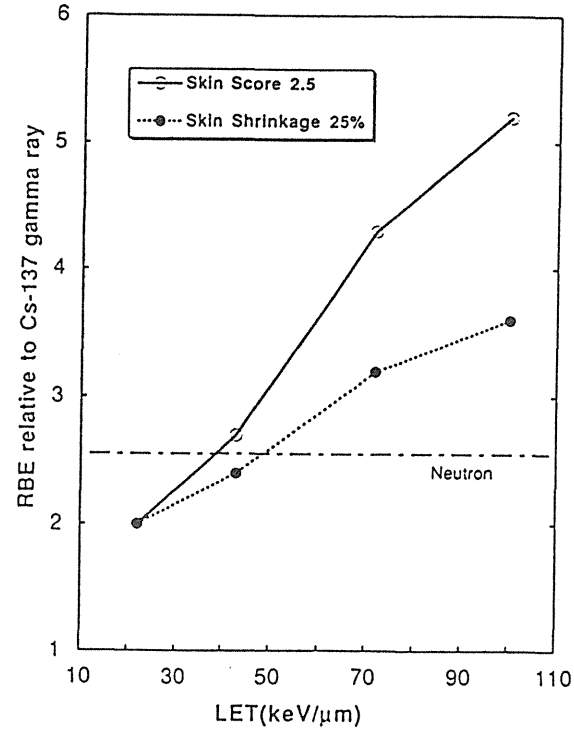

Fig.4 Dissociation of RBEs between Skin Reaction and Skin Shrinkage

2. Tumor

A murine fibrosarcoma, NFSa, was transplanted into the right hind legs of syngeneic C3H male mice and irradiated in vivo with single doses of carbons, fast neutrons and γ rays. A lucite range modulator spread out the Bragg peak of 135 MeV/n carbons to 30 mm wide by which tumors were irradiated. Tumor volume was measured every other day and tumor growth time, i.e. days for tumor to reach 5 times initial volume, was graphically obtained on tumor growth curves. As tumor volume at the time irradiation varied,depending on machine time, from 7mm to 10mm in diameter, growth delay for irradiated groups was expressed as relative growth delay which was obtained by a raio of (tumor growth time in an unirradiated control) to (tumor growth time in an irradiated group).

Fig.5 demonstrats that he shape of the dose-response curves for γ rays, fast neutrons, unmodulated plateau of carbons (23keV/μ m) and proximal SOBP(Spread-Out-Bragg-Peak) of carbons (61keV/μ m) was similarly downward concave. On the other hand, both middle SOBP (78keV/μ m) and distal SOBP(108keV/μ m) of carbons showed rather linear dose-responses. These results indicated that β term in the linear-quadratic model remained in both fast neutrons and carbons of plateau and proximal SOBP while α term was dominant in the distal and middle SOBPs. RBE values of carbons and fast neutrons were calculated at various isoeffects in Fig.5, and shown in **Fig.6**. Distal and middle SOBPs of carbons showed a large dependence of RBEs on doses;i.e.,RBEs of distal SOBP carbons decreased from 5 to 2.4 when doses increased form 1 to 25 Gy. Dependence of RBEs on doses was small for both proximal SOBP and unmodulated plateau of carbons. Fast neutrons showed a unique RBE-LET relation; RBEs of neutrons were larger than those for plateau /proximal SOBP of carbons, and remained large when doses increased. It is interesting to know that RBEs for distal/ middle SOBPs were larger than those for neutrons at doses of less than 10 Gy , but smaller than those for neutrons at doses of 20 Gy or over.

These results implied that the tissue damage caused by carbons is different form that by neutrons. The recoil protons secondarily produced by neutrons may be responsible to the difference.

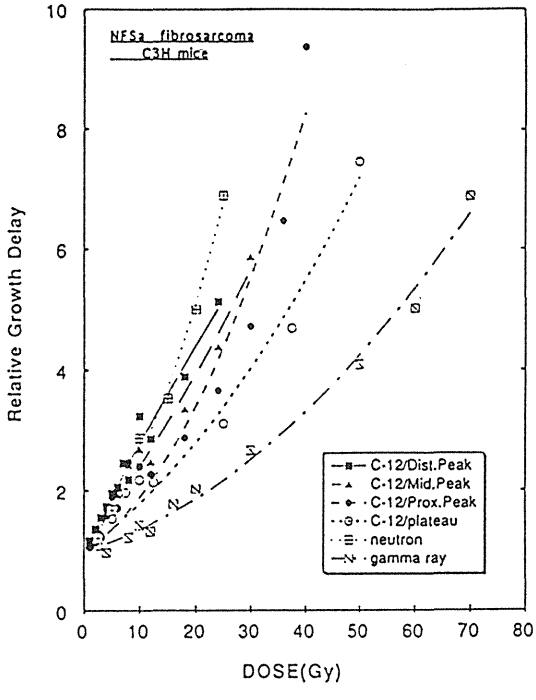

Fig.5 Tumor Growth Delay after Carbon-12, Fast Neutrons and Gamma Rays

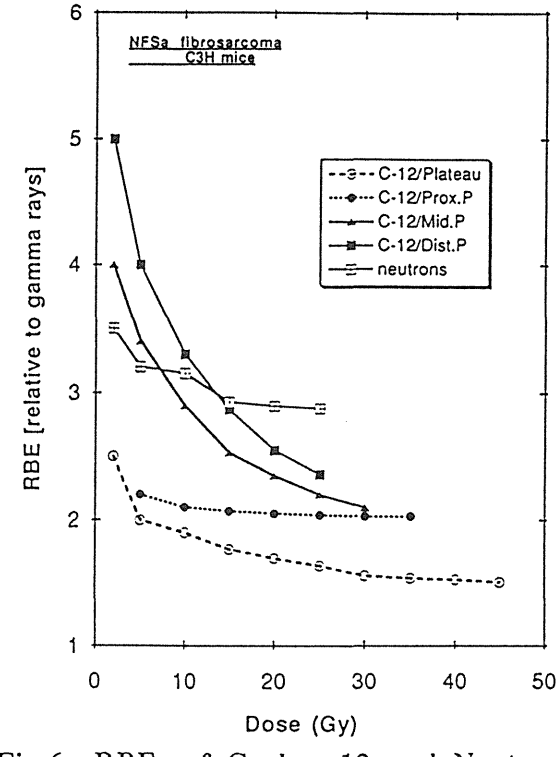

Fig.6 RBEs of Carbon-12 and Neutrons for Tumor Growth Delay

References

1. Hisashi Aizawa:Relative biological effectiveness of fast neutrons, observed in the skin reaction of mice, after single or fractionated irradiation. Nippon Acta Radiologica 33(7),602-616, 1973
2. Koichi Ando and Hideo Tatsuzaki:Volume effect;From a radiobiological point of view. Jpn.J.Cancer Clin.38(12),1339-1343, 1992
3. K.Ando, S.Koike, S.Furukawa, M.Kimoto, M.Iizuka, T.Kiuchi, T.Aruga, W.Shimizu, T.Sugita, C.K.Cho, T.Kanai, S.Matsushita and F.Yatagai: Saturation of skin damage after accelerated carbon particles.Int.Congress Radiation Oncology (ICRO '93) abstract 457, 1993

The irradiated volume dependency of early skin reaction after carbon ion beam irradiation.

*Hideo TATSUZAKI, *Toshiyuki OKUMURA, *Hideyuki TAKAHASHI, *Makiko MIYAKAWA, **Tatsuaki KANAI, **Shin-ichi MINOHARA, **Michio SUDOU, †Fumio YATAGAI.
*Institute of Clinical Medicine, University of Tsukuba; **Accelerator Physics and Enginearring, National Institute of Radiological Sciences; †Radioisotope Technology Division, Institute of Physical and Chemical Research.

Introduction

The tolerance dose of an organ is depend on some (or many) factors like LET, irradiated volume. The efects of irradiated volume on a tolerance dose with different LET beams should be clarify to develop better radiation therapy. So as to studing the above point, this experiments was performed using a skin of mouse as the target organ.

Materials and methods

Twelve weeks old female C_3H/He Slc mice (SPF) were used for this experiment.

All the irradiation was performed at the Institute of Physical and Chemical Research using ring-cyclotron. Two kinds of radiation with different LET was used. One is the entrance plateau portion of an original mono-peak beam of a 135 MeV/u carbon-ion beam and the other is middle portion of three cm spread out Bragg peak (SOBP) from the same carbon-ion beam. This SOBP is produced by rotating range modulator. The flatness of SOBP is adjusted biologically so as to get 10% survival of V79 cells uniformly. The LET values of these beams at skin surface was around 22 keV/μ and 71 keV/μ respectively. The beams were collimated to 25, 15, or 5 mm width slit-shape with copper final collimator. In this way, irradiated volume of legs were changed. The mice were irradiated under anesthesia using 65 mg/kg sodium pentobarbital i.p. injection.

Early skin reaction was used as an end-point. Seven days before irradiation, the lower hint leg of the mice was shaved using

razor blade for the preparation of an observation. The irradiated skins were observed every other day from seventh post-irradiation day to 35th post-irradiation day. An area independent skin score (Table) modified from Fowler's or Aizawa's one was used because irradiated area was different among three groups. The peak score during observation periods were used for the analysis.

Results

We show the preliminary results of these experiments. Fig.1, 2, and 3 show peak skin reaction of 25 mm slit irradiation, 15 mm slit irradiation, and 5 mm slit irradiation, respectively. The reaction is saturated above certain dose level with 15 mm and 5 mm slit irradiation. The saturation level of score is different between 15 mm slit and 5 mm slit group. Volume dependency is more eminent in higher dose region. Also these figure indicate that RBE difference tends to be small with small volume irradiation.

Table

Area independent skin score

score	descriptions
0.5	doubt of any difference from normal/ graying
1.0	slightly reddening
1.5	definite reddening, dry desquamation (+-)/ no hair with slight atrophy
2.0	severe reddening or dry desquamation (+) atrophy
2.5	dry desquamation (++)/ scales
3.0	moist desquamation (+-)
4.0	moist desquamation (+)
5.0	moist desquamation (++)

Figures

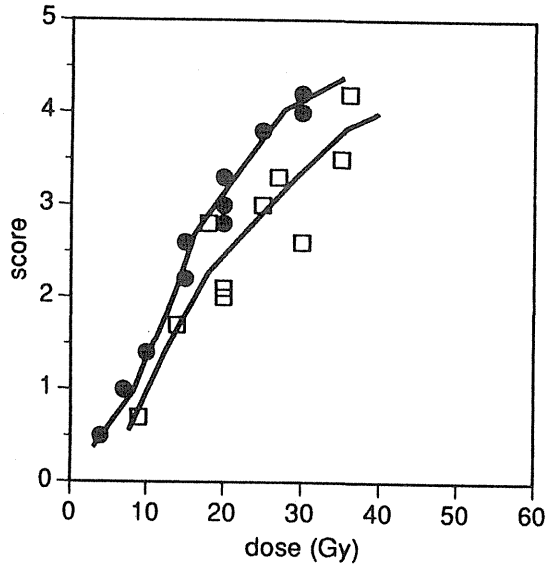

Fig.1 Peak skin score of 25 mm slit irradiation.
Open square shows entrance portion; closed circle shows SOBP.

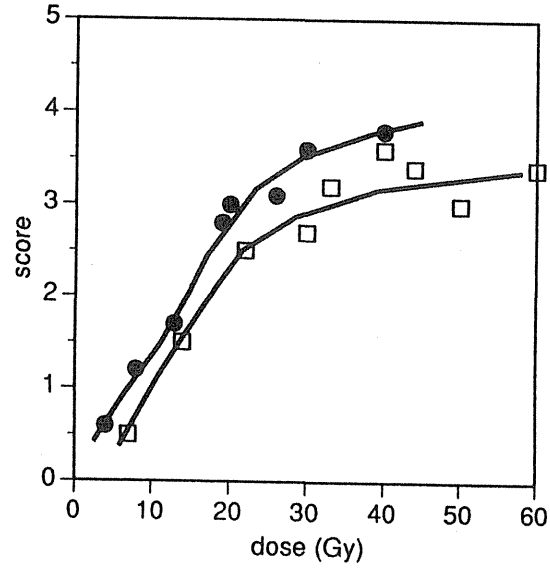

Fig.2 Peak skin score of 15 mm slit irradiation.
Open square shows entrance portion; closed circle shows SOBP.

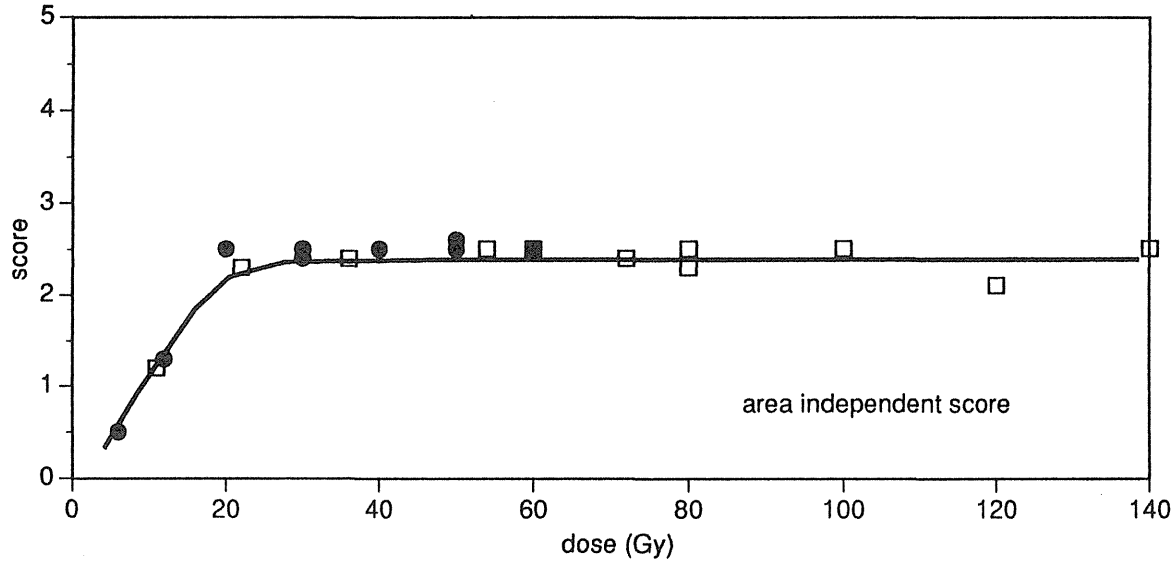

Fig.3 Peak skin score of 5 mm slit irradiation. Open square shows entrance portion; closed circle shows SOBP.

The effects of carbon beam on hemopoietic systhem in mice.

Atsushi Tsuboi, Eiichi Kojima, Kaoru Tanaka

It is necessary to obtain the quantitative data on the responses to radiation on normal tissues for therapeutic use of radiations. For that, we previously reported RBE values of carbon beam as the bases of the radiation effects on some normal tissues which were CFU-S and GM-CFC in bone marrow or spleen.

In the present paper, the effects of 135Mev/u carbon beam on Meg-CFC in bone marrow or spleen, blood cells in peripheral blood and survivals of mice were compared with the effects of 200 kVp x-rays on them.

8-10 weeks old male ddY-SLC mice were used all of the experiments. Anesthetized mice were irradiated with 200 kVp x-rays at 0.7 Gy/min or 135Mev/u carbon beam at 2-3 Gy/min. The cell preparations of bone marrow and spleen were performed as decribed in previous report. The bone marrow or spleen cells were seeded in 0.4 ml of a plasma culture including 10% lymphocyte conditioned medium. After 5 days incubation, the cultures were fixed with 5% glutaraldehyde and stained for acetylcholinesterase activity. The acetylcholine esterase positive colonies were scored as Meg-CFC. Whole blood were harvested from irradiated mice and collected in tubes containing the anticoagulant DPTA-2K. Leukicyte, erythrocyte and thrombocyte in the peripheral blood of irradiated mice were evaluated by using Sysmec K100 for 20 days after irradiations. The LD50/30 values were determined by monitering the numbers of survival mice daily during 30 days post-irradiation period.

Megakaryocyte progenitor cells (Meg-CFC) in bone marrow of irradiated mice were assayed to determine the dose relationships for 135 Mev/u and 200 kVp x-rays. The dose response to Meg-CFC in bone marrow exhibited no shoulders in both cases of the irradiations, carbon beam and x-rays. However, the slope of the dose response curve on cabon beam was little steepr than that of the dose response curve on x-rays. The D_o doses of Meg-CFC in bone marrow were 0.5 Gy for carbon beam and 1.0 Gy for x-rays. Therefore, the RBE value of carbon beam in term of Meg-CFC was 1.25 for bone marrow. On the other hand, the slope of the dose response for Meg-CFC in spleen of x-irradiated mice was great shallow which indicated extremely radioresistance to x-ray. One of the reasons is that presumably the spleen may be changed to hypoxic state by anesthetization. It is in general that the effects of high LET radiations on tissues were not much accelerated by hypoxic condition. Therefore, the RBE value of carbon beam for Meg-CFC in spleen resulted in extremely high, 4.1.

The kinetic of leukocyte, erythrocyte and thrombocyte in irradiated mice did not show any significant changes for 20 days post-irradiations with 2 Gy in between mice irradiated with x-ray and with carbon beam. As already reported, the survival fractions of CFU-S in spleen were not significantly different among mice irradiated with 2 Gy of the two radiation sources. Therefore, such survivals of stem cells may reflect to peripheral blood cells.

Figure I showed the dose response curves of survivals in mice

for 30 days after irradiations with graded doses of x-rays or carbon beam (open cycle : carbon beam, open triangle ; x-rays). The two response curves were provided for profit analysis and evaluated for RBE of carbon beam for LD50/30 which resulted in 1.4. The broken line in figure I indicate the dose response curve of 30 day survivals of mice irradiated with x-rays without anesthetization. Therefore, the present data of RBE for carbon beam will be varied when non anesthetized mice were irradiated with carbon beam.

Legend

Figure I , Dose-Mortality of mice for 30 ddays following single whole body irradiations with carbon beam or x-rays.
Open triangle : anesthetized mice of mortality irradiated x-rays.
Open cycle : anesthetized mice of mortality irradiated carbon beam.
broken line ; non anesthetized mice mortality irradiated x-rays.

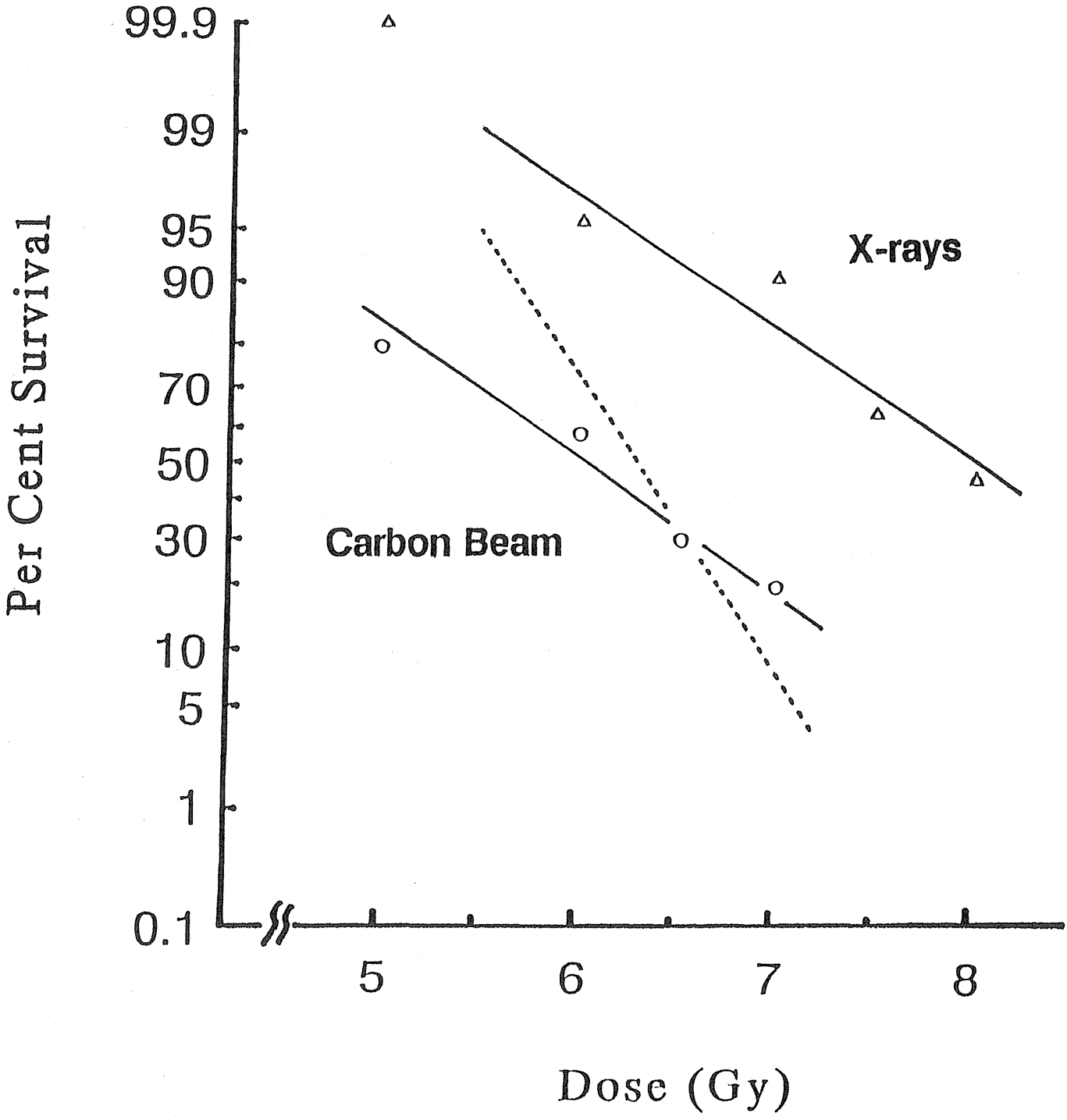
99.9
99
95
90
70
50
30
10
5
1
0.1
Per Cent Survival
X-rays
Carbon Beam
5
6
7
8
Dose (Gy)

Response of Mouse Intestine after Fractionated Doses of Accelerated Carbon-Ion with Spread-Out Bragg Peak

K. Fukutsu, T. Kanai, Y. Furusawa, T. Aruga, S. Murayama, S. Hori, S. Minohara, S. Koike, F. Yatagai*, and K. Ando
Natl. Inst. Radiol. Sciences, Chiba and *Inst. Phys. Chem. Res., Saitama 351-01.

Introduction

For a clinical trial of a heavy ion radiation therapy, it is necessary to know the effects of fractionated doses of accelerated heavy ion on various biological systems. Responses of mouse intestine after fractionated dose of carbon beam were examined. The carbon beam (135 MeV/u) accelerated by the RIKEN ring cyclotron facility, was modulated to have a spread-out Bragg peak of 3 cm width. The flatness of biological effect for the spread-out Bragg peak were investigated.

Materials & Methods

C3H female mice, age of 16 - 22 weeks old were used. Mice were irradiated to the whole body with Nembutal anesthesia at different depths in the spread-out Bragg peak (SOBP) and entrance part of unmodulated carbon beam. The SOBP was designed for 135 MeV/u carbon beam so that V79 cells were uniformly killed in the peak [1]. Responses of gamma-rays of a ^{137}Cs (0.62 Gy/min) unit for reference and of neutron beam of NIRS cyclotron were also used. Three equal dose of fractionated exposures were given at 4-hour intervals. The number of surviving ileum crypt cells per circumference was examined 3-1/2 days after irradiation by the method of Withers and Elkind [2].

Results & Discussions

Figure 1 shows the effects of anesthesia for gamma-ray and neutron. For gamma-rays irradiation, Nembutal anesthesia was found to reduce radiosensitivity of crypt cells against the single irradiation, but not against the fractionated irradiation. The doses required to reduce survivals to the level of ten crypt stem cells per circumference (D_{10} doses) were estimated as 15.1 Gy for single doses without anesthesia, 18.1 Gy for single doses with anesthesia, 23 Gy for fractionation. For neutron irradiation, no difference in radiosensitivity was found between

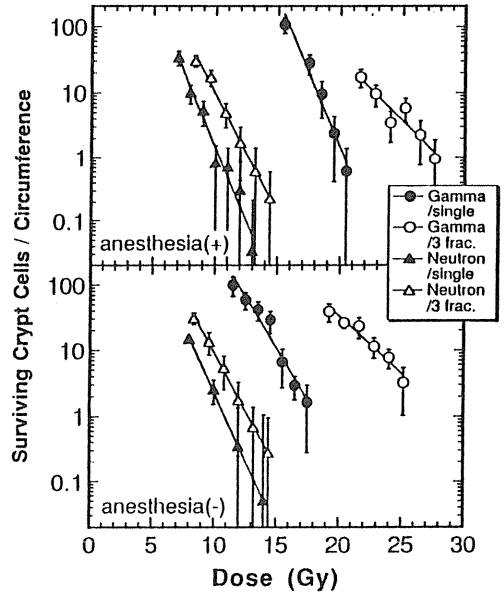

Fig. 1 Effects of anesthesia for gamma-ray and neutron.

with and without anesthesia. The D_{10} doses were estimated as 8.3 Gy and 9.9 Gy for single and fractionated doses, respectively. The mechanisms of reducing radiosensitivity with the Nembutal anesthesia are not known yet. For the investigation of the responses of carbon irradiation, Nembutal anesthesia was used to fix the depth of the crypt cells of the mouse.

Figure 2 shows the surviving crypt stem cells per circumference. Dose response curves of gamma-ray and unmodulated carbon are displaced towards higher doses, indicating that recovery occurs during fraction intervals. The dose modification factors at D_{10} doses were calculated as:

$DMF_{10} = D_{10}$ (fractionated irradiation) / D_{10} (single irradiation).

The DMF_{10} were 1.46 for unmodulated. For neutron and SOBP position, a few recovery occurs during fraction intervals. The DMF_{10}s were 1.22, 1.25, 1.23, and 1.14 for neutron, proximal, mid, and distal, respectively. The resultant RBE_{10}s for fractions were 2.29, 2.26, 2.54, and 3.22 for neutron, proximal, mid, and distal, respectively. Effects of neutron are nearly equal to between proximal and mid in SOBP.

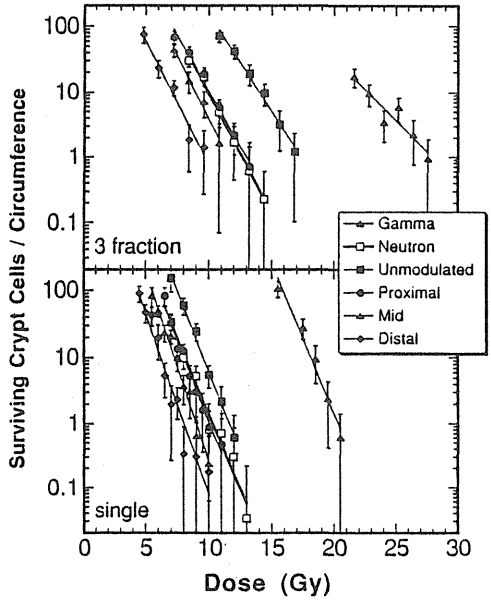

Fig. 2 Relationship between total dose and survival of crypt stem cells in mice exposed to single or 3 fractionated doses.

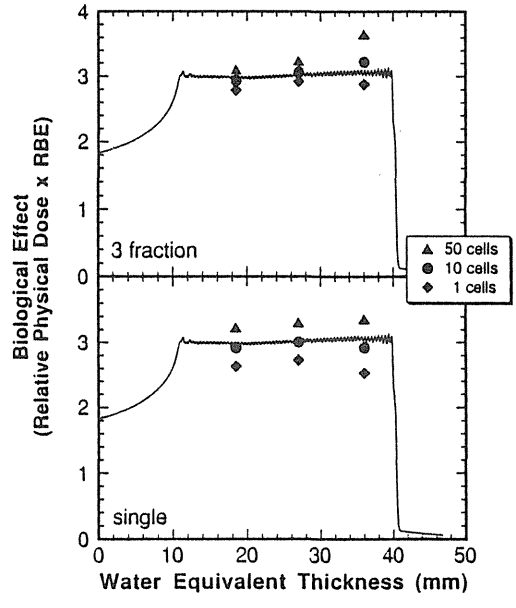

Fig. 3 Biological dose at 1, 10, and 50 cells survival level .

The biological doses for SOBP were calculated from the RBE obtained (Figure 3). The biological dose was defined as (total fractionated dose) x (RBE). The 50, 10, 1 cells indicated in the figure were estimated from the doses required to reduce survivals to the level of 50, 10, 1 crypt cells per circumference, respectively. As the survival level of the crypt cell is larger, the biological dose of the deeper region of the SOBP becomes larger than the proximal peak. The doses per

fractionation decrease according to change level from 1 cell of single doses to 50 cells of 3 fractionated doses. The dose response curves of crypt stem cells have large shoulder for low LET radiation [3]. These shoulders may affect the flatness of biological effect for low doses per fractionation. The variety of flatness of biological effects for fractionation will be investigated for multifractionations.

References

[1] T. Kanai, *et al.*, NIRS-M-90 HIMAC-003, pp.1-3, 1992.

[2] H. R. Withers and M. M. Elkind, Int. J. Radiat. Biol. 17, 261-267, 1970.

[3] H. R. Withers, *et al.*, Int. J. Radiat . Oncol. Biol. Phys. 1, 41-52, 1975.

Dose response relations in acute cell death of pancreatic islets after whole body irradiation of golden hamster with ^{60}Co gamma,70MeV proton and 135MeV carbon beams.

*Susumu TSUBOUCHI, **Kumiko FUKUTSU, **Hiromi ITSUKAICHI,** Masahiro MURAKAMI, **Kiyomi KASAI, **Yoshiya FURUSAWA,**Tatsuaki KANAI, **Sachiko KOIKE, **Kouichi ANDO,***Hiroshi OOHARA,****Fumio YATAGAI, and*****Eiichi KANO; *Lab. of Radiat. Biol.,Dept. of Radiol. Tech., Faculty of Health Sci., Suzuka Univ. of Med. Sci. and Tech.; Suzuka 510-02, ** National Inst. of Radiol. Sci.; Chiba 260, ***Dept. of Biol., Faculty of General Education, Okayama Univ., Okayama 700, ****RI Lab. , The Inst. of Phys. and Chem. Res., Wako 351-01, ****Dept. of Exptl. Radiol. and Health Physics, Fukui Med. School ;Fukui 910-11.

Dose response relations in acute cell death of pancreatic islet was studied at mainly 4 and 5.5hours after single or split dose irradiation of golden hamster with high dose rates,30-70Gy/min,of gamma, proton and carbon beams. As compared to the previous results of low dose rate irradiation of x-rays(4-5Gy/min) , dose dependence of the cell death with high dose rate irradiation was not always consisitent in all dose range, especially in high dose. In the case of low dose rate irradiation of X-rays, clear dose response relations of cell death was ovserved at 5 hours after irradiation with Do of 62.5 Gy and n of 3.2. One of the possibilities might be because of more rapid cell lysis in high dose rate irradiation. However this tendency was consisitent even at 3 hours after irradiation with high dose rate of carbon and gamma beams. Histologically uneven distribution of cell death in the islet was occasionally recognized and also vascular damages of pancreas was characteristic. Thus, it is suggested some sort of physiological factor,such as acute ischemia by arteritis might contribute this tendency in high dose rate. In spite of this unsolved problem, it was suggested that irradiation with high LET carbon and proton beams were less effective than that with gamma beams. But SLD repair (one hour interval) was not observed in all these three beam irradiaitons. Also the lack of repiar was previously observed in x-ray beam irradiation of low dose rate.

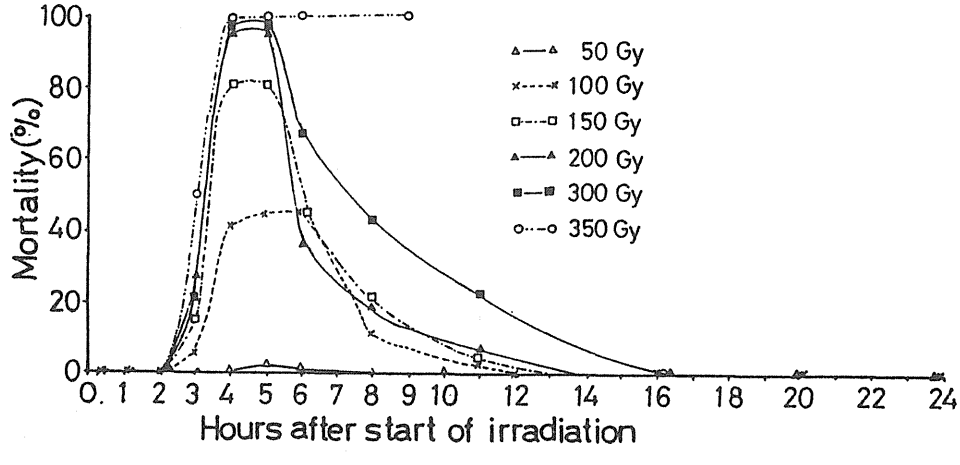

Fig. 1 Mortality of islet cells at various times after various doses of low dose rate of X-rays.

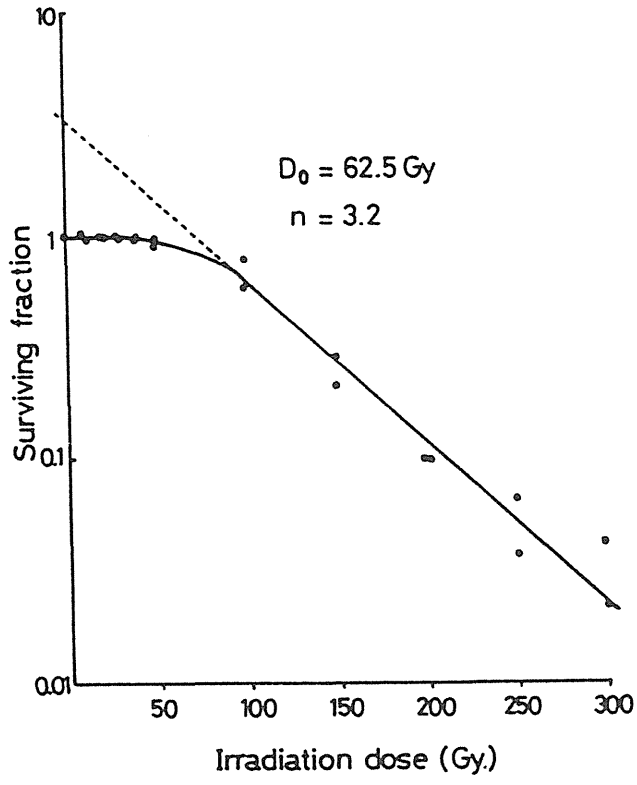

Fig. 2. Dose-survival curve of islet cells at 5 hours after start of X-irradiation with low dose rate.

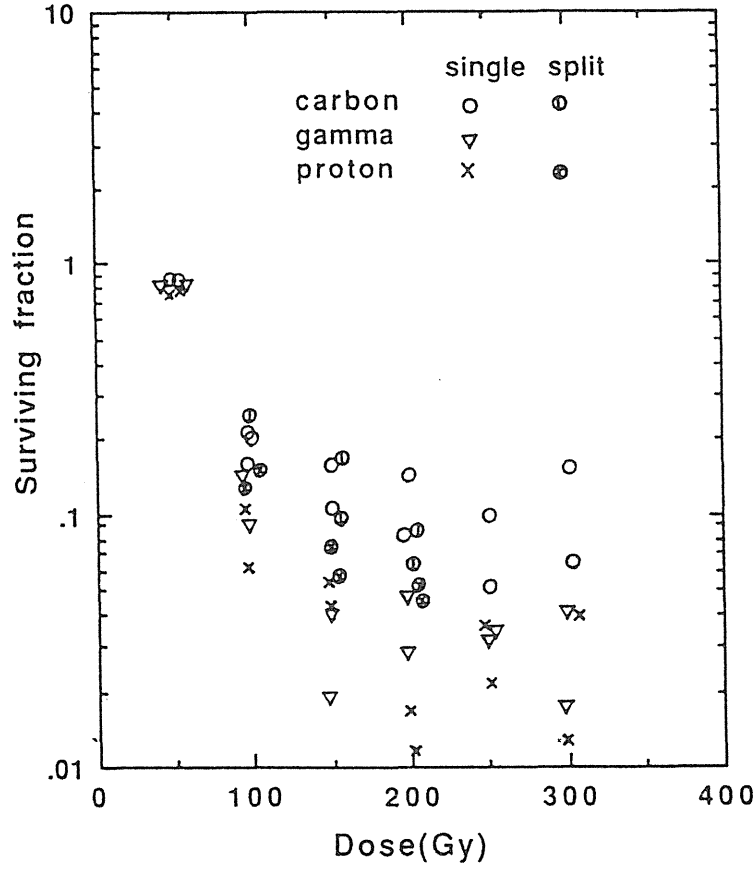

Fig. 3. Dose-suruvival of islet cells at 5.5 hours after start of gamma ,proton and carbon beam irradiations with high dose rate.

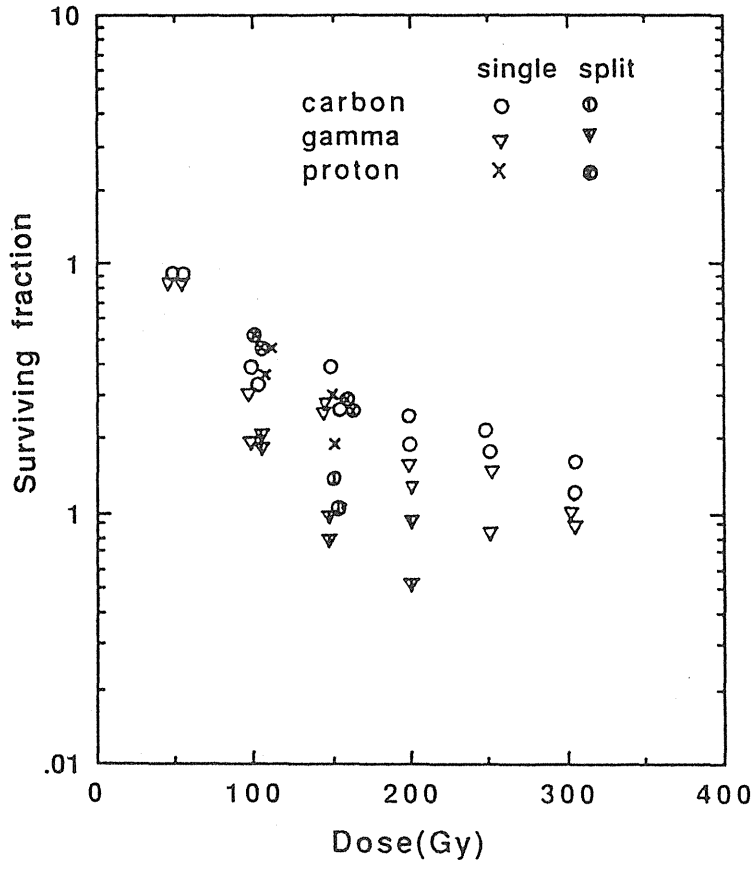

Fig. 4. Dose-suruvaival curve of islet cells at 4 hours after start of gamma, proton, and carbon beam irradiation with high dose rate.

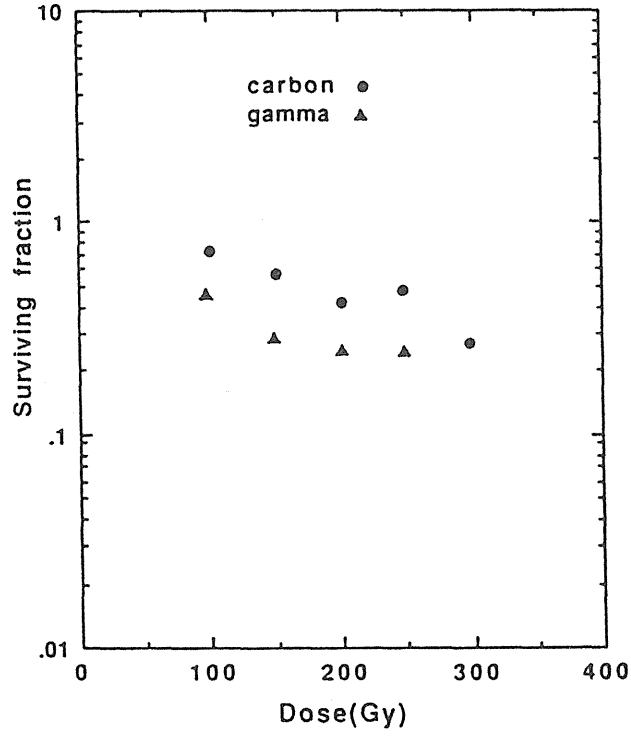

Fig. 5.Dose-suruvaival curve of islet cells at 3 hours after start of gamma, and carbon beam irradiation with high dose rate.

Effects of Accelerated Carbon-Ion on the Induction of Dominant Lethality in the Teleost Fish, *Oryzias latipes*

Yasuko HYODO-TAGUCHI, Tatsuaki KANAI, Shinichi MINOHARA and Yoshiya FURUSAWA

National Institute of Radiological Sciences, Chiba 263

The dominant lethal mutation test with mice has been considered one of the most important methods for the estimation of the mutagenic effects of chemicals on higher animals. In the small teleost fish, *Oryzias latipes*, it has been reported that the dominant lethal mutation test by using the hatchability of eggs is useful for estimation of the mutagenic effects of radiation and chemicals (Egami, et al, 1983). In the present experiment, we have studied the genetic effects of heavy ion on the male germ cells of the fish by using the dominant lethal test system.

One of albino strain of medaka (*bi-3R*) was used. A single pair of the adult fish lays a cluster of 10-40 eggs almost every morning in a laboratory aquarium if the fish were kept at 26°C. During the period of 6-9 days before irradiation, the numbers of fertilized and unfertilized eggs laid by each pair and the hatchability of the fertilized eggs were examined to determine non-irradiation control value. The male of each pair was irradiated with carbon-ion (135MeV/u) accelerated by the RIKEN ring cyclotron. The fish were exposed to heavy ion of 2, 5 and 10Gy at the mid position of spread-out bragg peak (dose average LET=70keV/μm). The irradiated fish were transported to the NIRS and each fish was kept with a non-irradiated female in an aquarium containing 2l of water. Each pair was kept under conditions of about 26°C and 14-h light/10-h dark cycle and observed every day. The numbers of fertilized and unfertilized eggs laid by each fish were counted every morning and each cluster of fertilized eggs was incubated separately in a petridish at 26°C. The incubation medium (D.W. containing 0.0001% methylene blue) was changed every day and dead embryos were removed. In the non-irradiated control, most embryos hatched 7-10 days after fertilization . The numbers of dead embryos and newly hatched fry were counted every day in each cluster. The hatchability was calculated as the percentage of hatched embryos per fertilized eggs. The hatchability of the non-irradiated control was 92±1 %; the relative hatchability rate (RHR) was calculated as follows: (hachability of the given group)/(hatchability of the control group)x 100. Dominant lethal rates were calculated as 1 minus RHR. The maturation stage at which spermatogenic cells were irradiated was judged by the time between irradiation and fertilization (Egami and Hyodo-Taguchi, 1967): fertilization 1-3 days after irradiation

corresponds to irradiated sperm, 4-9 days after irradiation corresponds to irradiated spermatides, 20-26 days after irradiation corresponds to irradiated spermatocytes and 30-36 days after irradiation corresponds to irradiated spermatogonia.

Table 1 shows the numbers of pairs of fish irradiated and the numbers of eggs examined. The fertility of eggs and the hathability eggs fertilized by each male was examined (Figs. 1 and 2). The fertility and hatchability of eggs laid 1-3, 4-6, 7-9, 20-26 and 30-36 days after irradiation was pooled. Considerable high level of the fertility of the male fish was kept within 10 days after irradiation in all irradiated groups (Fig. 1). At 20 and 30 days after irradiation the marked decrease in the fertility was observed in C-beam 10Gy-irradiated group. The hatchability changes in Fig. 2 show that (1) hatchability of eggs fertilized by irradiated males reduces markedly within 3 days after irradiation, and the effects are dose-dependent and (2) the effects of irradiation decrease if the interval between irradiation and fertilization becomes longer than 4 days. From these hatchability data, the dose-associated increase of production of the dominant lethality were observed in each spermatogenic cell stage in medaka after heavy ion irradiation (Fig. 3); a dose-dependent increase in dominant lethality was found for sperm, spermatid and spermatocytes within this dose range, whereas no marked increase of dominant lethality could be found for spermatogonia. Mature sperm was the most sensitive among the various stages of spermatogenetic cells. The high and low inducibility of dominant lethal in sperm and spermatogonia, respectively, was reported in this fish after X-irradiation (Egami, et al,1983 and Shima and Shimada, 1991).

On the basis of the present results and the works by Egami, et al (1983) and Shima and Shimada (1991), it seems to be evident that the effect of carbon-beam on the induction of dominant lethality was about 2 times higher than that of X-rays for sperm and spermatid of the fish.

Table 1 Number of fish pairs and eggs examined

Irradiation Dose, Gy	Number of pairs	Number of eggs examined
0(control)	37	2865
Carbon beam		
2	13	2854
5	9	2097
10	9	1578
X-rays		
5	6	1651

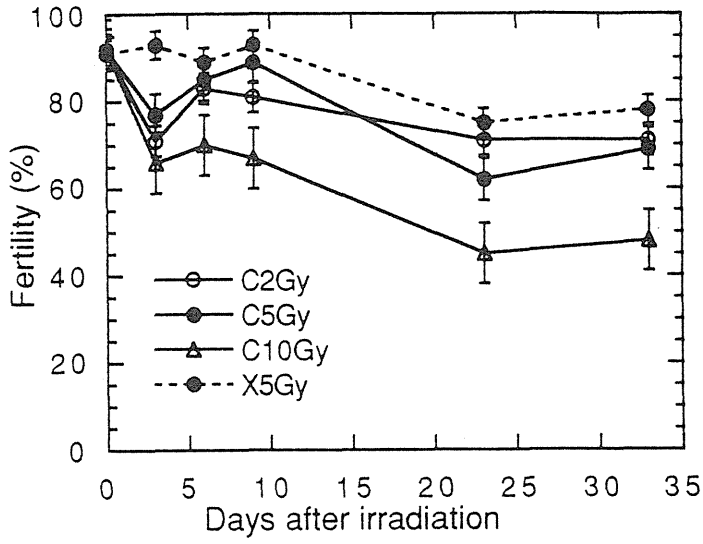

Fig. 1
Effects of carbon-ion and X-rays on fertility of the male fish.

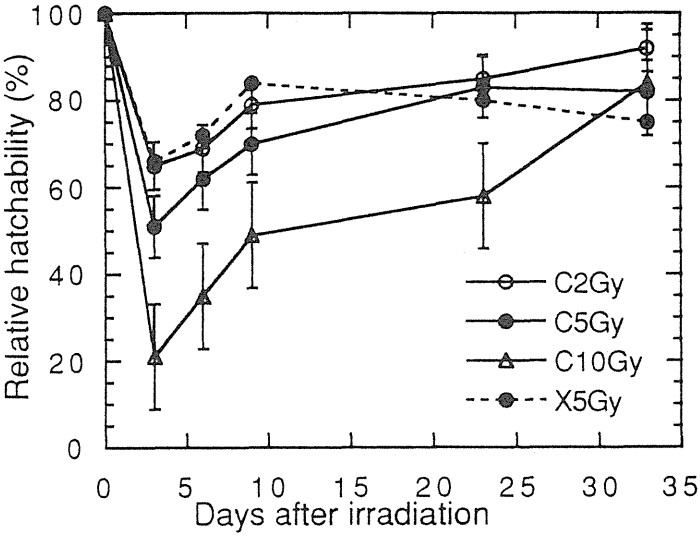

Fig. 2
Changes in hatchability of the eggs fertilized by the irradiated male gametes during about 35 days after irradiation.

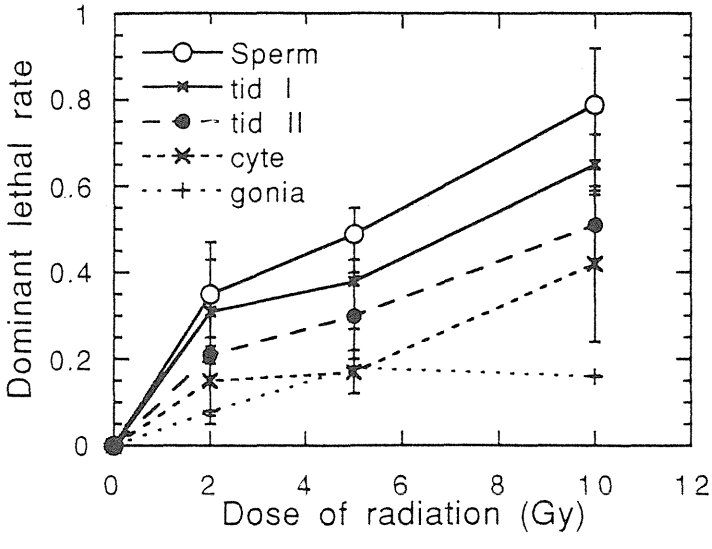

Fig. 3
Dominant lethal rates induced in male gametes of the fish by carbon-ion irradiation.

Apoptosis in Thymocytes and Lymphoma Cells Induced by Neutrons and X-rays.

Harumi Ohyama, Sachiko Koike and Kouichi Ando

Division of Clinical Research and Radiation Health,
National Institute of Radiological Sciences

There has been a growing interest in the last few years in understanding the mechanism of cell death known as apoptosis, or programmed cell death. Apoptosis is a distinctive mode of cell death with characteristic morphological and biochemical features that distinguished it from necrosis. Cells undergoing apoptosis display shrinkage, chromatin condensation, and internucleosomal breakage of DNA. The cell death is a process through which organisms get rid of unwanted cells, and plays essential roles in a number of important biological phenomena.

Thymocytes are highly radiosensitive and undergo typical apoptosis within a few hours after exposure to X-rays. Radiation-induced apoptosis has been observed in several normal tissues, such as intestinal crypt and salivary gland. Recently, apoptosis in several irradiated tumors has been recognized. However, there is few report concerning effects of heavy ion particles on apoptosis induction .

We have reported several characteristic features in radiation-induced apoptosis in thymocytes (1). We also found extremely radiosensitive thymic lymphoma cells which were susceptible to radiation-induced apoptosis after very low doses. In this preliminary study, we examined the effect of 30 MeV NIRS fast neutrons on the induction of apoptosis in thymocytes and thymoma cells, in comparison with that of X-rays.

Apoptosis in thymocytes as a function of dose

Although apoptotic cells increased gradually with time starting after 1 to 2 h following X-irradiation, the apoptotic processes proceeded rapidly in individual cells after onset. Apoptotic thymocytes showed distinct reduction in cell size, chromatin condensation, loss of surface microvilli and DNA fragmentation into oligonucleosomal units. Cell size reduction is one of the most characteristic features in the apoptosis in thymocytes. By measurement of cell size distribution with Coulter channelyzer, we observed appearence of a distinct apoptotic cell peak in irradiated thymocyte population in addition to normal viable cell peak.

Wistar rat thymocytes suspended in Krebs-Ringer phosphate were incubated for 4 h at 37^0 C following irradiation. As shown in Fig 1, apoptotic cells having peak at around 75 mm^3 increased depending on radiation dose. The effects of X-rays and neutrons are almost same, indicating that RBE value of neutrons for induction of apoptotic cell size reduction in thymocytes is approximately 1.

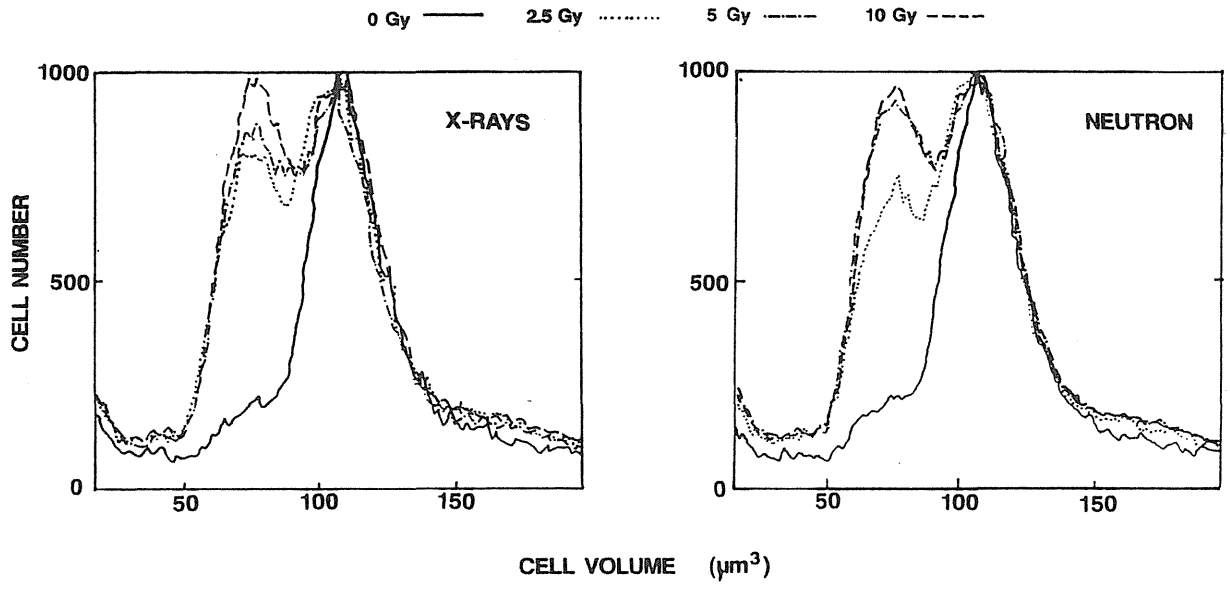

Fig. 1. Cell volume reduction of thymocytes induced by X-rays and neurons

Effects of neutron irradiation on SCA1 thymic lymphoma cells

SCA1, an established cell line from spontaneous thymic lymphoma in radiosensitive *scid* mouse, showed extremely high radiosensitivity and undergo apoptosis following X-irradiation. We noticed that cell size determination could not be used for measurement of apoptosis in the lymphoma cells. Microscopic observation revealed marked changes in nuclear morphology of the majority of cells at 4 h after 5 Gy X-irradiation. Therefore we developed a method to count apoptotic cells based on chromatin condensation, a characteristic morphological feature of apoptosis. Cells could be distinguished into normal or apoptotic cells and no intermediate cells existed in the irradiated population. The observation suggest that the transition from normal to apoptotic takes place extremely rapidly, as in the case of thymocytes. The DNA extracted from irradiated cells showed a typical "ladder" pattern after agarose electrophoresis, one of the most characteristic biochemical markers of apoptosis.

Four hours after exposure to 5 Gy X-rays or neutrons, apoptosis had reached to more than 80 % (Fig. 2). Doses lower than 5Gy were much more effective at inducing apoptosis with 1 Gy exposure, for example, producing 50% apoptosis. The results indicate that SCA1 has extremely high radiosensitivity and are killed rapidly via apoptosis by fairly low dose irradiation. Compared with thymocytes, the cells were more radiosensitive. As the doubling time was 9 h, it would be reasonable to assume that the apoptosis occurs mostly in interphase, without post-irradiation mitosis. The dose response curve for X-rays and neutrons is almost same, RBE value for the thymic lymphoma is also estimated to be nearly 1 .

Fig. 3 shows survival curves of SCA1 determined by colony formation assay after X-ray and neutron irradiation. The D_0 values are 0.39 and 0.28 Gy for X-rays and neutrons respectively, the curves have no shoulder. The RBE value is 1.4.

We also examined radiation-induced apoptosis in the other radiosensitive 3SB lymphoma cells established from radiation induced thymoma in B10 thy1-1 mouse (2). The effects of X-ray and neutron irradiation were almost similar as in case of SCA1 (data not shown).

In radiobiology, death of proliferating cells is in general defined as loss of colony forming ability. Majority of proliferating cells die after one or more round of cell division. Although the newly established lymphoma cells proliferate very rapidly with short doubling time, they undergo interphase death within 4 h after irradiation without undertaking mitosis. After longer incubation, number of apoptotic cells increased gradually depending on doses of irradiation. It is possible that some cells undergo apoptosis after mitosis. SCA1 is one of the most radiosensitive cells with the lowest D_0 value reported so far.

The present study indicate that the RBE values for induction of apoptosis in thymocytes and thymic lymphoma cells is nearly 1. It has been reported that RBE for neutrons varies or different tumor types , being high for slowly proliferating cells. It is well documented that neutron RBEs are higher for late than for early effects. The results show that neutron RBE for induction of apoptosis occured in short time in these cells are low. The mechanism remains to be elucidated. Present study confirmed that the apoptotic mode of cell death may represent an important response in the at least some irradiated tumor cells to fast neutrons.

Research on apoptosis has been stimulated by the finding that tumor cells die by apoptosis in response to a variety of cytotoxic therapeutic modalities, including ionizing radiation and chemotherapy. Many oncogenes and tumor suppressor genes has been recognized to participate induction or suppression of apoptosis. It was found that *bcl-2* oncogene suppressed apoptosis and tumor suppressor gene *p53* induced apoptosis in many cellular system including many tumors. These findings has forced a reconsideration of the mechanism whereby tumor cells can acquire or lose sensitivity to cytotoxic treatments. Therefore, for evaluation of heavy particle therapy, investigations on apoptosis will be required. Based on the present study, we are planning to examine the effect of heavy particle irradiation on induction of apoptosis in variety of normal tissues and tumors.

References

1) T. Yamada and H. Ohyama, 1988, Radiation-induced interphase death of rat thymocytes is internally programmed (apoptosis), *Int. J. Radiat. Biol.* 53, 65-75.

2) H. Ohyama, M. Muto and T. Yamada, 1992, Apoptosis in newly established radiosensitive mouse lymphoma cell lines. *Proc. Int. Conference on Low Dose Irradiation and Biological Defense Mechanisms*, Eds. T. Sugawara, L. Sagan and T. Aoyama, (Except Medica, Amsterdam-London-New York-Tokyo) , pp.361-364.

Fig. 2. Induction of apoptosis in SCA1 by neutorn and X-irradiation.

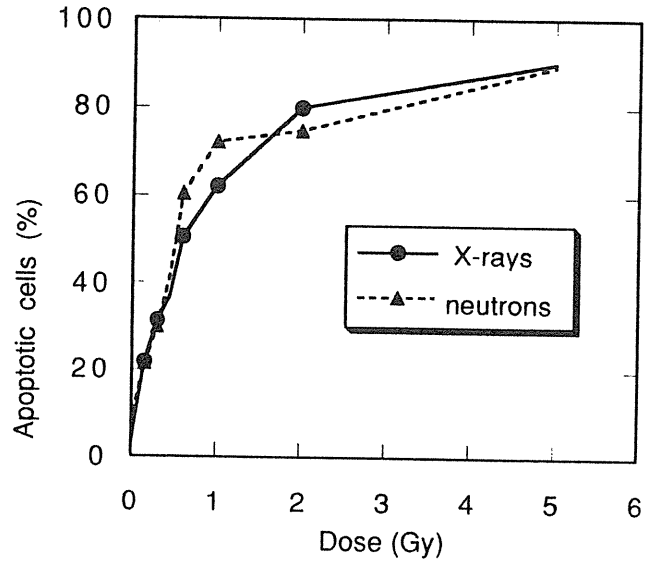

Fig. 3. Dose survival curves for SCA1 exposure to neutorns and X-rays.

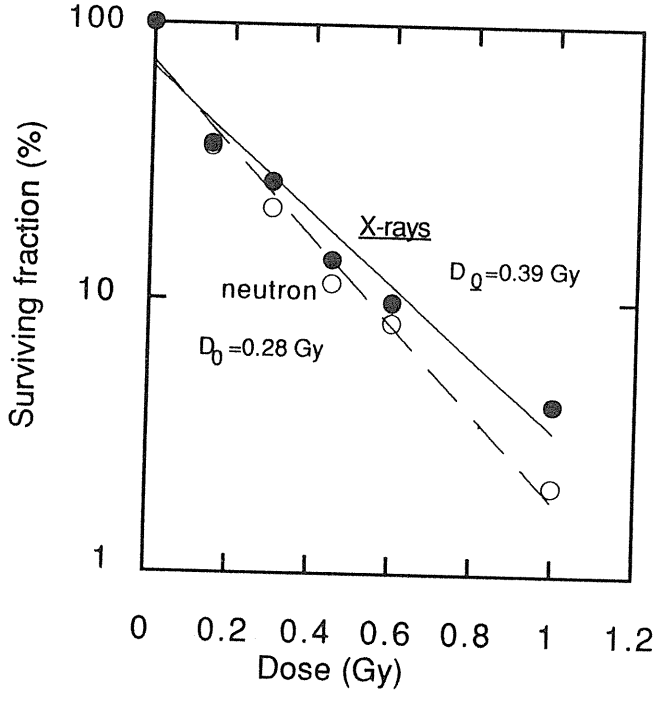

Irradiation Increases Manganese Superoxide Dysmutase Gene in Human Fibroblasts: Possible Mechanisms for Its Accumlatation

Makoto Akashi, Misao Hachiya, Saori Shimizu, Yoshiaki Osawa, and Gen Suzuki.

Division of Clinical Research and Radiation Health, National Institute of Radiological Sciences, Chiba, Japan, 263

Abstract

Fibroblasts are one of the mesenchymal cells and constitute a major element of components in bone marrow stroma as well as submucosal and subcutaneous tissue. Manganese superoxide dismutase (MnSOD) is a mitochondrial enzyme involved in scavenging of superoxide radicals (O_2^-). In this study, we examined the regulation of MnSOD gene by irradiation in WI38 human fibroblasts. We found that fibroblasts constitutively produced MnSOD; irradiation significantly increased the activity of MnSOD. The increase in MnSOD transcripts by irradiation was both time- and dose-dependent. Pretreatment with cycloheximide, a protein synthesis inhibitor, did not change accumulation of MnSOD mRNA by irradiation. WI38 fibroblasts constitutively produce low levels of IL-1. Induction of MnSOD mRNA by irradiation was blocked by anti-IL-1 antibodies. Inhibition of the cyclooxygenase pathway with indomethacin caused augmentation in the irradiation-induced MnSOD mRNA. These results suggest that induction of MnSOD gene after irradiation is regulated, at least in part, by IL-1 production, and increased levels of MnSOD transcripts also occur through a pathway of prostaglandin inhibition.

Introduction

Irradiation is one of stresses which produce physical and chemical damage to tissues. Irradiation induces neoplastic transformation as well as cell killing, and causes bone marrow suppression which leads to either bleeding or infection. In response to these stresses, cells induce or activate protein that protect themselves from external insults. Cytokines such as tumor necrosis factor (TNF) and interleukin-1 (IL-1) were observed to be produced after irradiation in hematopoietic cells and other cells. Recent studies have also shown that early-responsible genes such as C-jun, C-fos, or Egr-1 are induced after irradiation in either fibroblasts or epithelial cells.

Superoxide dismutase (SOD) are metalloenzymes that catalyze the dismutation of O_2^- (superoxide raidicals) to H_2O_2 (hydrogen peroxide) and O_2 (oxygen). SODs are important as initial components in the cellular defense against O_2^-. Three forms SODs with distinctive distributions characterized by their metal requirements are found; copper-zinc SOD (Cu/Zn-SOD) is mainly in the eukaryotes, and iron SOD (Fe-SOD) is mainly in the cytosol of prokaryotes. Production of Cu/Zn-SOD and Fe-SOD are constitutive. On the other hand, MnSOD is inducible by various stimuli such as IL-1, TNF, lipopolysaccharide (LPS), or hypoxia.

Mesenchymal cells including fibroblasts produce a variety enzymes or factors in response to various stimuli. Fibroblasts constitute a major element of bone marrow stroma as well as submucosal and subcutaneous tissue. Fibroblasts are important cells for repair tissue injury. In this study, we examined the effects of irradiation on expression of MnSOD gene, and also explored the mechanisms of the regulation of MnSOD gene by irradiation.

Materials and Methods

Cells and Culture.

Normal human embryonic lung fibroblasts (WI38, obtained from American Type Tissue Culture Collection) were cultured in amedium (Cosmo Bio Co. Ltd., Tokyo, Japan) supplemented with 7% fetal calf serum (FCS, Mitsubishi Kasei Co., Tokyo, Japan) in a humidified atmosphere containing 5% CO_2. Flasks containing confluent cells were used for experiments.

Irradiation.

Cells were irradiated with gamma ray by ^{137}Cs source emitting at a fixed dose rate of 12 Gy/minute as determined by dosimetry.

Reagents.

Anti IL-1α antibody(polyclonal rabbit anti-human IL-1) and anti IL-1β antibody (polyclonal rabbit anti-human IL-1) were kindly provided by Dr. Tsutomu Nishida (Otsuka Pharmaceutical Co Ltd, Tokushima, Japan).

Assay for MnSOD Activity.

The MnSOD activity was determined by nitroblue tetrazolium (NBT) methods using the xanthine-xanthine oxidase as source of O_2^-. Cells were sonicated in 0.005 mol/L potasium phosphate buffer (pH 7.8) on ice. The rate of NBT reduction was monitored by spectrophotometer at 560 nm. The unit of SOD was defined as the amount of enzyme activity which inhibits the NBT reduction rate by 50 %. The activity of MnSOD was assayed in the presence of 5 mmol/L sodium cyanide (NaCN) to inhibit CuZn-SOD. Endogenous activity of NBT reductase was subtracted.

Assay for Prostaglandin E_2.

The amount of PGE_2 secreted by WI38 fibroblasts in culture supernatants was measured by radioimmunoassay (RIA) as previously described. The cross reactivity between PGE_2 and PGD_2, or PGE_2 and PDF_2, was less than 0.01 % and the limit of detection by RIA was 0.25 pg.

Biological Activity of IL-1.

IL-1 activity in conditioned medium from WI38 cells was measured by enhanced ^3H-thymidine incorporation been exposed to phytohemoagglutinin (PHA).

DNA probes.

Human MnSOD cDNA (0.9 kilobase, Kb, EcoRI-BamHI) was derived from plasmid pCSF-1. B actin DNA probe (0.7 Kb, EcoRI-BamHI) was from pHFb A-3' ut plasmid. These probes were ^{32}P-labeled by random priming methods.

Isolation and blotting of RNA.

For total cytoplasmic RNA, WI38 cells were suspended in hypotonic buffer (10mmol/L Tris HCl pH7.8, 150 mmol/L NaCl, 1.5 mmol/L $MgCl_2$) and lysed with 0.65% Nonidet P-40. Cytoplasmic RNA was extracted by phenol/chloroform methods as previously described. Autoradiograms were developed at different exposures. The relative density of bands of hybridization of MnSOD mRNA in different lanes was scanned by the LKB Ultro Scan XL Laser densitometer using multiple exposure of the blot.

Results

Induction of MnSOD activity by irradiation in fibroblasts:

Confluent culture of WI38 fibroblasts were cultured for 16 hours after exposure to irradiation at different doses (10-80 Gy). As a control, unirradiated cells were cultured for

16 hours. Cells were harvested and tested for SOD activity by NBT-reduction method. Unirradiated fibroblasts constitutively had MnSOD protein (Fig.1). A significant increase of MnSOD activity was observed at 10 Gy of irradi-ation; the increase of MnSOD activity was almost in a dose-dependent fashion. At 80 Gy irradiation, MnSOD was approximately 4 times greater activity than constitutive production.

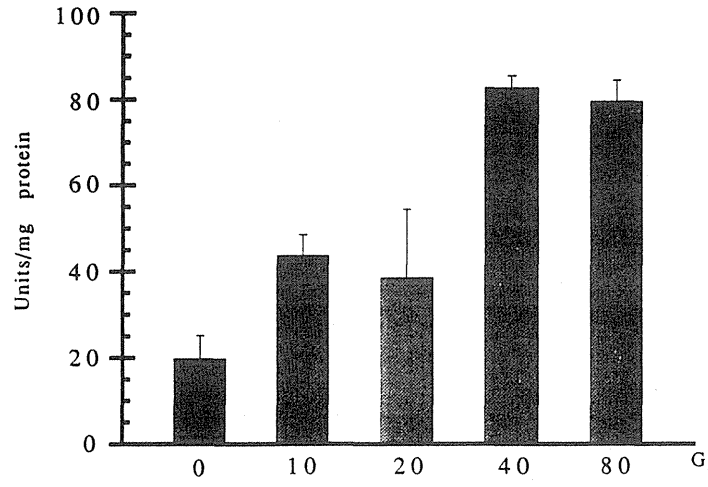

Figure 1. Increased activity of MnSOD in WI38 human fibroblasts exposed to irradiation. Cells were cultured for 16 hr after irradiation with 0-80 Gy. MnSOD activity was assayed by NBT-reduction method. Results represent mean and standard error of triplicate assay.

Dose dependent effect of irradiation on levels of MnSOD mRNA in fibroblasts.

Fibroblasts were cultured for 8 hours after 0-80 Gy irradiation. To determine the effect of irradiation on MnSOD gene expression, we performed Northern blots analysis of cytoplasmic RNA using ^{32}P-labeled MnSOD cDNA probes. Fibroblasts constitutively contained a low but detectable concentrations of mRNA coding for MnSOD. Irradiation with a dose of 10 Gy increased the MnSOD gene expression at a detectable level; the induction of MnSOD RNA was dependent on the dose of irradiation and the induction of MnSOD gene was maximal after exposed to 80 Gy irradiation (8 times)(Fig. 2).

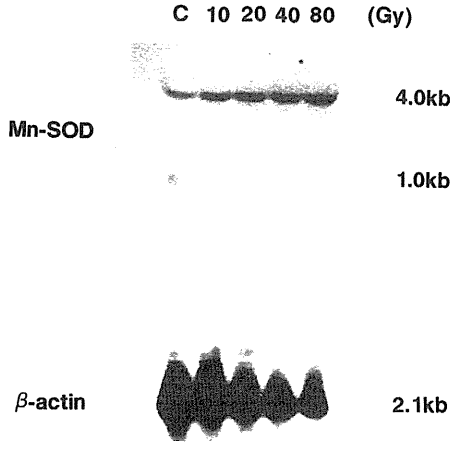

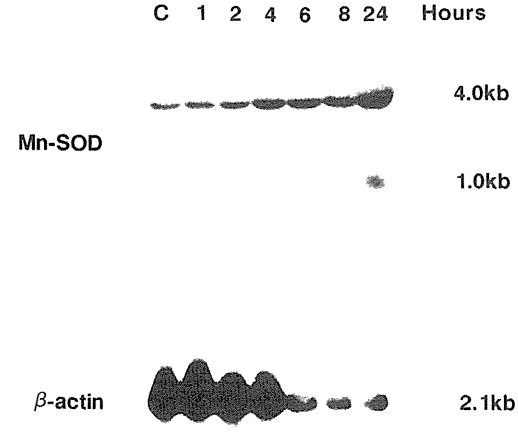

Figure 2. Dose dependent effect of irradiation on levels of MnSOD mRNA in fibroblasts. Cells were cultured for 4hr after irradiation. Cytoplasmic RNA (15 μg/lane) was prepared and analyzed by formaldehyde-agarose gel electrophoresis and transferred to a nylon membrane. Hybridization was with ^{32}P-labeled MnSOD cDNA (1.0 and 4.0 kb bands of hybridization) and β-actin DNA (2.1 kb).

Figure 3. Time dependent effect of irradiation on levels of MnSOD mRNA in fibroblasts. Cell were cultured for various duration (0-24hr) after irradiation at 40 Gy. Northern blots analysis of mRNA was performed by blotting cytoplasmic RNA (15 μg/lane).

Time dependent effect of irradiation on levels of MnSOD mRNA.

Fibroblasts were irradiated at 40 Gy and harvested sequentially at different durations. Northern blots analysis showed a significant increase was observed at 4 hours after irradiation; after this the levels of MnSOD mRNA increased until 24 hours (Fig. 3).

Effect of irradiation on expression of MnSOD mRNA in the absence of protein synthesis.

Fibroblasts cultured with cycloheximide (CHX; 0.2, 2, or 20 μg/ml) decreased protein synthesis by 74, 85, or 93 %, respectively as compared with untreated cells. Cells pretreated with CHX (20 μg/ml, 30 minutes) and followed by irradiation (80 Gy, 2 hours) did not enhance the accumulation of MnSOD RNA while irradiation alone significantly increased the level of MnSOD transcripts (Fig. 4).

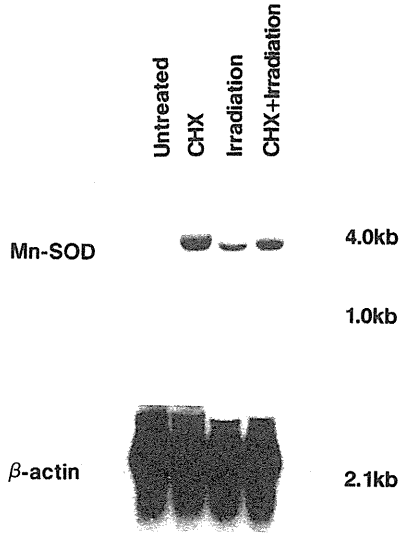

Figure 4. Effect of inhibitor of protein synthesis, cycloheximide (CHX), on expression of MnSOD mRNA after irradiation. Cells were either treated with irradiation (80 Gy, 4hr), CHX (20 μg/ml) or pretreated with CHX (0.5hr) and then irradiated (4 hr).

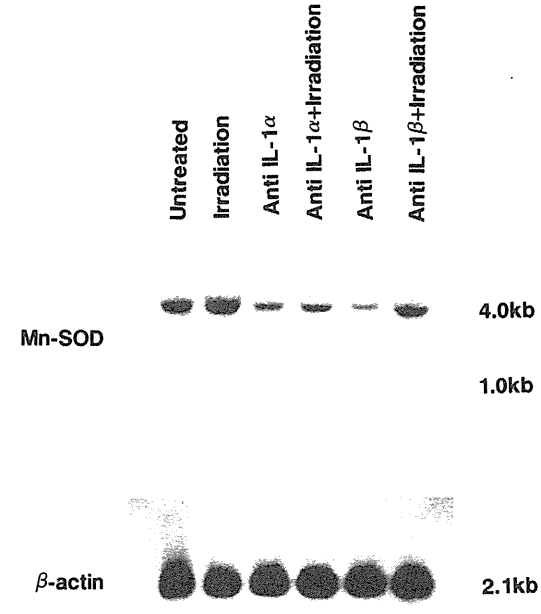

Figure 5. Effect of anti IL-1α and IL-1β antibodies on expression of MnSOD mRNA Cells were treated for 1 hr with either anti IL-1α or IL-1β antibody which neutralizes 100 U/ml of either IL-1α or IL-1β and irradiated at 80 Gy. After 4 hr, cells were harvested and levels of MnSOD mRNA were determined.

Effect of IL-1 production on expression of MnSOD mRNA after irradiation.

WI38 fibroblasts constitutively produce IL-1 protein at low levels. Northern blot analysis showed that WI38 cells contained very low levels of IL-1α and IL-1β mRNAs and there was no significant increase of levels of IL-1 RNAs after irradiation in these cells (data not shown). We also measured IL-1 bioactivity using thymocytes proliferation assay. Conditioned medium of WI38 cells cultured for 3 days contained less than 0.2 U/ml of IL-1 activity. To investigate further the involvement of IL-1 in expression of MnSOD RNA by irradiation, fibroblasts were preincubated with either anti IL-1α or IL-1β antibody for 1 hour which

neutralizes 100 U/ml of IL-1. Then, cells were irradiated with 80 Gy in the presence of either anti-IL-1α or β antibody. After 4 hours, cells were harvested and levels of MnSOD mRNA were determined. Neutralization of IL-1s with anti-IL-1 antibodies resulted in a decrease in levels of MnSOD mRNA in untreated cells. Treatment with anti-IL-1 antibodies inhibited the increase of these transcripts by irradiation (Fig. 5).

Effect of indomethacin on expression of MnSOD mRNA after Irradiation.

Previous studies have shown that cyclo-oxygenase metabolite prostaglandin E_2 (PGE_2) is a potent regulator of cytokines production and prostaglandins are synthesized by fibroblasts. In order to determine whether prostaglandins are involved in regulation of MnSOD gene by irradiation, induction of MnSOD mRNA by irradiation was examined in the presence of a cyclooxygenase inhibitor, indomethacin (Fig. 6). WI38 cells were initially cultured with different concentrations of IM (10^{-7}-10^{-5} M) for 0.5 hours and then exposed to 80 Gy irradiation. After 4 hours of cultures, cells were harvested and determined for MnSOD mRNA levels. Treatment of cells with indomethacin enhanced the induction of MnSOD mRNA by irradiation.

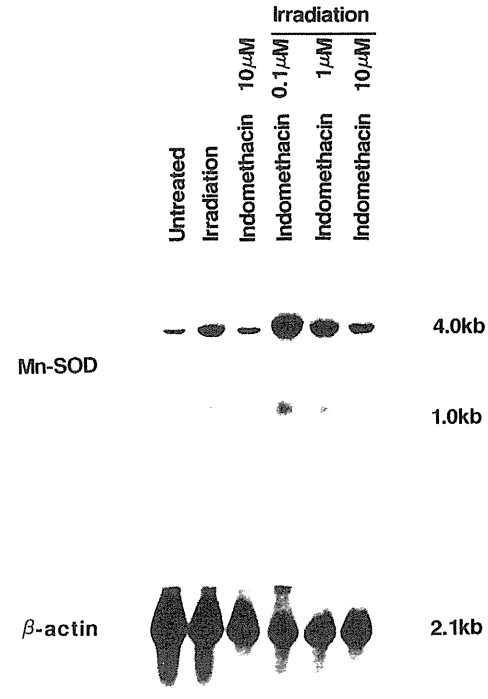

Figure 6. Effect of cyclooxygenase inhibition on the induction of MnSOD mRNA in irradiatied fibroblasts. Cells were pretreated with varying concentrations of indomethacin for 0.5 hr. Cells were irradiated in the presence of indomethacin and then cultured for 4 hr. Cytoplasmic RNA was extracted and each blot (15 μg/lane) was sequentially hybridized.

Dose dependent effect of irradiation on PGE_2 synthesis in WI38 fibroblasts.

To determine further involvement of prostaglandin in induction of MnSOD mRNA by irradiation, levels of PGE2 in culture supernatant were tested by RIA. Confluent cells were irradiated in the medium without FCS and cultured for 8 hours. A significant decrease of PGE_2 production was observed at 10 Gy of irradiation; the inhibition of PGE2 synthesis was dose-dependent (Table 1).

Table 1.
Synthesis of PGE2 in irradiated fibroblasts

Dose	pg/ml
Control	6.4 ± 1.0
10 Gy	3.0 ± 0.4
20 Gy	3.8 ± 0.8
40 Gy	2.5 ± 0.4
80 Gy	< 2.5

Discussion

The data presented here demonstrate that the levels of MnSOD mRNA can be modulated by irradiation in human fibroblasts; irradiation increases MnSOD transcripts in a dose and time dependent fashion. We also found that accumulation of MnSOD mRNA after exposure to irradiation occurs through, at least in part, indirect mechanisms; activation of IL-1 synthesis and inhibition of prostaglandin. Mitochondria is one of the major direct intracellular target sites for irradiation and chemical drugs. Recently, preferential oxidative damage to mitochondrial DNA rather than nuclear DNA after irradiation has been reported . Studies have shown that MnSOD, a mitochondrial enzyme, is involved in resistance to irradiation and overexpression of MnSOD promotes the survival of cells exposed to irradiation. Thus, our results suggest that the increased activity of MnSOD might be an important biological response to irradiation, since O_2^- generated after irradiation causes DNA breakage which sometimes results in lethal injuries of tissues.

WI38 fibroblasts constitutively produced IL-1 at a low level and treatment of cells with either anti-IL-1α or β antibody increased the constitutive expression of MnSOD mRNA. Investigators have shown that IL-1 stimulated expression of Mn SOD in fibroblasts. These studies suggest that IL-1 stimulates these cells to produce MnSOD in an autocrine manner. This constitutive expression of IL-1 could be augmented after appropriate stimulation. Other investigators have demonstrated that irradiation induced IL-1 and ultraviolet (UV) irradiation also induced release of IL-1 in human keratinocytes. In this study, no significant change could be detected in the levels of IL-1 transcripts. However, anti-IL-1 antibodies blocked induction of MnSOD gene by irradiation. Our results indicate that irradiation induces expression of MnSOD mRNA through the autocrine loops in the endoplasmic reticulum since exogenously added antibodies can only interrupt an autocrine loop on the exterior of the cells. Further studies are required.

Prostaglandins play an important role in the pathogenesis of the inflammation and augmented synthesis of prostaglandin by fibroblasts in response to various stimuli is a prominent feature of inflammatory reactions. PGE_2 synthesized by cyclooxygenase metabolism of arachidonic the second messenger cAMP. Studies have shown that PGE_2 is a potent regulator of cytokine production and PGE_2 synthesis is enhanced in fibroblasts with stimuli such as IL-1. Ultraviolet irradiation has been also shown to increases PGE_2 release in human skin keratinocytes. In the present study, inhibition of cyclooxygenase enhanced the induction of MnSOD mRNA. Our data suggest that induction of MnSOD mRNA by irradiation is likely to be mediated through cyclooxygenase pathway.

Mesenchymal cells including fibroblasts produce a variety of factors in response to various stimuli. Fibroblasts constitute a major element of bone marrow stroma as well as submucosal and subcutaneous tissue. We have shown that WI38 fibroblasts constitutively transcribe MnSOD gene and produce the increased level of MnSOD in response to irradiation. Irradiation is considered immunosuppressive and increases production of O_2^-; O_2^- causes

DNA breakage and lipid peroxidation. Thus, it seems paradoxical that irradiation induces MnSOD in fibroblasts. Since MnSOD protects or promotes the recovery of cells exposed to stress including irradiation, fibroblasts may be primarily responsible cells for irradiation in the repair of tissue injury.

Acknowledgment: This work was supported in part by Grant-in-Aid for Science Research from Ministry of Science and Culture (No. 04671542). We would like to thank Ikuko Furusawa for her assistance.

Errata; LET dependency of the initial recombination written in "Beam Modulation for Heavy-ion Radiotherapy" in the 2nd workshop on "Physical and Biological Research with Heavy ions", HIMAC 003, 1-3, 1992. and in "Irradiation of 135 MeV/u carbon and neon beams for studies of radiation biology", HIMAC 004,p27,p28, 1993. should be corrected. The revised version of the LET dependence of the initial recombination will be described as follows. This paper is submitted to RIKEN accelerator report.

Initial Recombination in a Parallel Plate Ionization Chamber Exposed to Heavy-ion Beams

Tatsuaki Kanai, Michio Sudou, Shinichi Minohara, and Fumio Yatagai

We have installed an irradiation system at E5 room of the RIKEN Ring Cyclotron Facility for studies of radiation biology using heavy-ion beams. The biological and physical data are used to modify the heavy-ion beams for the heavy-ion radiation therapy.[1] In the biological studies and radiation therapies using heavy-ion beams, an accurate determination of the absorbed dose is essential. Dosimetry for the heavy-ion beams was described in a separate paper.[2] Fluence of the uniform irradiation field was measured by a plastic scintillator, and dose at the entrance position of the depth dose distribution was obtained by multiplication of the fluence by the stopping power of the heavy ions at the position. Then, the depth dose distribution was normalized by the dose at the entrance position. The depth dose distributions are usually measured by a parallel plate ionization chamber. As discussed in a previous paper,[2] initial recombination plays an important role in measuring the ionization current of an air-filled parallel plate ionization chamber. The ion collection efficiency in the parallel plate ionization chamber is not 100 % because of the initial recombination. The LET dependence of the ion collection efficiency was measured for several gases and differential W-values of the gases for the 135MeV/u carbon and neon ions were deduced.

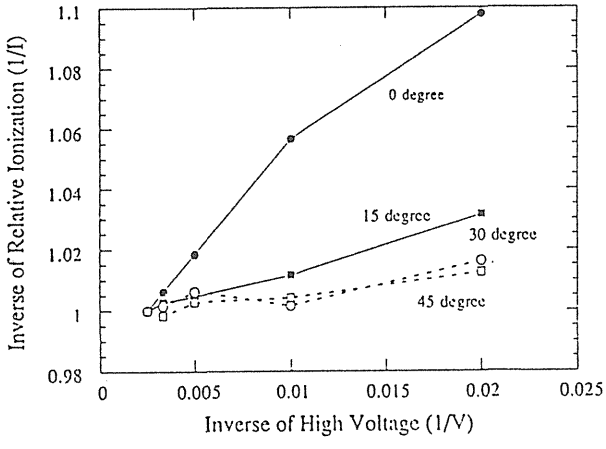

Fig. 1. Plots of the inverse of the ionization current against the inverse of the applied high voltage. Angle between the beam direction and the electric field was changed.

Two types of parallel plate ionization chamber were used for the measurements of the initial recombination. One has an entrance window of 2.5 μm thick aluminized polyester sheet and the other has an entrance window of 1 mm thick Lucite sheet. A signal electrode of 5 mm in diameter is surrounded by a guard ring that is against disturbance of electric field near the boundary of the signal electrode. A gap between the signal and the high voltage electrodes is 2 mm. Usual operating bias of the high voltage electrode is 400 V, which is 2000 V/cm electric field. The initial recombination of the parallel plate ionization chamber depends on an angle between the heavy-ion beam and the electric field of the chamber. The thin-window chamber was used for this angular dependence. Only air can be used as a gas of the cavity of the chamber. The gas in the thick-window chamber can be replaced. The recombination for several gases was measured by this thick-window chamber.

The chamber was irradiated by uniform heavy-ion beams at the irradiation site of the irradiation facility.[1] Ionization current was measured by an electrometer Keithley 617. The LETs of the heavy-ion beams were changed by changing absorber thickness of the irradiation facility.[1] Ionization currents of the parallel plate ionization chamber were measured by changing the voltage applied to the high voltage electrode. The inverses of the ionization current were plotted against the inverse of the applied high voltage. The data corresponding to $1/V < 0.01$, that is, $V > 100$, can be fitted by a straight line. Decrease of the ion collection efficiency at such a high electric field can be regarded as the decrease due to the initial recombination.

The differential W-values of air, nitrogen, argon, carbon dioxide, and tissue equivalent gas for 135MeV/u carbon and neon ions were measured by the same methods described in the previous report.[2] The ion currents were corrected by the recombination effect.

Figure 1 shows the angular dependence of the initial recombination. The slope in a region of $1/V < 0.01$ represents the initial recombination. When the beam was parallel to the electric field (0 degree in the figure), the slope was steepest. When the angle was over 30 degrees, the initial recombination could be neglected. Fig. 2 shows the results of LET dependence of the gradient of the slope at $V > 100$ for air. It can be said that the recombination depends only on the LET of the heavy-ion beams and increases roughly linearly with LET. The experimental data is now being analyzed using model calculation. For argon and nitrogen gases, the decreases of ion collection efficiency due to the initial recombination were not observed.

Table 1. summerizes the differential W-values of those gases for 135 MeV/u carbon and neon ions.

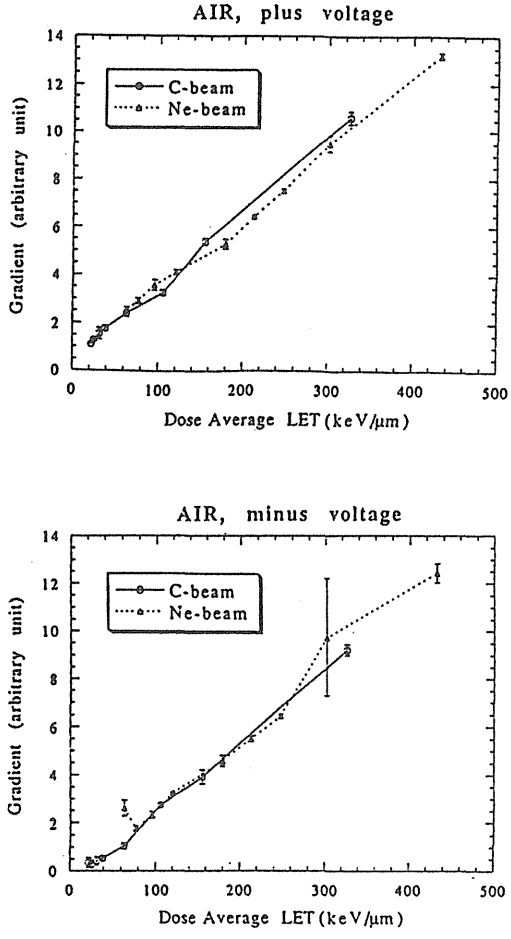

Fig. 2. Typical result of LET dependence of the slope of plots of the inverse of the ionization current against the inverse of the applied high voltage at V > 100. The upper and lower graphs show the results for ion and electron collection, respectively.

Table 1. Differential W-values for 135 MeV/u carbon and neon ions. The results in references [2) 3)] and [4)] are also written for comparison.

	C 135MeV/u	Ne 135 MeV/u	Photon/Electron[3)]
Air	33.5 eV	34.2 eV	33.85 eV
N_2	35.8 eV	36.6 eV	34.8 eV
Ar	23.6 eV	24.3 eV	23.8 ~ 26.4 eV
CO_2	21.4 eV	21.9 eV	33.0 eV
TEG	28.6 eV	29.3 eV	29.2 eV

	^{4}He 18.3 MeV/u[4)]
TEG	29.2 +/- 0.9 eV

	C 129.4 MeV/u	^{3}He 10.3 MeV/u	C 6.7 MeV/u [2)]
Air	33.7 +/- 0.9 eV	34.5 +/- 1.0 eV	36.5 eV +/- 1.0 eV

References

1) T.Kanai et al.: HIMAC report 004 (NIRS-M-91) NIRS publication, (1993).
2) T.Kanai et al.: Radiation Research ,135, 293-301(1993).
3) ICRU report 31 (International Commission on Radiation Units and Measurements, Washington), (1979).
4)T.Kanai and K.Kawachi: Radiation Research, 112, 426-435 (1987).